

Development of Novel Carbon Sorbents for CO₂ Capture

Final Technical Report

Start Date: October 1, 2008

End Date: November 30, 2013

Principal Author: Dr. Gopala N. Krishnan, Associate Director
Materials Research Laboratory

Contributors: Dr. Marc Hornbostel, Dr. Jianer Bao, Dr. Jordi Perez,
Mr. Anoop Nagar, and Dr. Angel Sanjurjo

Date Report Issued: March 2014

DOE Award Number: Cooperative Agreement No. DE-NT0005578

Submitting Organization: SRI International
333 Ravenswood Avenue
Menlo Park, CA 94025

Project Partners: ATMI, Inc.
7 Commerce Drive, Danbury, CT 06810

The University of Toledo
Department of Chemical and Environmental Engineering,
3048 Nitschke Hall, 1610 N Westwood Ave, Toledo, OH 43607

Prepared for: U.S. Department of Energy
National Energy Technology Center
3600 Collins Ferry Road
Morgantown, WV 26505
Attention: Mr. Andrew O'Palko

DISCLAIMER

This report was prepared as an account of work sponsored by an agency of the United States Government. Neither the United States Government nor any agency thereof, nor any of their employees, makes any warranty, express or implied, or assumes any legal liability or responsibility for the accuracy, completeness, or usefulness of any information, apparatus, product, or process disclosed, or represents that its use would not infringe privately owned rights. Reference herein to any specific commercial product, process, or service by trade name, trademark, manufacturer, or otherwise does not necessarily constitute or imply endorsement, recommendation, or favoring by the United States Government or any agency thereof. The views and opinions of authors expressed herein do not necessarily state or reflect those of the United States Government or any agency thereof.

ABSTRACT

An innovative, low-cost, and low-energy-consuming carbon dioxide (CO₂) capture technology was developed, based on CO₂ adsorption on a high-capacity and durable carbon sorbent. This report describes the (1) performance of the concept on a bench-scale system; (2) results of parametric tests to determine the optimum operating conditions; (3) results of the testing with a flue gas from coal-fired boilers; and (4) evaluation of the technical and economic viability of the technology. The process uses a falling bed of carbon sorbent microbeads to separate the flue gas into two streams: a CO₂-lean flue gas stream from which > 90% of the CO₂ is removed and a pure stream of CO₂ that is ready for compression and sequestration. The carbon sorbent microbeads have several unique properties such as high CO₂ capacity, low heat of adsorption and desorption (25 to 28 kJ/mole), mechanically robust, and rapid adsorption and desorption rates.

The capture of CO₂ from the flue gas is performed at near ambient temperatures in which the sorbent microbeads flow down by gravity counter-current with the up-flow of the flue gas. The adsorbed CO₂ is stripped by heating the CO₂-loaded sorbent to ~ 100°C, in contact with low-pressure (~ 5 psig) steam in a section at the bottom of the adsorber. The regenerated sorbent is dehydrated of adsorbed moisture, cooled, and lifted back to the adsorber. The CO₂ from the desorber is essentially pure and can be dehydrated, compressed, and transported to a sequestration site. Bench-scale tests using a simulated flue gas showed that the integrated system can be operated to provide > 90% CO₂ capture from a 15% CO₂ stream in the adsorber and produce > 98% CO₂ at the outlet of the stripper. Long-term tests (1,000 cycles) showed that the system can be operated reliably without sorbent agglomeration or attrition.

The bench-scale reactor was also operated using a flue gas stream from a coal-fired boiler at the University of Toledo campus for about 135 h, comprising 7,000 cycles of adsorption and desorption using the desulfurized flue gas that contained only 4.5% v/v CO₂. A capture efficiency of 85 to 95% CO₂ was achieved under steady-state conditions. The CO₂ adsorption capacity did not change significantly during the field test, as determined from the CO₂ adsorption isotherms of fresh and used sorbents. The process is also being tested using the flue gas from a PC-fired power plant at the National Carbon Capture Center (NCCC), Wilsonville, AL.

The cost of electricity was calculated for CO₂ capture using the carbon sorbent and compared with the no-CO₂ capture and CO₂ capture with an amine-based system. The increase in the levelized cost of electricity (L-COE) is about 37% for CO₂ capture using the carbon sorbent in comparison to 80% for an amine-based system, demonstrating the economic advantage of CO₂ capture using the carbon sorbent. The 37% increase in the L-COE corresponds to a cost of capture of \$30/ton of CO₂, including compression costs, capital cost for the capture system, and increased plant operating and capital costs to make up for reduced plant efficiency. Preliminary sensitivity analyses showed capital costs, pressure drops in the adsorber, and steam requirements for the regenerator are the major variables in determining the cost of CO₂ capture.

The results indicate that further long-term testing with a flue gas from a pulverized coal-fired boiler should be performed to obtain additional data relating to the effects of flue gas contaminants, the ability to reduce pressure drop by using alternate structural packing, and the use of low-cost construction materials.

CONTENTS

DISCLAIMER.....	ii
ABSTRACT.....	iii
CONTENTS.....	iv
LIST OF TABLES.....	vi
LIST OF ILLUSTRATIONS.....	vii
I. EXECUTIVE SUMMARY	1
I.1 SORBENT CHARACTERIZATION.....	2
I.2 bench-scale testing.....	3
I.3 FIELD testinG.....	5
I.4 PRELIMINARY PROCESS EVALUATION.....	6
I.5 CONCLUSIONS AND RECOMMENDATIONS	7
II. INTRODUCTION.....	9
II.1 Current State of the Art.....	9
II.2 Project Overview	11
III. determination of sorbent properties.....	12
III.1 CO ₂ ADSORPTION CHARACTERISTICS.....	12
III.2 CO ₂ DESORPTION CHARACTERISTICS	15
III.3 Heats of adsorption and desorption of CO ₂	18
III.4 adsorption of other gases on the carbon sorbent.....	21
III.5 surface functional groups.....	27
III.6 physical and mechanical properties	28
IV. Screening Tests with the Sorbent Formulation.....	31
IV.1 Screening tests	31
IV.2 Improvements to the sorbent.....	35
V. bench-scale parametric testing	37
V.1 Bench-Scale Reactor Design.....	37
V.2 Adsorber Bed Flow Distribution.....	38
V.3 Parametric Tests in a Bench-Scale System.....	39
V.4 Design of an Integrated Adsorber-Stripper System.....	46
V.5 Operation of the Integrated Adsorber-Stripper System	48
V.6 Results from the Integrated System	50
V.7 Design of a Large Bench-Scale Integrated System.....	53
V.8 Initial Operation of the LARGE Bench-Scale System	56



V.9	Stable Operation of the Bench-Scale System	59
V.10	Long-Term Testing	62
VI.	Field Test of the Advanced Carbon Sorbent Process	66
VI.1	Installation of the Integrated Reactor System at the University of Toledo.....	66
VI.2	Operation of the System with the Flue Gas at the University of Toledo.....	66
VI.3	Analysis of the Sorbent after the Field Test at the University of Toledo	73
VI.4	FIELD TEST AT THE university of toledo	77
VII.	PRELIMINARY PROCESS EVALUATIONS	91
VII.1	model validation.....	91
VII.2	evaluation of the process to capture CO ₂ with carbon sorbent.....	99
VII.3	Updating the Process Economics.....	106
VIII.	CONCLUSIONS AND RECOMMENDATION.....	110
IX.	REFERENCEs	112

LIST OF TABLES

III-1. Measured Parameters Related to Surface Functionalities for ACS-1.....	28
III-2. Physical Properties of the ACS-1 Sorbent.....	28
III-3. Attrition Resistance of the ACS-1 Sorbent.....	300
VI-1. Process Parameters and Their Values Used in the Field Test at the University of Toledo.....	71
VI-2. Comparison of Inorganic Elements in the Fresh and Field Test Sorbents	76
VI-3. Comparison of Adsorbed Gases in the Fresh and Field Test Sorbents	76
VI-4. Design Parameters and Their Values Used in the Field Test at NCCC	77
VII-1. Comparison of SRI Modeling Results with NETL Published Results on Supercritical Pulverized Coal-Fired Power Plants	91
VII-2. Process Assumptions of a Supercritical Power Plant with No-CO ₂ Capture.....	94
VII-3. Comparison of NETL and SRI Results for the Case with No-CO ₂ Capture.....	94
VII-4. Process Assumptions of a Supercritical Power Plant with Econamine CO ₂ Capture.....	97
VII-5. Comparison of NETL and SRI Results for the Case with Econamine CO ₂ Capture.....	97
VII-6. Comparison of Auxiliary Load and Net Plant Performance for the Cases with No-CO ₂ capture and CO ₂ Capture with Econamine.....	98
VII-7. Process Assumptions of a Supercritical Power Plant, CO ₂ Capture with Carbon Sorbents.....	101
VII-8. Comparison of Supercritical Power Plants Using SRI Model	101
VII-9. Comparison of SRI Results for the Case with CO ₂ Capture by Carbon Sorbent and by Econamine process.....	102
VII-10. Sensitivity Analysis of the Parameters for CO ₂ capture with Carbon Sorbents	104
VII-11. Characteristics of the CO ₂ Capture System	106
VII-12. Characteristics of a Supercritical Power Plant with CO ₂ Capture	107
VII-13. Auxiliary Loads and Power Plant Performance.....	108
VII-14. Cost of CO ₂ Capture	109

LIST OF ILLUSTRATIONS

III-1. The quantity of CO ₂ adsorbed on the ACS-1 sorbent as a function of CO ₂ partial pressure at 5°C.	13
III-2. The adsorption isotherms of CO ₂ on the ACS-1 sorbent at various temperatures.	14
III-3. The Dubinin-Polanyi plot of the CO ₂ adsorption isotherm at 20°C.	15
III-4. The adsorption of CO ₂ on ACS-1 sorbent at 30°C in pure CO ₂ and its desorption at temperatures in the range 40 to 110°C.	16
III-5. The mass change of the sorbent at various temperatures with different CO ₂ -Ar gas mixtures.	17
III-6. The CO ₂ loading on the sorbent as a function of temperature and gas composition.	17
III-7. The isostere plots of CO ₂ adsorption on ACS-1 sorbent at various coverages.	18
III-8. The heat of adsorption of CO ₂ on ACS-1 sorbent as a function of CO ₂ loading.	19
III-9. The isostere plots of CO ₂ adsorption on ACS-1 sorbent at various coverages in the temperature range 30° to 110°C.	20
III-10. The heat of desorption of CO ₂ on ACS-1 sorbent as a function of CO ₂ loading.	20
III-11. The quantity of N ₂ adsorbed on the ACS-1 sorbent as a function of N ₂ partial pressure at various temperatures.	21
III-12. The quantity of O ₂ adsorbed on the ACS-1 sorbent as a function of O ₂ partial pressure at various temperatures.	22
III-13. The quantity of Ar adsorbed on the ACS-1 sorbent as a function of Ar partial pressure at various temperatures.	23
III-14. The quantity of H ₂ O vapor adsorbed on the ACS-1 sorbent as a function of the relative pressure at various temperatures.	24
III-15. The adsorption isotherm of SO ₂ gas on ACS-1 sorbent at 20 and 90°C.	25
III-16. The adsorption isotherm of NO gas on ACS-1 sorbent at 20°C.	25
III-17. The heat of adsorption of N ₂ , O ₂ , and Ar on ACS-1 sorbent as a function of their coverage on the sorbent.	26
III-18. The heat of adsorption of water vapor on ACS-1 sorbent as a function of its loading on the sorbent.	27
III-19. A magnified picture of a single ACS-1 sorbent granule.	29
III-20. The compressive strength of the ACS-1 granules.	29
III-21. The photograph of an attrition tester.	30
IV-1. The breakthrough of CO ₂ as a function of time at 25°C at various humidity levels.	32
IV-2. The calculated loading of CO ₂ as a function of time at 25°C at various humidity levels. ...	32
IV-3. The calculated loading of CO ₂ as a function of relative humidity at 5°, 15° and 25°C.	33
IV-4. The rate of desorption of CO ₂ from the ACS-1 sorbent as it is heated to the regeneration temperature.	34
IV-5. The CO ₂ loading on the ACS-1 sorbent as it is heated to different regeneration temperatures.	34

IV-6. The CO ₂ capacity of the ACS-3 sorbent during cycling at 30 and 115°C in a CO ₂ atmosphere.	35
IV-7. The surface area of the original and improved sorbents.	36
IV-8. The difference in the CO ₂ loading at 30° and 110°C of the ACS sorbents.....	36
V-1. Schematic diagram of the integrated absorber-stripper column.	38
V-2. Photograph of the structured packing used in the bench-scale reactor and a demonstration of the packing effectiveness at distributing the flow of sorbent granules.....	39
V-3. Photographs of sorbent granules moving down the adsorption column.....	40
V-4. Variation in sorbent linear velocity as a function of gas flow velocity.	41
V-5. Pressure drop across the adsorber column as a function of air flow rate.	42
V-6. Example adsorption run showing the removal of CO ₂ while solid sorbent flows through the reactor. (Time in seconds).....	43
V-7. The residual CO ₂ concentration in the reactor exit gas at various gas flow rates.	43
V-8. Absorber section capture efficiency as a function of the simulated flue gas feed rate.....	44
V-9. Capture efficiency as a function of the CO ₂ residence time in the adsorber.	45
V-10. Fixed bed desorption of CO ₂ using direct contact heating with low-pressure steam.	46
V-11. Photograph of the integrated absorber-stripper system.	47
V-12. CO ₂ concentration in the absorber exit gas stream.	49
V-13. CO ₂ concentration in the stripper exit gas.	49
V-14. Temperature rise during steam injection.	50
V-15. Product purity vs output flow rate.	52
V-16. Capture efficiency vs output flow rate.....	52
V-17. Optimal purity and efficiency vs gas residence time in the absorber.	53
V-18. Schematic diagram of the large bench-scale integrated absorber-stripper column.	54
V-19. Photograph of the 6-in-diameter x 20-ft-tall integrated system.....	55
V-20. System performance during Run 2.	57
V-21. Performance of the system in Run 5.....	58
V-22. Results of Run 13 showing stable operation without loss of capture efficiency.	59
V-23. CO ₂ product purity and capture efficiency during 50-h test of the integrated system.	60
V-24. CO ₂ product purity and capture efficiency using reduced granule size sorbent.....	61
V-25. Photograph of fines recovered from exhaust filter at end of 50-h test series.	61
V-26. Efficiency of CO ₂ capture and purity of the product gas leaving the stripper in the first 200 cycles.....	63
V-27. Efficiency of CO ₂ capture and purity of the product gas leaving the stripper in 800 to 1,000 cycles.....	63
V-28. CO ₂ absorption isotherms of the sorbent before and after the 1,000-cycle test.	64
V-29. Steady-state CO ₂ capture efficiency and product gas CO ₂ purity after improvements.	65
VI-1. The integrated reactor installed at the University of Toledo boiler site.....	67

VI-2. Schematic diagram of the integrated reactor assembly.....	68
VI-3. A photograph of the of the integrated reactor assembly.	69
VI-4. A photograph of the sorbent inlet and flue gas outlet sections.	69
VI-5. A photograph of the stripper and rotary valve sections.....	70
VI-6. A photograph of the sorbent dehydrator, cooler, screw feeder, and pneumatic recycle sections.....	70
VI-7. Percentage of CO ₂ capture and the CO ₂ purity of the stripper gas.....	72
VI-8. A plot of the CO ₂ capture efficiency and product gas purity in the field test after 100 h of operation.	73
VI-9. CO ₂ adsorption isotherms before and after the field test.....	74
VI-10. Comparison of the CO ₂ adsorption characteristics of freshly and field-tested sorbents...	75
VI-11. Thermogravimetric analysis of the sorbent after the field test.....	75
VI-12. Piping and instrumentation diagram of the system installed at NCCC.....	79
VI-13. Schematic of the integrated adsorber-stripper column.....	80
VI-14. Drawing of the structure to support the integrated column.....	81
VI-15. Photograph of a heat exchanger for recovering thermal energy from the sorbent.....	82
VI-16. Pneumatically operated sorbent flow control valve (pinch valve design).....	82
VI-17. Photograph of the inside of the column filled with structural packing.	83
VI-18. Photograph of the code-compliant enclosures.....	83
VI-19. Operational verification of a differential pressure gauge.....	84
VI-20. Operational verification of the CO ₂ flow meter sensor.....	85
VI-21. Operational verification of the temperature sensor.	85
VI-22. Operational verification of air flow meter.....	86
VI-23. The skid is being lifted from the assembly floor to the truck by a crane.	86
VI-24. Skid to demonstrate CO ₂ capture by carbon sorbent is on the truck to transport it to National Carbon Capture Center.....	87
VI-25. The skid lifted from the truck at the NCCC installation.	88
VI-26. The skid installed at the NCCC site.	89
VII-1. Process flow diagram of a PC power plant without CO ₂ capture.	93
VII-2. Process flow diagram of a PC power plant with CO ₂ capture with Econamine process..	96
VII-3. Process flow diagram of a PC power plant with CO ₂ capture using carbon sorbents. ...	100

I. EXECUTIVE SUMMARY

The overall objective of this program for the Department of Energy (DOE) is to develop an innovative, low-cost, and low-energy-consuming carbon dioxide (CO₂) capture technology based on adsorption on a high-capacity, low-cost carbon sorbent. The specific objectives are to: (1) validate the performance of this concept on a bench-scale system; (2) perform parametric experiments to determine the optimum operating conditions under simulated flue gas conditions; (3) evaluate the performance of the bench-scale system with a flue gas from coal-fired boilers; and (4) evaluate the technical and economic viability of the technology. The information obtained in this successful project will be used to design a pilot-scale unit that will treat a slipstream from an operating coal-fired power plant in a future phase.

The CO₂ capture process that SRI International investigated uses a falling bed of advanced carbon sorbent (ACS) to separate an incoming stream of flue gas into two streams: a lean flue gas stream from which > 90% of the CO₂ has been removed and a pure stream of CO₂ that is ready for compression and sequestration. The carbon sorbent microbeads developed for this process by the project partner, ATMI, Inc., have a unique suite of properties:

- High CO₂ capacity: The sorbent has a high capacity for CO₂ adsorption (20 wt% at 1 atm CO₂) and good selectivity for CO₂ over other flue gas components.
- Rapid adsorption and desorption rates: The adsorption of CO₂ occurs on the micropores of the sorbent with very low activation energy (< 5 kJ/mole), allowing rapid adsorption and desorption so that the sorbent can be cycled very rapidly.
- Low heat of adsorption and desorption: The relatively low heats (28 kJ/mole) indicate that this process has a low heat demand for regeneration and low cooling requirements.
- Long lifetime: The sorbent is mechanically robust, which gives the sorbent a long lifetime.
- Low capital cost: This process is unique in that it uses no corrosive chemicals or liquids, just carbon particles and is operated dry. These mild conditions the use of inexpensive construction materials for the reactor.

The integrated adsorption-stripper reactor system takes advantage of this full set of properties to achieve simple, efficient separation of CO₂ in a continuous, easily scalable process using commercially available materials and equipment. The capture of CO₂ from the flue gas is performed at near ambient temperature using a falling reactor in which the sorbent granules flow down by gravity counter-current with the up-flow of the flue gas. The adsorbed CO₂ is stripped by heating the CO₂-loaded sorbent to ~ 100°C, in contact with low-pressure (~ 5 psig) steam in a section at the bottom of the adsorber. The regenerated sorbent is dehydrated of adsorbed moisture, cooled, and lifted back to the adsorber. The CO₂ from the desorber is essentially pure

and can be dehydrated, compressed, and transported to a sequestration site. The initial low capital cost combined with other characteristics such as (1) long life and high capacity sorbent, (2) high mass transfer rate, and (3) low energy requirements results in a very competitive process for CO₂ recovery.

I.1 SORBENT CHARACTERIZATION

Determination of Sorbent Properties: The CO₂ adsorption and desorption isotherms were determined for a carbon sorbent, designated as ACS-1, made commercially by ATMI, Inc. for industrial applications. The equilibrium amount of CO₂ adsorbed on the sorbent as a function of process parameter is an important criterion that is needed to devise a viable process. The amount of CO₂ adsorbed was determined as a function of temperature and partial pressure of CO₂ in the gas. The adsorbed quantity increases with the partial pressure of CO₂, but decreases with increasing temperature. The CO₂ loading on the sorbent was about 20 and 16 wt% at 5°C and 20°C, respectively, in pure CO₂. Both the CO₂ adsorption and desorption processes are rapid. No hysteresis was observed between adsorption and desorption isotherms at temperatures of 5°C to 30°C.

The heats of adsorption and desorption of CO₂ on a sorbent are: 1) the heat that needs to be removed during adsorption; 2) and the heat that needs to be supplied for desorbing the CO₂ from the sorbent. The isosteric heats of adsorption, calculated from the adsorption isotherms, are only 25 to 28 kJ/mole (245 to 275 Btu/lb) of CO₂, far less than the value of 70 to 85 kJ/mole for the CO₂ adsorption on an amine solvent in a competing concept. In addition, the carbon sorbent has a high thermal conductivity (1.2 W/m.K) so that the sorbent will be isothermal during operation.

The CO₂ desorption characteristics of the sorbent were determined in the temperature range 40°C to 110°C using thermogravimetric analysis (TGA). These experiments showed that CO₂ desorbs as the sorbent is heated and the sorbent regeneration can be performed at a relatively low temperature of 90°C even in a CO₂-rich stream. The regeneration temperature has only a minor effect on the residual CO₂ on the sorbent. The TGA and BET techniques complemented each other, and the data obtained from these two techniques agreed with each other reasonably. The isosteric heat of desorption was about 25 kJ/mole of CO₂, similar to the heat of adsorption.

Improvements to the Sorbent: The CO₂ adsorption characteristics were evaluated also with two structurally improved sorbents fabricated by ATMI. The modification resulted in a ~ 25% increase in surface area and a similar increase in CO₂ loading when the sorbent is cycled between 30°C and 110°C in a CO₂ atmosphere.

Screening Tests with Sorbent Formulations: Fixed-bed reactor experiments demonstrated removal of more than 90% of CO₂ from an air-15% CO₂ gas stream at 5°C to 20°C. The adsorption of CO₂ on the sorbent was rapid, and the exiting reactor gas contained less than 0.1% CO₂ in this temperature range. The amount of CO₂ captured on the sorbent increased

with decreasing adsorption temperature, but it decreased slightly with increasing amounts of moisture in the feed gas.

The fixed-bed reactor was also used to determine the desorption characteristics of a sorbent that contained previously adsorbed CO₂ from a humid air containing 15% CO₂ at 20°C. The regeneration was performed in the temperature range 90°C to 106°C in a flowing stream of CO₂ gas. The rate of desorption of CO₂ was very rapid, and it was relatively insensitive to the regeneration temperature. The residual level of CO₂ in the sorbent decreased slightly with increasing temperature.

The advanced carbon sorbent microbeads made by ATMI have exceptional compression strength and attrition resistance for a high-surface-area sorbent, which makes them suitable for moving- or fluidized-bed reactor applications. The attrition resistance index was less than 0.01 wt% per hour compared to a nominal value of 4 wt% per hour for a typical fluid-bed cracking catalyst. The sorbent microbeads are highly spherical and smooth and have a low repose angle.

I.2 BENCH-SCALE TESTING

Bench-Scale Parametric Testing: A novel reactor design that allows a low-pressure drop while preserving an efficient gas-solid contact is necessary for the present application. A falling-bed reactor was designed that takes advantage of the unique high adsorption and desorption kinetics, high fluidity, and high attrition resistance of our carbon sorbent microbeads. In this design, the granular sorbent flows (falls) from top to bottom of the reactor. The gas containing the CO₂ flows upward in a counter-current mode to maximize the rate and extent of absorption. Experimental testing indicated that a commercially available structural packing was suited for this application. This capability demonstrates that no special design of the packing is necessary, and it accelerates the development of CO₂ capture using this technology. Initial tests were conducted using a bench-scale reactor with a 2-in. inside diameter (ID) and an adsorber height of 3 ft.

Efficient adsorption of the CO₂ from the flue gas requires that the sorbent microbeads be uniformly distributed on the surface of the packing and intimately mixed with the counter flowing gas. The structural packing distributed the sorbent microbead flow uniformly in a very short length of the packing (4.5 in.) and demonstrated that no special distributor design is necessary.

Pressure-drop experiments showed that the falling-bed reactor provides a relatively low pressure drop for the gas flow. The pressure drop is a function of the gas velocity and the sorbent flow. In the absence of sorbent flow, the measured pressure drop was only 0.1 in H₂O/ft packing (0.004 psi/ft) at a gas velocity of 2.4 ft/s. When the sorbent microbeads were flowing at a rate of 0.25 lbs/(min-ft²), an acceptable flow rate, the pressure drop increased to 0.4 H₂O/ft packing (0.014 psi/ft).

The rate of sorbent microbeads moving down the reactor was a function of the gas velocity. The measured sorbent falling velocity varied from about 7 in/s to 3.8 in/s as the air velocity increased from 0.5 to 2 ft/s. This variation of the solid velocity will allow the solid and gas residence time to be controlled by appropriate choice of parameters such as reactor height, baffle design, and cross-section area for a given gas flow rate.

CO₂ adsorption experiments were performed in the bench-scale reactor with varying gas flow rates at a constant feed CO₂ concentration and with varying CO₂ concentrations at a fixed gas flow rate. These experiments showed rapid capture of CO₂ by the advanced carbon sorbent and achieved a nearly complete capture of CO₂ with a gas residence time of ~ 6 s in an air stream containing 15% CO₂ under ambient conditions. As expected, the capture efficiency decreased with decreasing gas residence time: capture efficiencies of 90% and 65% were recorded with residence times of 5 and 4 s, respectively.

Experiments showed that sorbent regeneration and desorption of adsorbed CO₂ are rapid when the CO₂-loaded sorbent is in direct contact with low-pressure steam at ~ 100°C. The rate of CO₂ evolution was essentially controlled by the rate of sorbent heating by steam. Direct heating of the sorbent microbeads with steam has tremendous advantages in that: (1) the rate of heat transfer is extremely rapid; and (2) any residual steam in the regenerator exit gas stream can be condensed and removed, providing pure CO₂ gas.

Integrated Reactor Testing: Based on the success of the CO₂ capture and release experiments, an integrated system was designed, built, and tested at SRI. The falling microbead system enables the integration of adsorption and stripping of the CO₂ in a single vertical column. The upper portion of the column functions as the absorber through which fresh or regenerated sorbent microbeads move down by gravity while the feed gas containing CO₂ flows upward. The CO₂-lean gas exits at the top of the reactor. The CO₂-laden sorbent moves down through a middle section to desorb any adsorbed O₂ and N₂. In the bottom stripper section, CO₂ is stripped from the sorbent by direct contact with steam.

This novel reactor design has several advantages:

1. It simplifies the transport of solid microbeads from the absorber to the stripper; only the regenerated sorbent needs to be transported from the bottom of the stripper to the top of the absorber.
2. Since adsorbed O₂ and N₂ are removed in the middle section, the CO₂ from the stripper can be pure.
3. It allows sorbent regeneration with steam directly contacting the sorbent to release the adsorbed CO₂. Direct contact with steam provides a very high heat transfer and efficient use of steam.

The integrated reactor system was operated to determine optimum conditions necessary to capture CO₂ from a simulated flue gas and provide a pure CO₂ gas stream that can be sequestered. The process variables include simulated flue gas flow, sorbent flow, steam flow, and the exit gas flow rates.

In the integrated reactor, the residual CO₂ in the adsorber exit gas and the purity of CO₂ in the stripper exit gas were affected by both the feed gas rate and the stripper exit gas rate. When the stripper exit gas flow is low, more CO₂ is entering the reactor through the feed gas than CO₂ flowing out in the stripper gas. In that case, the remaining CO₂ must exit with the adsorber exit gas stream. Under these conditions, the CO₂ purity is high but the capture efficiency is reduced. When the stripper exit gas flow rate is high, there is not enough CO₂ entering the column to produce a pure CO₂ stream, and some of the feed air exits at the stripper exit port, resulting in high capture efficiency but low purity. When the stripper exit gas flow matches the input flow of CO₂ contained in the flue gas, the system achieves both high purity and high capture efficiency.

Tests with the integrated reactor showed that a gas residence time of 6 to 7 s in the absorber section achieved a capture efficiency of 98% and a product CO₂ purity of 97%. Under these conditions, the product CO₂/feed CO₂ ratio approached a value of 1. The bench-scale experiments demonstrated that the falling granule bed reactor design is suitable for rapid cycling of the sorbent, and that the carbon sorbent microbeads have rapid CO₂ adsorption and desorption kinetics and excellent attrition resistance. Both high CO₂ capture efficiency and high product CO₂ purity were achieved in an integrated reactor.

Bench-scale tests at SRI using a simulated flue gas showed that the integrated system can be operated to provide > 90% CO₂ capture from a 15% CO₂ stream in the adsorber and produce > 98% CO₂ at the outlet of the stripper. Long-term tests (1,000 cycles) showed that the system can be operated reliably without sorbent agglomeration or attrition.

I.3 FIELD TESTING

The bench-scale reactor was also operated using a flue gas stream from a coal-fired boiler at the University of Toledo campus. The reactor at SRI was dismantled and reinstalled at the new site. The system was operated for about 135 h, comprising 7,000 cycles of adsorption and desorption using the desulfurized flue gas that contained only 4.5% v/v CO₂. We were able to achieve 85 to 95% CO₂ capture under steady-state conditions. The field unit was operated during the daytime for ~ 8 to 10 h/day over a period of 2 weeks. During the test period, the flue gas flow and solid circulation were maintained without any significant problem. The major difficulty encountered was maintaining the temperatures of the stripper and the dehydrator, especially in the cold weather encountered in Ohio in the middle of winter. When we implemented the external heating of the walls of the stripper and the dehydrator and added additional insulation, we obtained reliable performance of the integrated system with both high CO₂ capture efficiency and CO₂ product gas purity.

In the field test, the sorbent microbeads were circulated for about 7,000 cycles of adsorption and stripping. The CO₂ adsorption capacity did not change significantly during the field test, as determined from the CO₂ adsorption isotherms of fresh and used sorbents. These

results are consistent with the performance of the system observed with the simulated gas tests at SRI.

The process was also tested using the flue gas from a PC-fired power plant at the National Carbon Capture Center (NCCC), Wilsonville, AL. The system used at the NCCC was designed to handle a flue gas flow that is about 10 times higher than that used at the University of Toledo. The adsorber of this field test unit was designed to be a 1.5-ft-square, 10-ft-tall column that will handle a flue gas stream of 70 cfm (~250 tons CO₂/year, or 40 kWe). The components were fabricated and assembled in a skid at the SRI campus in Menlo Park, CA which was then transported by truck to the NCCC site at Wilsonville, AL. The skid was installed at the site using cranes.

After installation, shake-down runs were performed with the system. Corrective actions were taken to prevent both gas and sorbent particles leaks from the reactor. The pneumatic lift design was changed to allow lifting of the required rate of sorbent from the bottom of the sorbent cooler to the top of the adsorber. This change in the design required an increase in the diameter of the lift tube and a higher flow rate of lift air than the original design and so the disengagement section at the top of the adsorber was modified also.

Initial results showed a CO₂ capture efficiency of ~65% and a CO₂ product gas purity approaching 65%. In previous operations both at SRI and the University of Toledo, the CO₂ product gas purity takes certain period of time to achieve high values.

I.4 PRELIMINARY PROCESS EVALUATION

Initial Preliminary Process Evaluation. A process evaluation model was developed using Aspen Plus and Steam-Pro programs and validated this model against the published data by NETL. The model estimated the cost of electricity in a 550 MWe PC-fired power plant without CO₂ capture and CO₂ capture using the Econamine process under conditions similar to those described in a NETL publication. The estimated levelized cost of electricity (LCOE) for these two cases agreed very closely with the NETL published values. The LCOE is 6.4 ¢/kWh for the case in which CO₂ is not captured compared to the published value of 6.33 ¢/kWh. In the case in which CO₂ is captured using the Econamine process, it is 11.58 ¢/kWh compared to the published value of 11.47 ¢/kWh. A preliminary cost analysis using this process model showed that the CO₂ capture with advanced carbon sorbents can be accomplished at a 37% increase in the cost of electricity, far less than the 80% increase in LCOE for the amine process.

A preliminary sensitivity analysis was conducted to understand which parameters will have the greatest impact on the performance of the power plant. The variables that have significant effect on the COE are the capital cost associated with the CO₂ capture unit and the steam consumption for the regeneration of the sorbent. Decreasing the capital cost by 30% in relation to the base case decreased the change in the LCOE from 44% to 36%. The other important variables were the quality and quantity of steam used for regeneration and the pressure drop of the absorber. The advanced carbon sorbent is non-corrosive; therefore, inexpensive

construction materials can be used, thereby decreasing capital costs. The sorbent has minimum water adsorption, and this characteristic will reduce the steam load in comparison to the amine process, wherein a significant amount of water needs to be heated and evaporated. The sensitivity analysis provided a set of capital and operating parameters that are necessary to achieve the DOE goal of 30% increase in the LCOE for carbon capture.

Update of the Process Evaluation: The initial process evaluation was updated using the data collected in the bench-scale tests. The pressure drop across the adsorber was increased to 1 psi. The heat input to the stripper was increased to 500 Btu/lb CO₂ to include the sensible heat supplied to the sorbent in heating from the adsorber temperature to stripper temperature and auxiliary heat to remove steam condensed on the sorbent in the stripper. The CO₂ working capacity of the sorbent was reduced to 5 wt%, consistent with the experimental results.

In this model, the net power output kept constant at 550 MWe and coal feed rate are changed to accommodate changes in the auxiliary load. Note that the auxiliary loads are significantly smaller for the carbon-sorbent case compared with the amine-based case. Because of reduced steam requirement in the stripper, the coal feed rate is reduced to obtain the net plant output. The net plant efficiency (HHV) is reduced only by 3.3% in the case of CO₂ capture by the carbon sorbent.

The cost of electricity was calculated for CO₂ capture using the carbon sorbent and compared with the no-CO₂ capture and CO₂ capture with an amine-based system. The increase in the cost of electricity (COE) is about 37% for CO₂ capture using the carbon sorbent in comparison to 80% for an amine-based system, demonstrating the economic advantage of CO₂ capture using the carbon sorbent. The 37% increase in the COE corresponds to a cost of capture of \$30/ton of CO₂, including compression costs, capital cost for the capture system, and increased plant operating and capital costs to make up for reduced plant efficiency.

1.5 CONCLUSIONS AND RECOMMENDATIONS

Based on experimental and analytical work performed, the following conclusions can be made:

- Bench-scale tests with a flue gas from a coal-fired boiler showed that the advanced carbon sorbent process can capture > 90% CO₂ and produce a product stream that is nearly pure CO₂.
- The integrated adsorber-stripper system takes advantage of the unique high adsorption and desorption kinetics, high fluidity, and high attrition resistance of the carbon sorbent microbeads. Tests in the bench-scale system demonstrated that a commercially available structural packing is suitable for this application. A stable operation of the integrated system was demonstrated both at SRI using a simulated flue gas and in the field using flue gas from a coal-fired boiler.

- The system was able to operate with a flue gas stream containing only 4.5% CO₂ (v/v). When the system operating parameters were adjusted for a target capture efficiency of 90%, a CO₂ level corresponding to 85 to 95% CO₂ capture was observed at the adsorber exit under steady-state conditions. We obtained a CO₂ product gas purity of ~ 100% under those conditions.
- During the field test, the flue gas-flow and sorbent circulation were maintained without any significant problems. The major difficulty encountered during the test period was maintaining the temperatures of the stripper and the dehydrator, especially in the cold weather encountered in Ohio in the middle of the winter. When we implemented the external heating of the walls of the stripper and the dehydrator and added additional insulation, we obtained reliable performance of the integrated system with both high CO₂ capture efficiency and CO₂ product gas purity.
- The sorbent was stable with no change in sorption capacity over thousands of adsorption and desorption cycles (~ 7,000).
- The sorbent has an extremely low attrition loss, as judged by an extrapolated sorbent lifetime that accounts for attrition over many years of continuous operation.
- The sorbent microbeads flow down smoothly even when heated directly with steam because steam condenses inside the pores of the microbeads.
- A single column with the adsorber on the top and the stripper on the bottom is an efficient design, minimizing the solid transport.
- The preliminary estimate of the process using the advanced carbon sorbent indicates that the COE of CO₂ capture and sequestration will increase by 37% over the base case of no-CO₂ capture. The increase in COE by using an advanced carbon sorbent for CO₂ capture is estimated to be less than half that of an amine-based solvent system for CO₂ capture.
- Preliminary sensitivity analyses showed capital costs, pressure drops in the adsorber, and steam requirements for the regenerator are the major variables in determining the cost of CO₂ capture.

Based on the above conclusions, the following recommendations are made:

- The results indicate that further long-term testing with a flue gas from a pulverized coal-fired boiler should be performed to obtain additional data relating to the effects of flue gas contaminants, the ability to reduce pressure drop by using alternate structural packing, and the use of low-cost construction materials.

II. INTRODUCTION

Concern over the impact of greenhouse gas emissions and increasing CO₂ concentrations in the atmosphere are driving the search for low-cost and efficient technologies to capture and sequester CO₂ emissions. Coal-fired power plants are large stationary sources of CO₂, and the capture and sequestration of CO₂ from these power plants hold the potential for deep reductions in greenhouse gas emissions. A typical 500-MWe plant emits 2 to 3 million tons of CO₂ per year. Capturing and sequestering this very large volume of CO₂ is a major challenge.

The process that was investigated is based on the use of a high-capacity carbon sorbent for adsorbing CO₂ from the flue gas stream and subsequent regeneration by heating the loaded sorbent to a moderate temperature. The adsorption process is less energy intensive than other processes such as the amine-based process. The sorbent regeneration is performed at a relatively moderate temperature (~ 100°C) requiring only a moderate quantity of low pressure steam, thus decreasing the energy penalty for capturing and separating CO₂ from the flue gas.

SRI International, in collaboration with ATMI, Inc., performed a multi-year effort to develop a novel, high CO₂-capacity carbon sorbent with moderate thermal requirements for regeneration. We also tested the process at the University of Toledo using the flue gas from a coal-fired steam boiler. The overall objective of the program was to develop an innovative, low-cost, and low-energy-consuming CO₂ capture technology. The specific objectives were to: (1) validate the performance of this concept on a bench-scale system; (2) perform parametric and long-term experiments to determine the optimum operating conditions; and (3) evaluate the technical and economic viability of the technology. The information obtained from this project will be used to design a pilot unit that will treat a slipstream from an operating coal-fired power plant in a future phase.

II.1 CURRENT STATE OF THE ART

Commercially available post-combustion CO₂ capture technologies are amine-based processes and mainly use the monoethanolamine (MEA) process, which is capable of achieving high-efficiency CO₂ capture and generating a concentrated CO₂ stream for sequestration. However, the amine-based process has many drawbacks, including: (1) the reagents are expensive and degrade in the flue gas environment; (2) the amine-CO₂ system is corrosive in concentrated form; (3) the reaction of CO₂ with a primary amine is highly exothermic; (4) the regeneration of the CO₂ absorbed amine is energy intensive; and (5) the process is a large consumer of auxiliary power. Assuming a fleet-wide CO₂ reduction of around 50% and a total energy penalty for MEA-CO₂ systems of between 30 and 40%, it would be necessary to construct an additional 100 to 150 GW of capacity in the United States just to offset the resulting energy penalty of CO₂ capture and sequestration [Figueroa, 2006]. Advanced amine processes under development make incremental improvements but do not eliminate any of the above disadvantages. If the amine-based technology is applied for post-combustion CO₂ capture on the

U.S. power generation fleet, it will significantly impact the cost of electricity in the United States. Rising electricity prices would have a drastic impact on the U.S. economy.

Siemens Energy sector is developing a post-combustion CO₂ capture process based on an amino-acid salt solution that is claimed to be less sensitive to oxidation than an amine solution [Jockenovel et al., 2008]. The process has been tested at a pilot-scale in Europe, and the regeneration energy requirement was reported to be 120 kJ/mole of CO₂. Alstom has tested the chilled-ammonia process at a pilot-scale. WE Energie, Pleasant Prairie, WI has tested at 5 MWth and, at the Mountaineer power plant in New Haven, WV, tests have been done at a demonstration scale of 58 MWth. The regeneration steam requirement was again reported to be 123 kJ/mole of CO₂ [Kozak et al., 2011].

Several research programs are under way regarding the use of solid sorbents to capture CO₂ from flue-gas streams. Choi et al [2009] reviewed the CO₂ adsorption behavior of several different classes of solid carbon dioxide adsorbents, including zeolites, activated carbons, calcium oxides, hydrotalcites, organic-inorganic hybrids, and metal-organic frameworks. No clear winner was apparent in this review. Krutka et al [2010] reported the results of bench-scale tests on several solid sorbents for CO₂ capture. The regeneration energy requirements varied from 900 to >6,000 Btu/lb CO₂ (~ 90 to > 600 kJ/mole). Pilot-scale tests (1 kW) with one sorbent were conducted at the Southern Company's Martin Lake power plant using a circulating fluidized bed configuration. They noted that the regeneration of the CO₂-loaded sorbent was slow, although 90% CO₂ capture was obtained in the adsorber (riser) portion of the system. They indicated a rotary kiln configuration may be needed for the regeneration step in contrast to a fluidized-bed configuration used normally in a circulating fluidized bed system.

TDA Research reported the use of alkalized alumina sorbent using a series of fixed-bed reactor geometry [Elliott et al., 2012]. Both adsorption and regeneration are performed at elevated temperatures of 110° to 150° C. This scheme requires that the flue gas is heated to the adsorption temperature. The CO₂-loading of the sorbent was relatively low at ~ 0.9 wt%. TDA Research is also studying the use of mesoporous carbons functionalized to enhance CO₂ adsorption [Alpetkin et al., 2012]. Although CO₂ was physisorbed with low heat of adsorption (20 kJ/mole), the bench-scale tests results showed only adsorption at 22° C and 1.3 psig CO₂ and deep vacuum desorption (- 13.7 psig). SO₂ at 300 ppm and NO at 70 ppm did not affect CO₂ adsorption over 40 cycles. In a fixed-bed reactor, only 2 wt% CO₂ was adsorbed on the bed at the time of CO₂ breakthrough.

Recently, metal organic framework (MOF) sorbents have been reported for capturing CO₂ from flue gas streams [Mason 2011]. Although the Zn- and Mg-based MOF sorbents showed excellent CO₂/N₂ selectivity, the CO₂ working capacities were relatively low when the adsorption and desorption were performed at 40° and > 100° C. Working capacities were 5 and 10 wt% when desorption was performed at 100° and 130° C, respectively. MOF sorbents are fragile and intolerant to many flue gas components including moisture, SO_x, and NO_x, and have relatively low thermal conductivity. The working capacity will be even lower than the reported

values if they require support by a strong ceramic support to provide mechanical stability. The future of MOF sorbents for practical flue gas CO₂ capture may be years away.

Based on the results reported in the literature, a need exists still for the development of a low-cost, low-energy consuming process for the capture of CO₂ from the flue gas of a coal-fired power plant.

II.2 PROJECT OVERVIEW

SRI International, in collaboration with ATMI, Inc., performed a multi-year effort to develop a novel, high CO₂-capacity carbon sorbent with moderate thermal requirements for regeneration. The overall objective of the program was to develop an innovative, low-cost, and low-energy-consuming CO₂ capture technology. The specific objectives were to: (1) validate the performance of this concept on a bench-scale system: (2) perform parametric experiments to determine the optimum operating conditions: and (3) evaluate the technical and economic viability of the technology.

The project consists of the following tasks:

1. Project management and planning
2. Determination of the relevant properties of the sorbent
3. Improvements to the sorbent
4. Screening tests with sorbent formulations
5. Initial process evaluation
6. Bench-scale parametric testing
7. Update of the process evaluation
8. Long-term testing
9. Performance and economic analysis.

The results of the work performed were described in quarterly technical reports and continuation applications covering Budget Periods 1, 2, and 3.

III. DETERMINATION OF SORBENT PROPERTIES

In this process to capture the CO₂ from existing pulverized coal (PC)-fired power plants, CO₂ will be absorbed on carbon sorbent microbeads and subsequently desorbed regenerating the sorbent, which cycles back to the adsorber. In evaluating the suitability of a sorbent for this application, several chemical, physical, and mechanical properties were determined. The following properties were measured and the results are described below:

1. Quantity of CO₂ adsorbed as a function of temperature and pressure
2. Quantity of CO₂ desorbed as a function of temperature and pressure
3. Heats of CO₂ adsorption and desorption
4. Adsorption of moisture
5. Adsorption of SO₂ and NO
6. Compressive strength
7. Attrition resistance.

III.1 CO₂ ADSORPTION CHARACTERISTICS

The CO₂ adsorption characteristics of an advanced carbon sorbent, designated as ACS-1, made by ATMI, were determined in the temperature range 5 to 30°C from the adsorption isotherms obtained using the Brunauer–Emmett–Teller (BET) technique. The equilibrium amount of CO₂ adsorbed on the sorbent was measured as a function of temperature and CO₂ partial pressure.

A Micromeritics ASAP 2020 Surface Area and Pore Size Analyzer was used to determine the adsorption isotherms of CO₂ on the sorbent. In this technique, the sorbent was heated in vacuum at 110°C to remove any adsorbed gas on the sample. The sample, after this degassing step, was cooled to the adsorption temperature and was exposed to pure CO₂ gas at ~ 0.01 atm while maintaining a constant temperature. The equilibrium pressure and volume of CO₂ adsorbed on the sample were measured. The sample was then exposed to a higher pressure of CO₂ stepwise up to a pressure of 1 atm at the same temperature to obtain an adsorption isotherm. Additional data were also obtained while reducing the CO₂ pressures from 1 atm to 0.3 atm to desorb the gas from the sorbent (desorption isotherm).

Figure III-1 illustrates the CO₂ adsorption isotherm of ACS-1 at 5°C. It shows that the quantity of CO₂ adsorbed increases with the pressure of CO₂. At 1 atm pressure more than 100 cm³ [STP – standard temperature (0°C) and pressure (1 atm)] of CO₂ is adsorbed per gram of the sorbent. This quantity of the CO₂ adsorbed corresponds to 20 wt% CO₂ loading. Figure III- 1 also includes the desorption isotherm at 5°C. The desorption isotherm is nearly

identical to the adsorption isotherm indicating that the adsorption of CO₂ on the sorbent is reversible even at this low temperature.

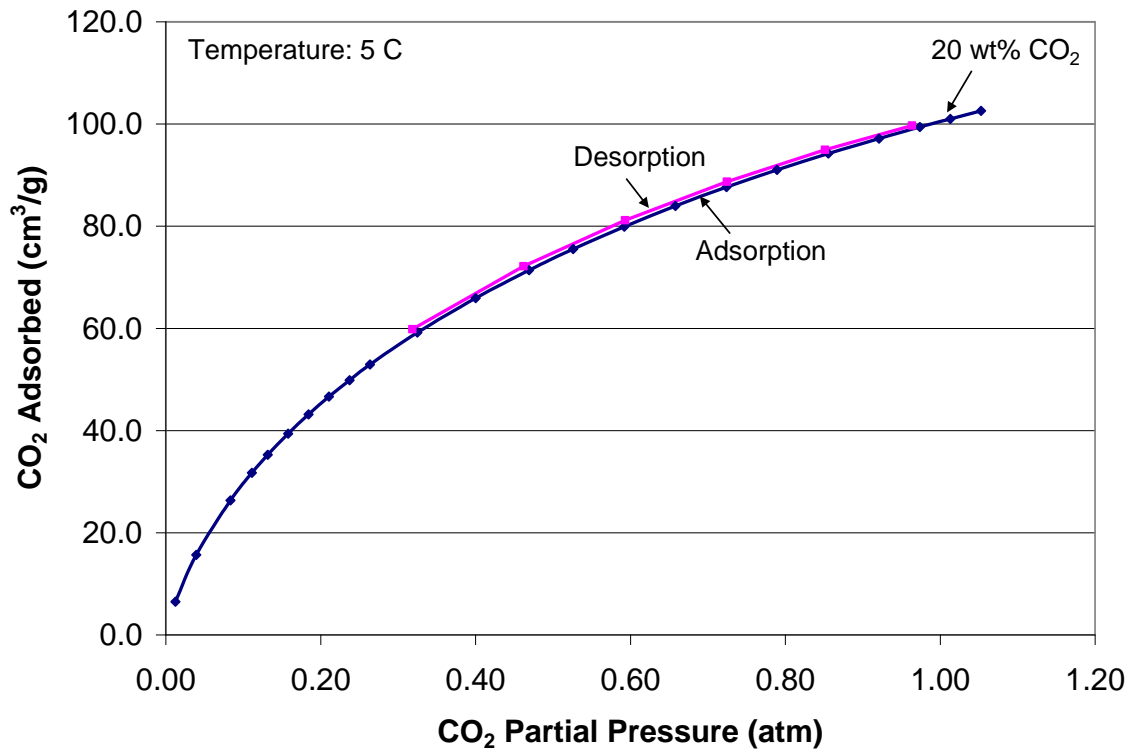


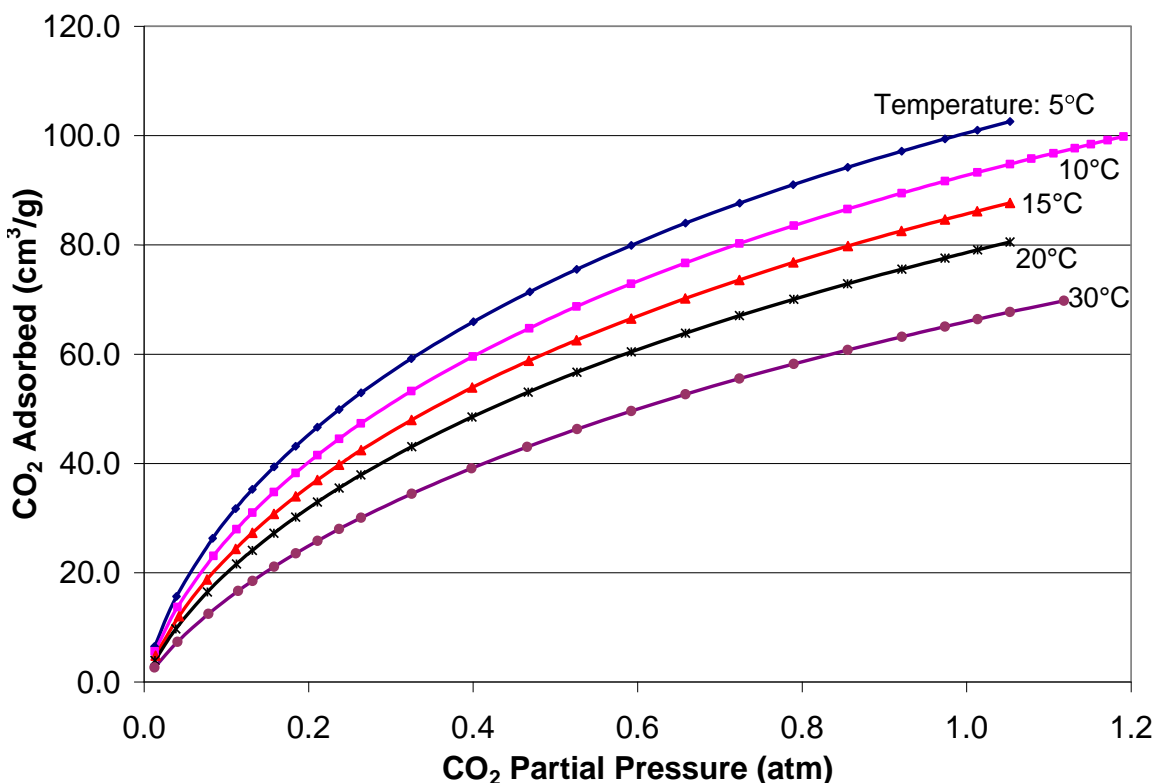
Figure III-1. The quantity of CO₂ adsorbed on the ACS-1 sorbent as a function of CO₂ partial pressure at 5°C.

Similar isotherms were obtained at 10°, 15°, 20°, and 30°C (Figure III-2). At these temperatures, the quantity of CO₂ adsorbed increased with the partial pressure, as expected. Desorption isotherms in this temperature range were also nearly identical to the adsorption isotherms and they were not shown in Figure III-2 for clarity purposes.

The data from adsorption isotherms illustrate that the quantity of CO₂ adsorbed decreases as the temperature increases. These results suggest that the CO₂ adsorption step should be conducted at the lowest possible temperature to obtain the maximum loading.

The surface area of the ACS-1 sorbent was determined from the CO₂ adsorption isotherm at 20°C. Walker and Patel [1970] showed that the Dubinin-Polanyi equation can be used to calculate the surface area of coals from a CO₂ adsorption isotherm at ambient temperature. That Dubinin-Polanyi equation states that

$$\text{Log}(V) = \text{Log}(V_0) - BT^2/\beta \times \text{Log}^2(P_0/P)$$



III-2. The adsorption isotherms of CO₂ on the ACS-1 sorbent at various temperatures.

Where V is the amount of CO₂ adsorbed at an equilibrium pressure P , V_0 is the monolayer volume, P_0 is the saturation pressure at temperature T , β is an affinity constant of adsorbate relative to nitrogen, and B is a constant [Marsh and Siemieniewska, 1965]. If $\text{Log}(V)$ is plotted against $\text{Log}^2(P_0/P)$, the zero intercept is equal to $\text{Log}(V_0)$. Figure III-3 illustrates the CO₂ adsorption isotherm plotted as the Dubinin-Polanyi relation. The V_0 obtained in this plot is 194 cm³ (STP)/g. The molecular area for CO₂ at 293 K was taken as 0.253 nm² (Walker and Patel, 1970). This value for molecular area is higher than (0.17 nm²) used normally in the BET equation at the liquid nitrogen temperature (78 K) because the adsorbate density decreases with increasing temperature. The calculated the surface area of ACS-1 sorbent was 1318 m²/g using the above parameter values.

As noted earlier, about 100 cm³/g of CO₂ was adsorbed on the sorbent at 5°C in the presence of pure CO₂ at 1 atm. This quantity of adsorbate will cover only about 51% of the sorbent as a monolayer, indicating that multilayer adsorption may not occur at atmospheric pressure at temperatures greater than 5°C.

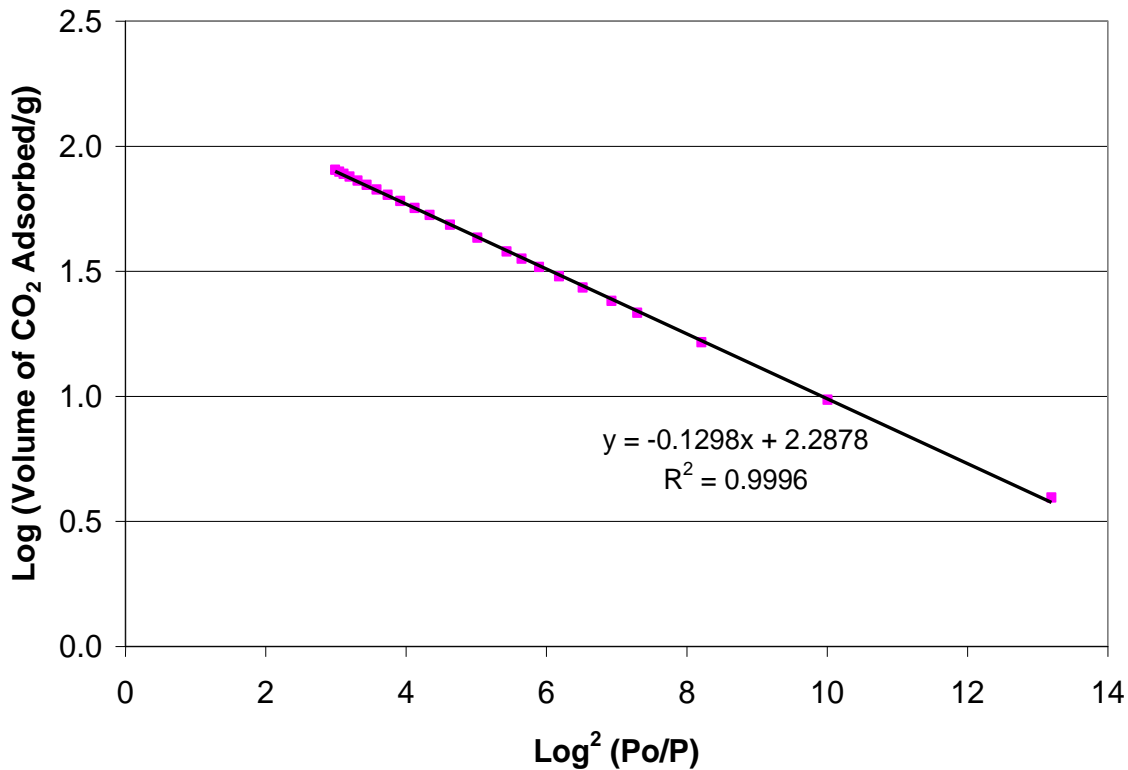


Figure III-3. The Dubinin-Polanyi plot of the CO₂ adsorption isotherm at 20°C.

III.2 CO₂ DESORPTION CHARACTERISTICS

The isotherms obtained by the BET technique showed that CO₂ desorbs rapidly from the sorbent as evidenced by the absence of hysteresis between adsorption and desorption isotherms even at low temperatures. In a CO₂ capture process, CO₂ will be desorbed at elevated temperatures to desorb the maximum amount of adsorbed CO₂. A thermogravimetric method was used to determine the desorption of CO₂ at elevated temperatures.

A Perkin Elmer TGA 7 thermal analyzer was used to determine the CO₂ desorption characteristics of the ACS-1 sorbent. In this test, a small quantity of the sorbent was heated in a stream of Ar to 110°C to remove the adsorbed gases. It was then cooled to 30°C and was exposed to a gas stream containing various levels of CO₂ in an Ar stream and the mass change of the sorbent was measured. After reaching a steady state, the sample was heated stepwise to 40, 50, 70, 90, and 110°C and held at each temperature for 60 min. Figure III-4 illustrates the change in the mass of the sorbent at 1 atm CO₂ as a function of temperature. The change in the mass is due to the CO₂ desorption from the sorbent. Note that the CO₂ desorbs rapidly even in pure CO₂ and the rate of desorption is mainly determined by the temperature rise.

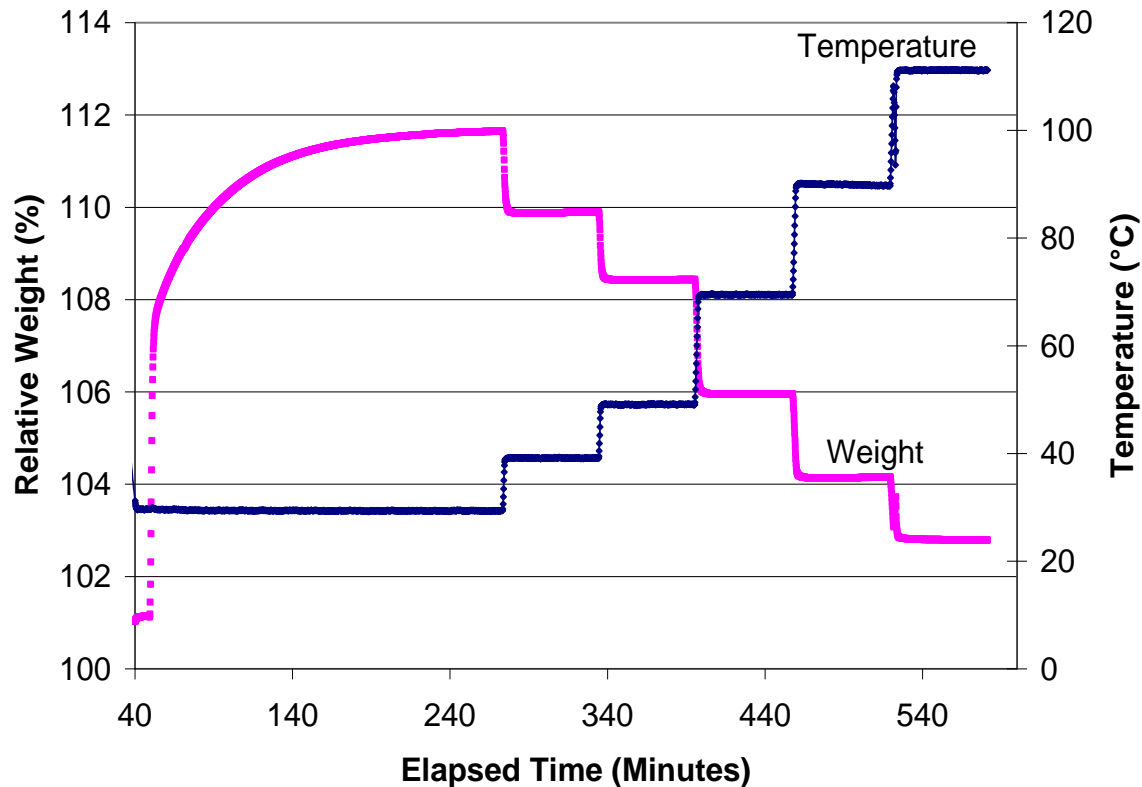


Figure III-4. The adsorption of CO₂ on ACS-1 sorbent at 30°C in pure CO₂ and its desorption at temperatures in the range 40 to 110°C.

Similar plots illustrating the CO₂ loading on the sorbent for CO₂ partial pressures from 25% to 75% CO₂ are shown in Figure III-5. Data was also collected for a gas mixture of 15% CO₂-balance Ar. This data is not shown in the figure for clarity reason. In that case, the time at which the sample was kept at various temperatures was shorter than that shown in Figure III-5. For the 15% CO₂ run, the relative sorbent weight was 103.8 wt% during adsorption at 30°C, and it was 103.0, 102.4, 101.4, 100.9, and 100.5 wt% at temperatures 40, 50, 70, 90, and 110°C, respectively.

The data from these measurements can be used to determine the equilibrium CO₂ loading at various temperatures and gas mixtures containing different partial pressures of CO₂, as shown in Figure III-6. The data indicate that the amount of CO₂ remaining on the sorbent decreases with temperatures and the partial pressures of CO₂ in the gas mixture in contact with the sorbent.

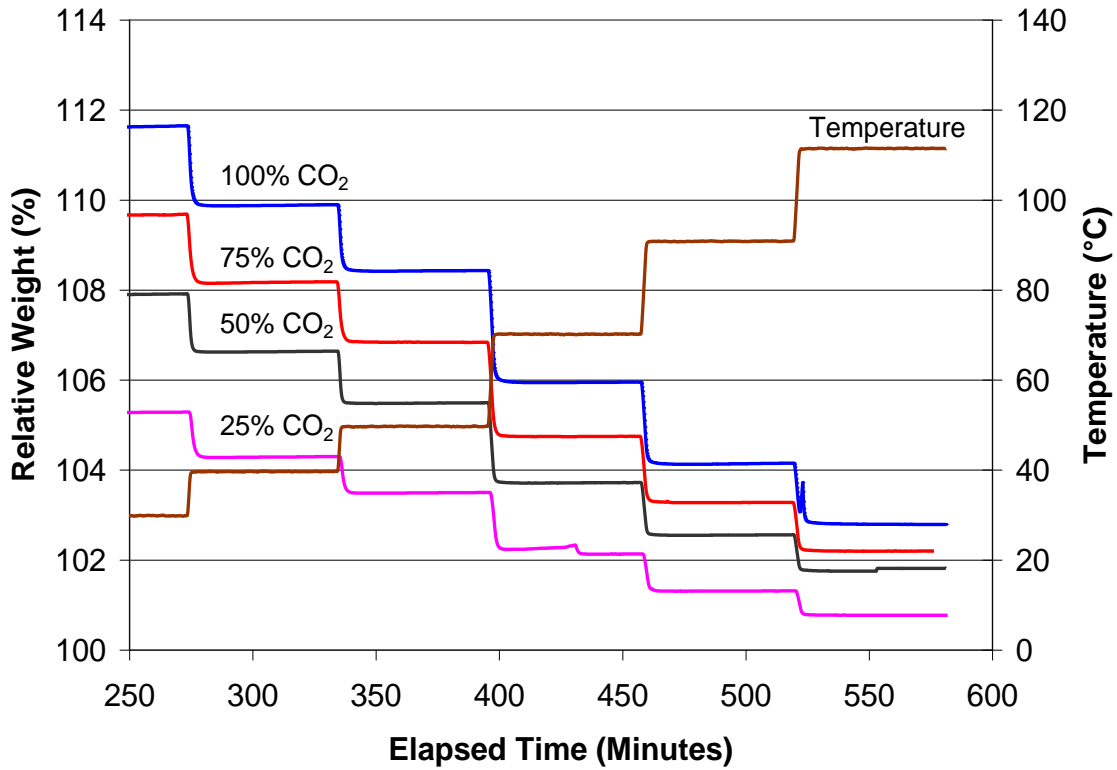


Figure III-5. The mass change of the sorbent at various temperatures with different CO₂-Ar gas mixtures.

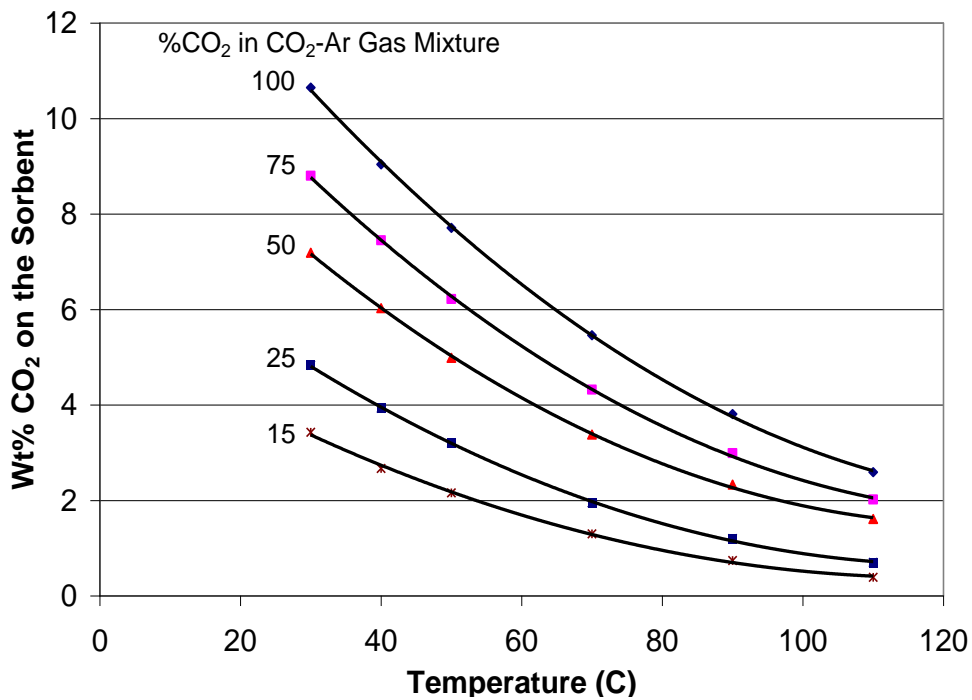


Figure III-6. The CO₂ loading on the sorbent as a function of temperature and gas composition.

III.3 HEATS OF ADSORPTION AND DESORPTION OF CO₂

The heats of adsorption and desorption of CO₂ on the sorbent are: 1) the heat that needs to be removed during adsorption; and 2) the heat that needs to be supplied for desorbing the CO₂ from the sorbent, respectively. The heat of adsorption of CO₂ on the ACS-1 sorbent at various coverages can be calculated from the slopes of isosteres using the relationship:

$$d(\ln P)/d(1/T) = \Delta H_{ads}/RT \quad (1)$$

Where ΔH_{ads} is the isosteric heat of adsorption, R is the gas constant, T is the temperature, P is the equilibrium partial pressure of CO₂ adsorbed. The isosteres (constant adsorbate coverage plots) were calculated at various coverages from the adsorption isotherms shown in Figure III-2. These plots are shown as the variation of logarithmic equilibrium partial pressures of CO₂ as a function of inverse temperature (Figure III-7).

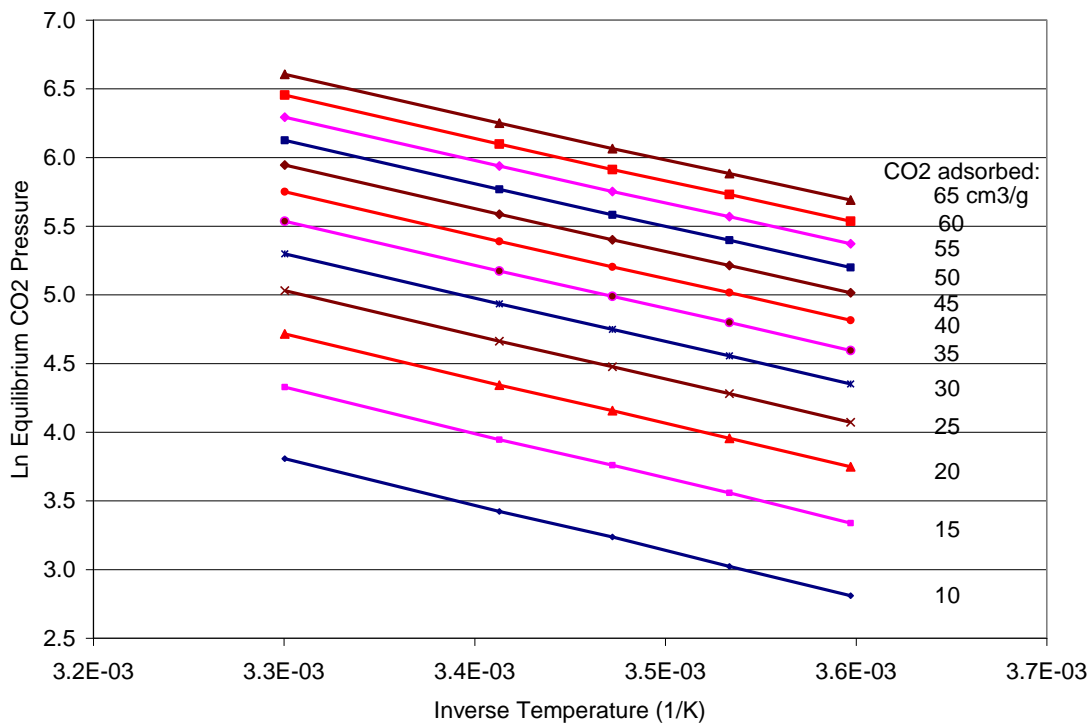


Figure III-7. The isostere plots of CO₂ adsorption on ACS-1 sorbent at various coverages.

The calculated heat of adsorption as a function of the extent of CO₂ adsorbed is shown in Figure III-8. The data indicate that the heat of adsorption is somewhat high at low coverages, but it approaches the latent heat of vaporization of CO₂ at high coverages. The measured heat of adsorption (28 kJ/mole) is significantly less than the heats of adsorption of CO₂ on primary amines such as monoethanolamine (80 kJ/mole)

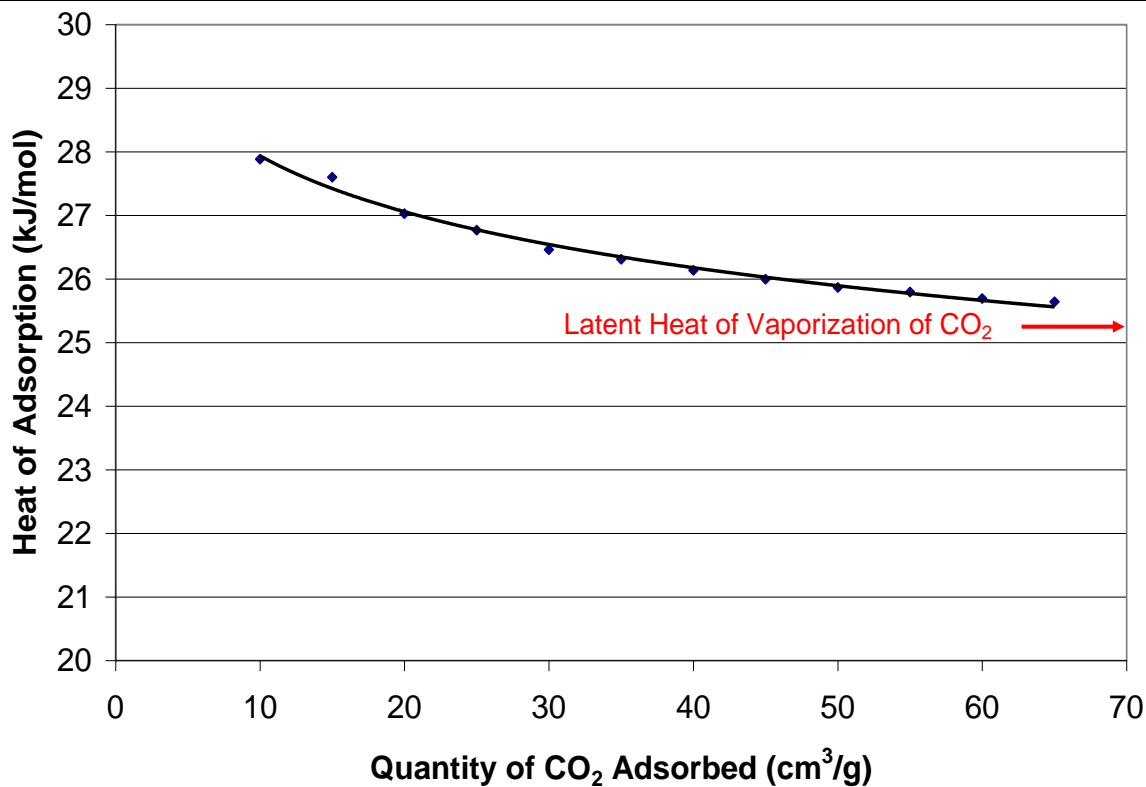


Figure III-8. The heat of adsorption of CO₂ on ACS-1 sorbent as a function of CO₂ loading.

Isostere plots were also calculated from the data collected in the TGA experiments (Figure III-9). From the slopes of these isosteres, the heat of desorption was calculated and the results are shown in Figure III-10. The average heat of desorption is 27 kJ/mole (range: 24.2 to 28.7 kJ/mole), similar to the value calculated from the BET adsorption. The data is somewhat scattered because the TGA technique is not as precise as the BET technique. However, the near similar values obtained with both techniques indicates that the adsorption and desorption heats are similar.

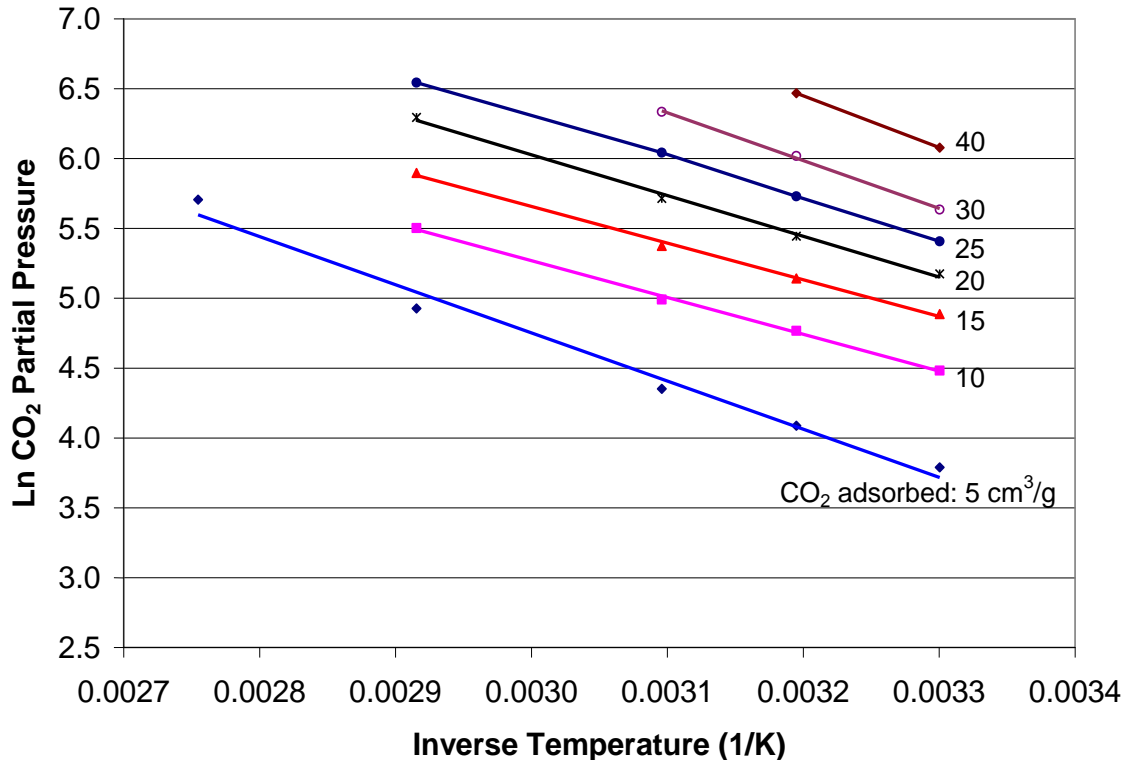


Figure III-9. The isostere plots of CO₂ adsorption on ACS-1 sorbent at various coverages in the temperature range 30° to 110°C.

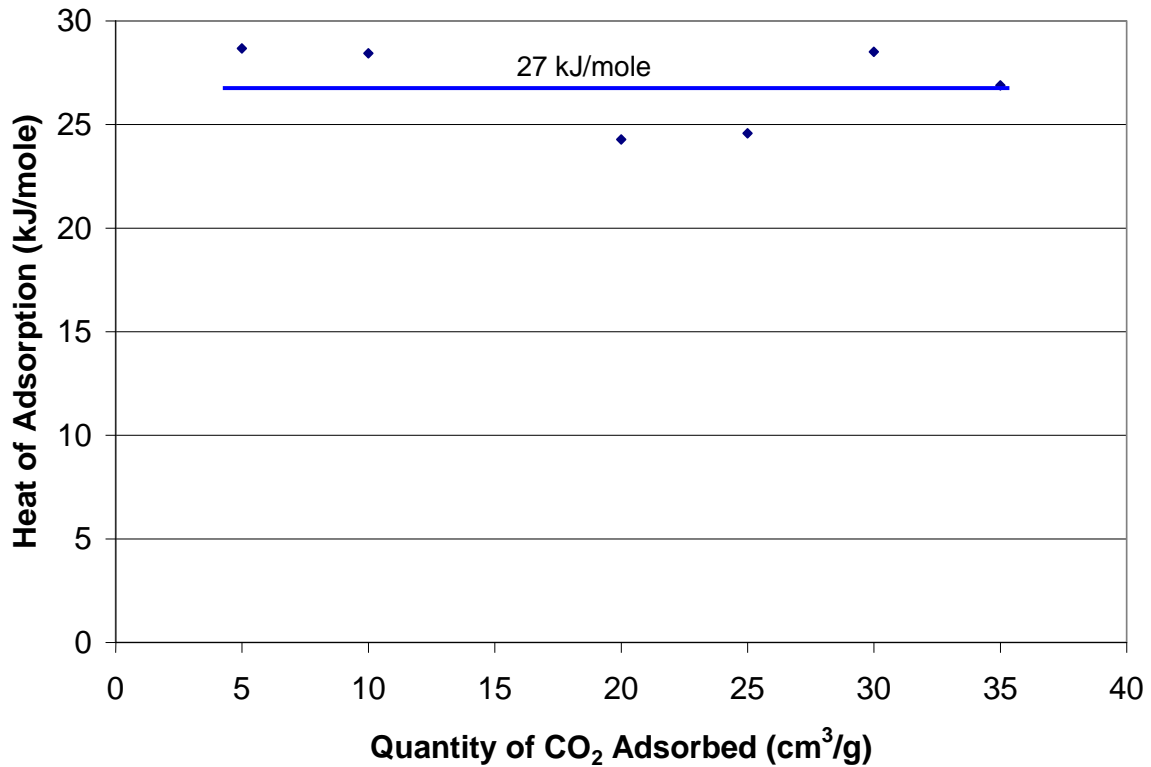


Figure III-10. The heat of desorption of CO₂ on ACS-1 sorbent as a function of CO₂ loading.

III.4 ADSORPTION OF OTHER GASES ON THE CARBON SORBENT

The adsorption characteristics of O₂, N₂, Ar, H₂O vapor, SO₂, and NO on the ACS-1 carbon sorbent were determined. Flue gas from PC-fired boiler contains these components and their adsorption characteristics on the sorbent must be known. The equilibrium amounts of O₂, N₂, Ar, and H₂O vapor adsorbed on the sorbent as a function of temperature and their partial pressures were determined to understand whether they will be adsorbed significantly on the carbon sorbent.

The BET technique was used to determine the adsorption isotherms of these gases in the temperature range 5° to 30°C. The adsorption capacity as a function of temperature and pressure can be calculated from the adsorption isotherms. The isosteric heats of adsorption were calculated from the adsorption isotherms. .

Figure III-11 illustrates the N₂ adsorption isotherm at 5° to 25°C. It shows that the quantity of N₂ adsorbed increases with the pressure of N₂. Note that the quantity of N₂ adsorbed is about 6 times less than the amount of CO₂ adsorbed at that temperature even though the partial pressure of N₂ gas (0.66 atm) is at about 5 times more than that of CO₂ [Klara, 2007].

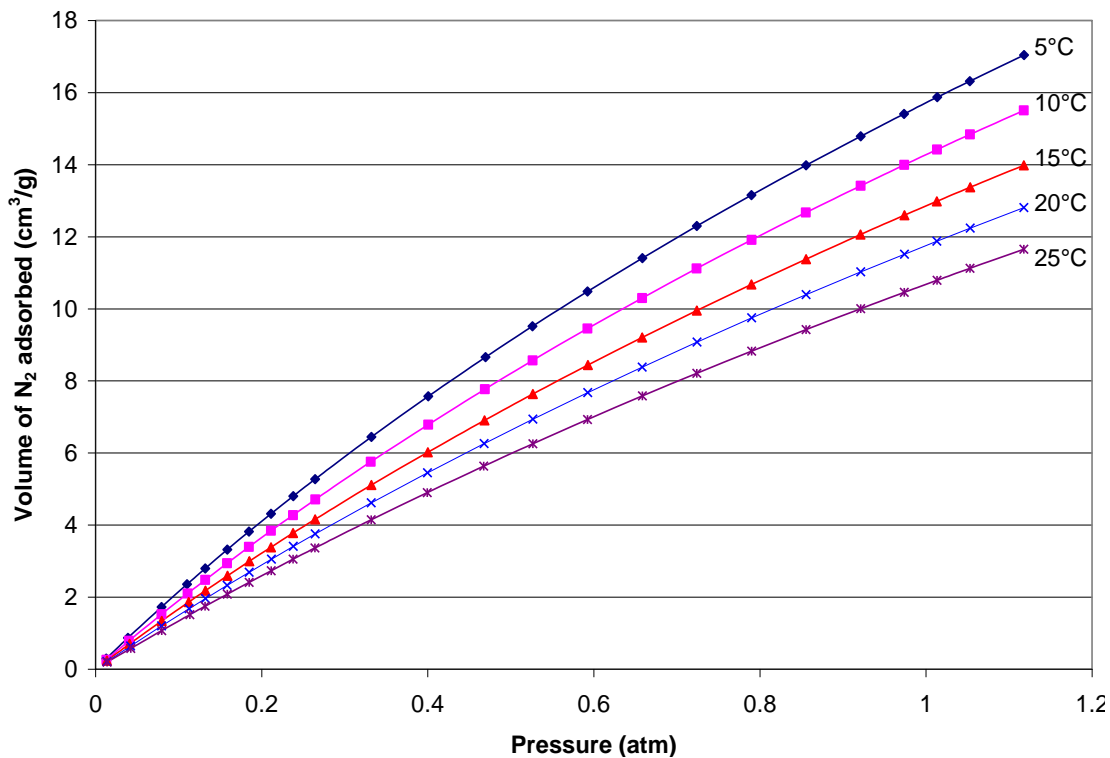


Figure III-11. The quantity of N₂ adsorbed on the ACS-1 sorbent as a function of N₂ partial pressure at various temperatures.

Similar results are obtained with O₂ (Figure III-12). These results are not unexpected because CO₂ will adsorb more strongly than N₂ or O₂ on carbon sorbents. The adsorption of O₂ on the sorbent will be relatively small because the O₂ partial pressure in the flue gas is only 0.02 atm [Klara, 2007].

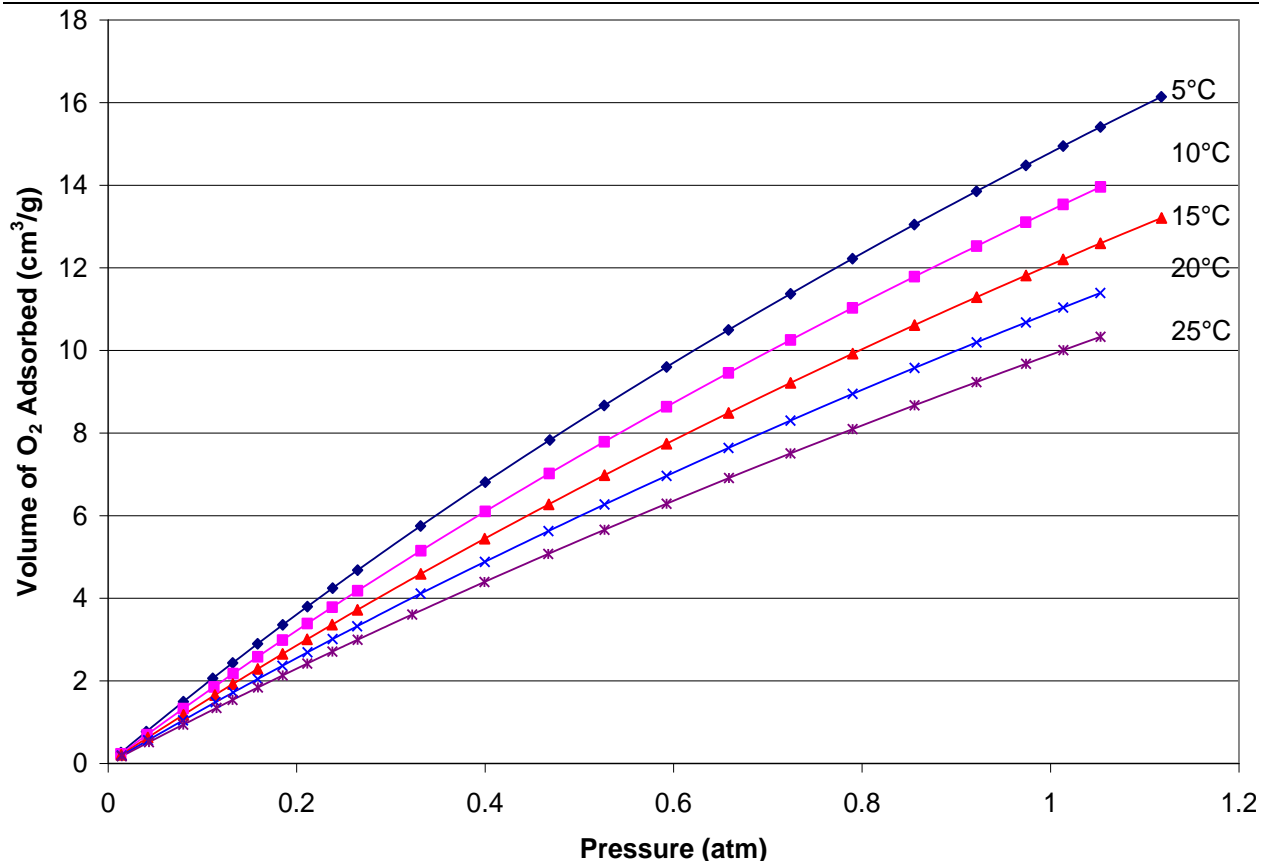


Figure III-12. The quantity of O₂ adsorbed on the ACS-1 sorbent as a function of O₂ partial pressure at various temperatures.

Figure III-13 illustrates the Ar adsorption isotherms in the temperature range of 5 to 25°C. Ar gas is present in the flue gas at a partial pressure less than 0.01 atm. The Ar isotherms appear to be similar to those of N₂ and O₂ even though Ar is a noble gas. This similarity may be due to the fact that the adsorption isotherms were obtained at a temperature far greater than the boiling points of these gases. The boiling point of Ar is -186°C, which is only 10°C higher than that of N₂. At near ambient conditions, N₂, O₂, and Ar appear to physisorb similarly on the micropores of the ACS-1 sorbent.

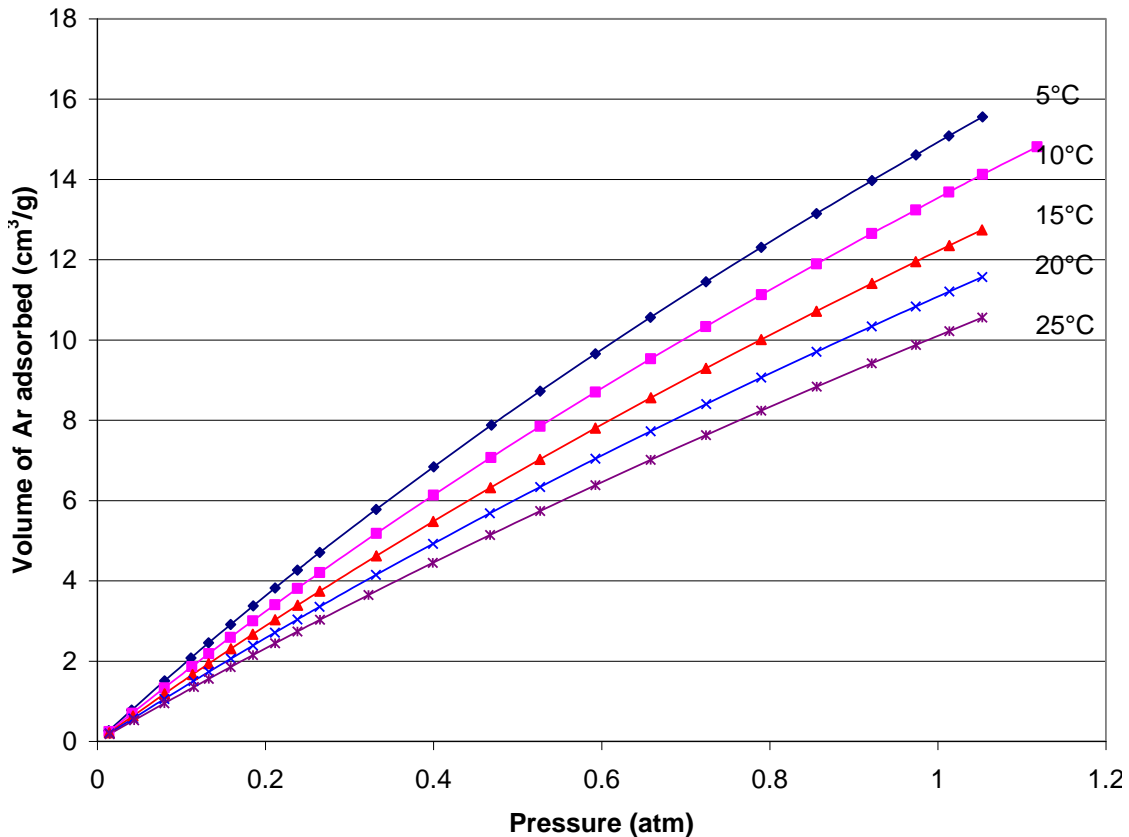


Figure III-13. The quantity of Ar adsorbed on the ACS-1 sorbent as a function of Ar partial pressure at various temperatures.

Figure III-14 illustrates the adsorption isotherms of water vapor on the sorbent in the temperature range of 5 to 25°C. Water vapor is present in the flue gas at near saturation as the flue gas leaves the wet flue gas desulfurization step. Hence, obtaining adsorption data of the water vapor on the sorbent is essential. The isotherms are plotted as the volume of moisture adsorbed as a function of relative pressure, P/P_0 where P_0 is the saturation pressure at that temperature. The quantity of moisture adsorbed increases with the relative pressure at a constant temperature, but it decreases with increasing temperature at a constant relative pressure. At P/P_0 greater than ~ 0.3 , liquid condensation occurs, increasing the amount of water adsorbed on the sorbent. This characteristic is due to the fact that at a concave surface, the vapor pressure of a liquid is lower than on a flat surface, as given by the Kelvin principle. The walls of the micropores inside the sorbent are highly concave, providing a suitable surface for condensation at a far lower temperature than the boiling point of water.

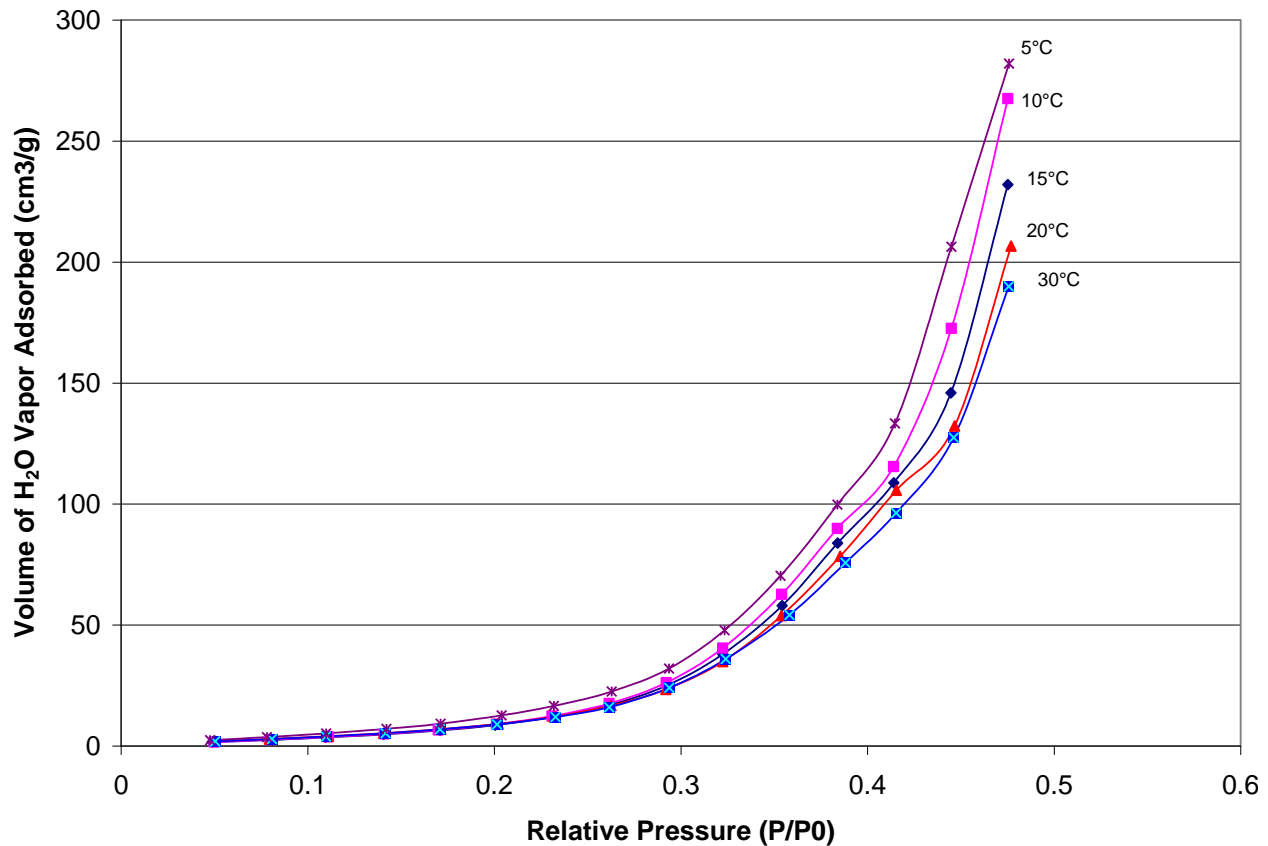


Figure III-14. The quantity of H₂O vapor adsorbed on the ACS-1 sorbent as a function of the relative pressure at various temperatures.

During CO₂ capture in PC-fired flue gas, the sorbent will be exposed to SO₂ and NO that are present in the flue gas. The SO₂ and NO adsorption characteristics of the ACS-1 sorbent were determined. These tests were conducted at partial pressures that are very high compared to the concentrations expected in a flue gas. After wet flue gas desulfurization and SO₂ polishing, the concentration of SO₂ in the flue gas is expected to < 10 ppm (< 0.01 torr). The data shown in Figure III-15 illustrate that SO₂ is adsorbed on ACS-1 sorbent, and the amount adsorbed decreases with temperature. These data do not represent equilibrium adsorption because the desorption rate of SO₂ from the sorbent is extremely slow.

A similar adsorption isotherm for NO is shown in Figure III-16. Again, the rate of desorption of NO from the sorbent at 20°C was very slow.

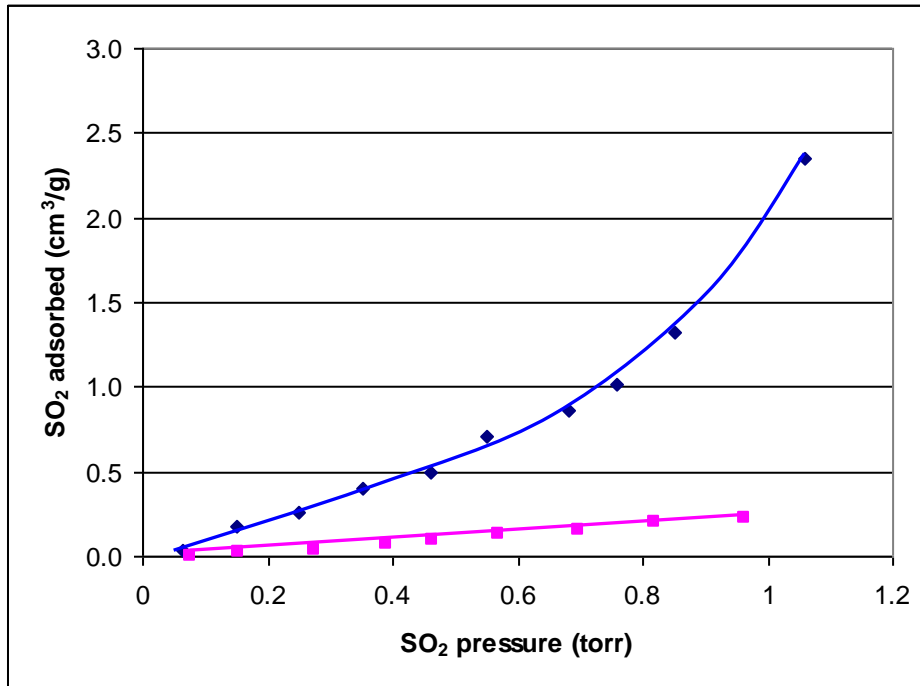


Figure III-15. The adsorption isotherm of SO₂ gas on ACS-1 sorbent at 20 and 90°C.

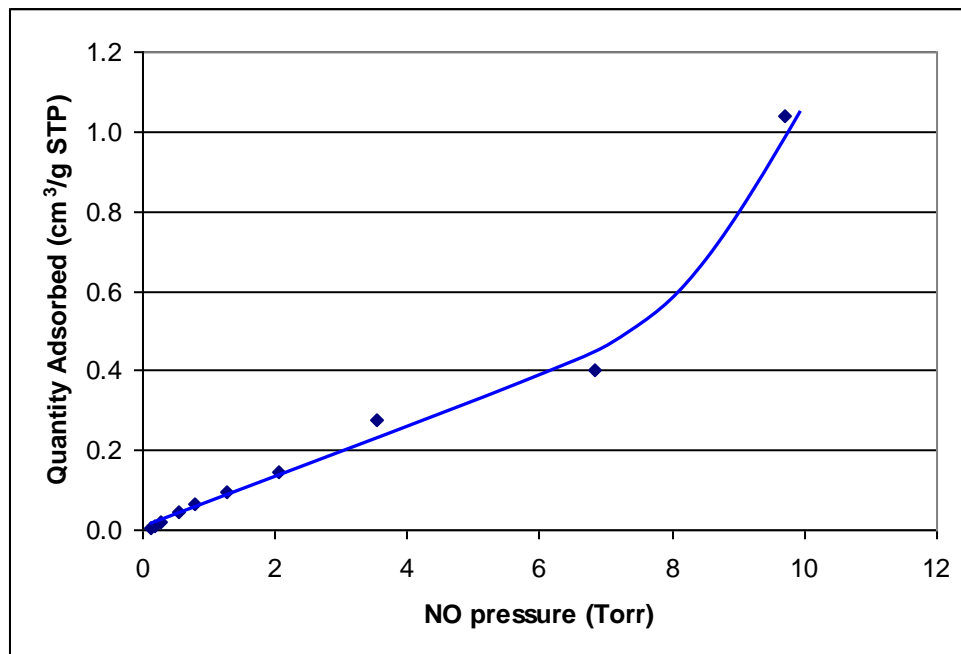


Figure III-16. The adsorption isotherm of NO gas on ACS-1 sorbent at 20°C.

From the adsorption isotherms shown in Figures III-11 through III-13, isosteres (constant adsorbate coverage plots) were calculated at various coverages. The heats of adsorption of N_2 , O_2 , and Ar gas on the ACS-1 sorbent at various coverages were calculated from the slopes of these isosteres (Figure III-17). The data indicate that the heats of adsorption are relatively small and constant in the coverage range tested. The observed heats of adsorption are higher than the heat of vaporization for these gases because the adsorption is being conducted at a temperature far higher than the boiling point.

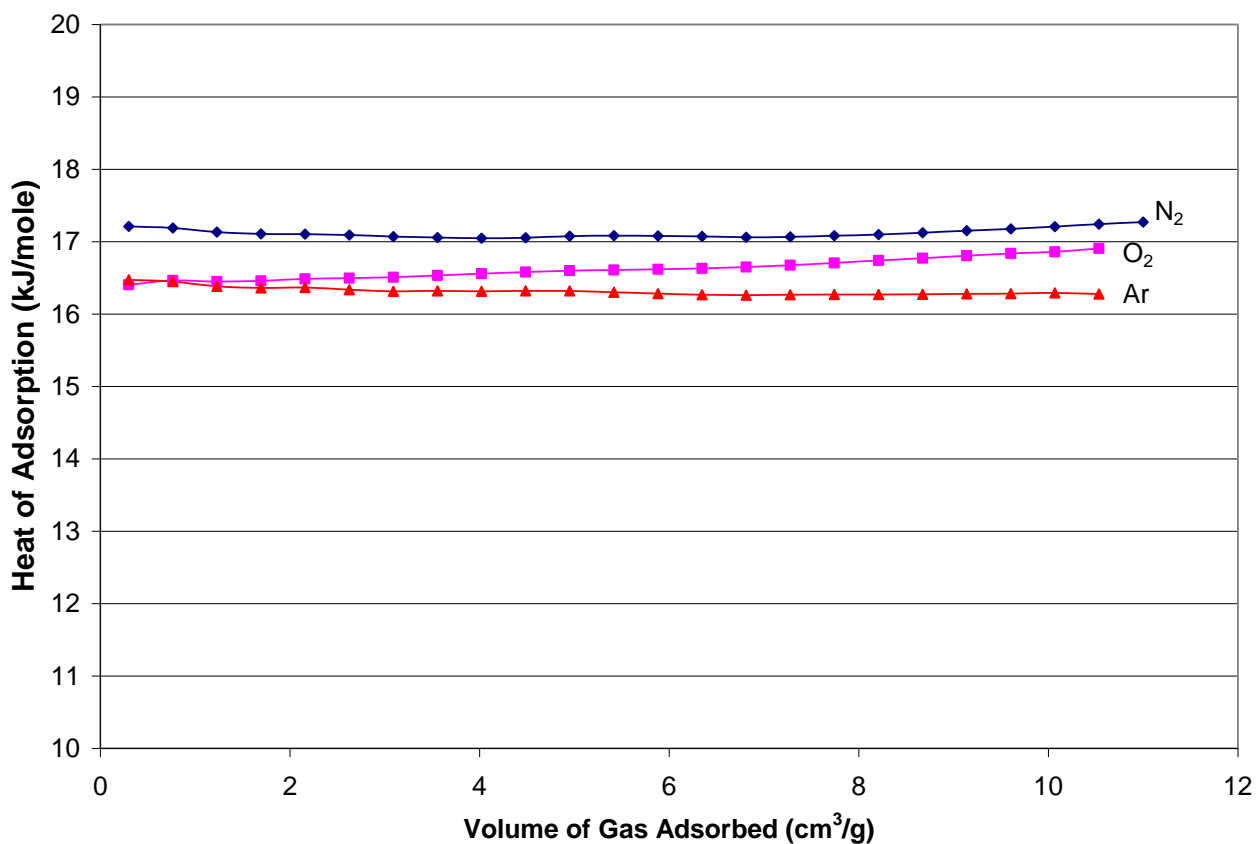


Figure III-17. The heat of adsorption of N_2 , O_2 , and Ar on ACS-1 sorbent as a function of their coverage on the sorbent.

The heat of adsorption of water vapor on the ACS-1 sorbent was also measured as a function of its coverage (Figure III-18). The heat of adsorption is relatively low at a low coverage, and it increases slightly as the coverage or the amount of water vapor adsorbed. At moisture loadings greater than $50 \text{ cm}^3/\text{g}$, the heat of adsorption is constant at a value close to the heat of vaporization of water ($\sim 45 \text{ kJ/mole}$). The decrease in the value of heat of adsorption at the low coverages indicates that the surface is likely to be hydrophobic. As we noted earlier, at higher coverages, liquid condensation occurs in the micropores. The similarity in the heat of adsorption of H_2O on the carbon sorbent and the heat of vaporization of water indicates that, in the case of carbon sorbent, water vapor is adsorbing on the liquid water that is condensed inside the micropores.

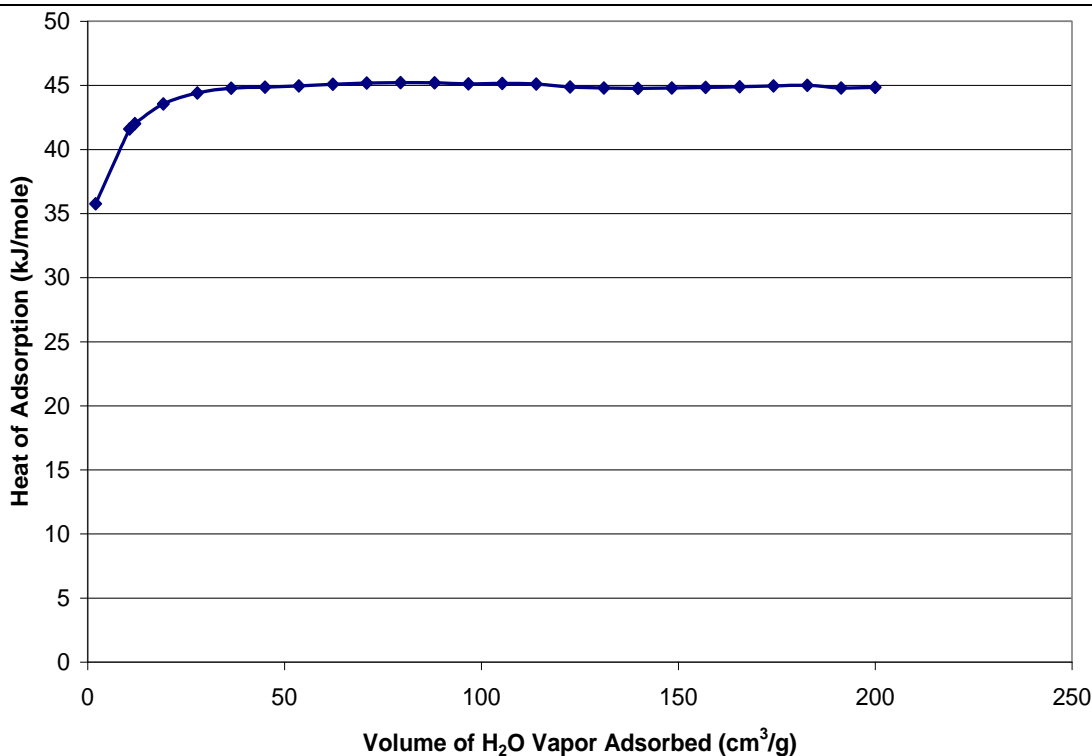


Figure III-18. The heat of adsorption of water vapor on ACS-1 sorbent as a function of its loading on the sorbent.

III.5 SURFACE FUNCTIONAL GROUPS

The presence of basic sites on the surface facilitates the adsorption of CO₂ on the sorbent because CO₂ is considered to be acidic in nature. The type and the quantity of the functional sites on the surface of the sorbent can be determined by titration with various acids and bases. The pH was measured using a water extraction method. Before analysis, the sorbent samples were dried at 120°C overnight to remove the adsorbed gases. One gram samples of the carbon were added to 10 mL of deionized water and stirred for 3 h. The pH of the resulting solution was measured to be 6.7. The oxygenated surface groups were determined according to the method of Boehm. A known amount of carbon (0.2 g) was placed in 10 mL of the following 0.05 M solutions: sodium hydroxide, sodium carbonate, and hydrochloric acid. The vials were sealed and shaken for 24 h. The excess of base or acid present in the solution was determined by titrating with HCl and NaOH, respectively. The number of acid sites of various types were calculated under the assumption that NaOH neutralizes carboxylic, phenolic, and lactonic groups, whereas Na₂CO₃ neutralizes carboxylic and lactonic groups. The number of surface base sites was calculated from the amount of hydrochloric acid that reacted with the carbon. These results suggest that the surface of the ACS-1 sorbent contains small amounts of both acidic and basic groups (Table III-1). The observed low heat of adsorption for CO₂ on the surface (25 kJ/mole) may be due to the fact that the surface does not contain significant amount of strong basic sites and CO₂ adsorbs mainly as physisorption.

Table III-1. Measured Parameters Related to Surface Functionalities for ACS-1

Parameter	Value
Surface pH	6.7
Basic Groups (10^{-3} mole/g)	0.3
Carboxyl Groups (10^{-3} mole/g)	<0.01
Lactone Groups (10^{-3} mole/g)	0.3
Phenol Groups (10^{-3} mole/g)	0.05

III.6 PHYSICAL AND MECHANICAL PROPERTIES

The various physical properties of the ACS-1 sorbent are listed in Table III-2. The sorbent has a high surface area of more than $1270 \text{ m}^2/\text{g}$ and micropore volume of $0.4 \text{ cm}^3/\text{g}$ that are conducive to a high CO_2 loading. The relatively high thermal conductivity of the sorbent will provide increased heat transfer rate during heating and cooling of the sorbent bed.

Table III-2. Physical Properties of the ACS-1 Sorbent

Parameter	Value
Density (g/cm^3)	1.10
Heat Capacity ($\text{J}/\text{g}\cdot^\circ\text{K}$)	1.0
Thermal Conductivity (298°K), $\text{W}/\text{m}\cdot^\circ\text{K}$	0.82
BET Surface Area, (m^2/g)	1300
Micropore volume (cm^3/g)	0.38

The sorbent granules made by ATMI were spherical in nature (Figure III-19), and the majority of the particles varied from 150 to $250 \mu\text{m}$ in diameter. For the CO_2 capture application, the sorbent may need to flow through absorber and regenerator columns counter current to the gas flow. The flow characteristics of the granules may be inferred from the angle of repose. We found the angle of repose of the dry sorbent granules to be 29° , similar to that of a dry sand bed. The angle of repose is the maximum angle of a stable slope determined by friction, cohesion, and the shape of the particles. We measured the angle by forming the granules into a conical pile and measuring the angle of the cone. A low angle of repose indicates that the friction between the particles is low and they move easily with respect to one another.

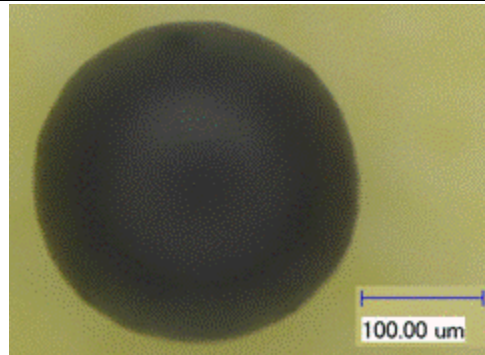


Figure III-19. A magnified picture of a single ACS-1 sorbent granule.

The compressive strength of ACS-1 sorbent granules was measured using a sensitive mechanical tester. The stress-vs-strain curves, shown in Figure III-20, indicate that the granules are brittle because of the very low displacement and abrupt fracture. The microbeads failed under tensile stress around the equator of the beads. From the measured load at fracture, we calculate that the compressive strength of the granules to be ~ 12,000 psi, a very high value for a porous substance. The differences in the test patterns are due to differences in the size of the granules that were tested. The compressive strength of a flat bar of this material was measured to be 18,000 psi in a separate test. The differences in the strength values between the flat bar and granules may be due to fact that a sphere is not the ideal geometry for determining compressive strength.

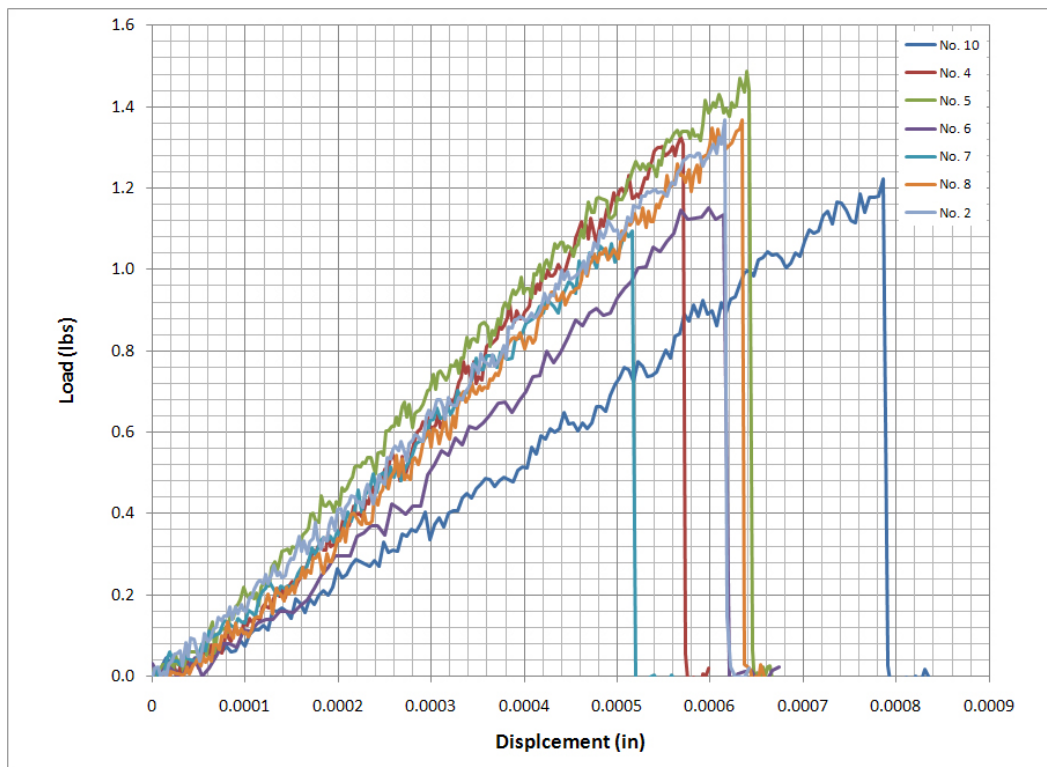


Figure III-20. The compressive strength of the ACS-1 granules.

The attrition resistance of the granules was measured using the standard ASTM D5757 air jet test procedure, which is designed for fluidized bed reactor catalysts (Figure III-21). A batch of 50 g of granules was placed inside a conical vessel on the top of a disc that had three 0.015-inch (0.038 cm) diameter holes. Air is passed through the disc at a rate of 10 liters/min to fluidize the granules. During fluidization, the granules are accelerated by the high velocity air jet (~ 500 m/s at the orifice) and impact with each other. Any solid powder that may separate from the granules due to attrition is carried away by the flowing air. The entrained powder is collected in a filter and measured. For the carbon sorbent, the amount of material lost was found to be only 0.01 and 0.03 g after 1 h and 5 h of testing, respectively, (Table III-3). The attrition rate index, defined as the rate of weight loss between 1-h and 5-h of testing was only 0.01 wt% per hour. This low value indicates that the ACS-1 sorbent is very tough and significantly more attrition resistant than FCC catalysts that have typically an attrition index of 4% per hour. Note that this attrition test is a very severe test and, during use, the carbon microbeads are not subjected to the aggressive impact forces used in the test.

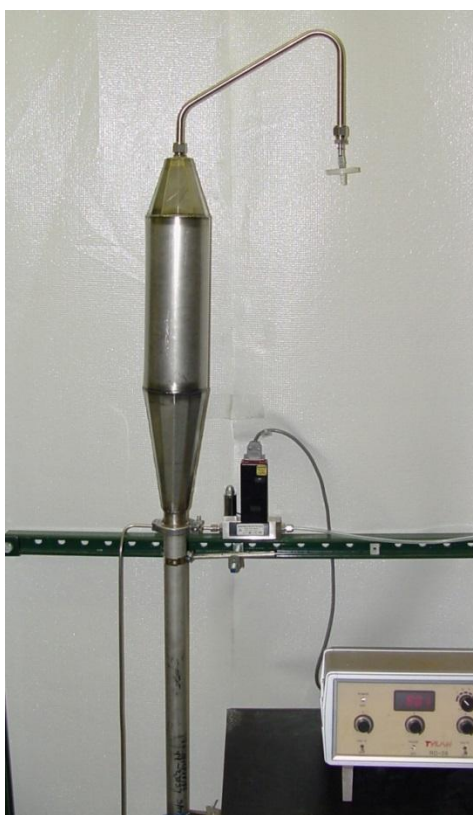


Figure III-21. The photograph of an attrition tester.

Table III-3. Attrition Resistance of the ACS-1 Sorbent

Parameter	Value
Attrition after 1 h of testing (g)	<0.03
Attrition after 5 h of testing (g)	<0.05
Attrition rate index (% weight loss/h)	<0.01

IV. SCREENING TESTS WITH THE SORBENT FORMULATION

IV.1 SCREENING TESTS

A fixed-bed reactor system was used to determine the rate of CO₂ adsorption on the sorbent. The reactor had a nominal ID of 2.2 cm, and it was filled with the sorbent to a bed height of 18 cm. The particle size of the sorbent was in the range 0.3 to 0.6 mm. The bed was kept at a constant temperature using a liquid-cooled jacket at the outer walls. About 200 cm³/min of air containing 15% CO₂ was passed through the bed and the CO₂ composition of the exit gas was monitored using a CO₂ specific infrared detector. In some tests, moisture was introduced into the feed gas from about 20% to 80% relative humidity values. Before the adsorption test, the sorbent was heated to ~100°C in a stream of dry N₂ to desorb any CO₂, moisture, or other adsorbed gases.

Figure IV-1 illustrates the observed breakthrough of CO₂ from the bed at 25°C. The data shows that, for a period of time, the CO₂ level in the exit gas is below 0.05%, which is the detection limit of the CO₂ detector, indicating that > 90% removal of CO₂ is feasible with this sorbent. After the breakthrough, the CO₂ concentration in the reactor exit gas rises rapidly approaching the feed gas concentration in a relatively short period of time. As expected, the breakthrough occurs after a longer period of time with a dry gas mixture than with a gas stream containing moisture. The breakthrough time decreases as the relative humidity value increases. For comparison, the breakthrough curves are also indicated for CO₂ in an empty reactor and in a reactor filled with dense alumina particles (Blank run). The rise time with the carbon sorbent is only marginally slower than that for the empty reactor or reactor with the alumina particles. This observation provides an indication that the adsorption-desorption of CO₂ on the sorbent is rapid.

Figure IV-2 shows the calculated CO₂ loading on the sorbent as a function of time at various humidity levels. In this calculation, the CO₂ is assumed to be adsorbed uniformly on the bed. The calculated loading is independent of the humidity level until near the breakthrough time. The amount of CO₂ captured decreases slightly with the amount of moisture in the feed gas.

Similar experiments were also carried out at 5 and 15°C. The amount of CO₂ captured on the sorbent increases as the adsorption temperature decreases, as shown in Figure IV-3. The CO₂ loading on the sorbent is nearly independent of the relative humidity at 5 and 10°C, and this observation is likely to be due to the fact that the partial pressure of moisture decreases with temperature for a given relative humidity value.

These preliminary results suggest that the ACS-1 sorbent is capable of removing more than 90% of CO₂ from a flue gas. The moisture level in the feed gas decreases the loading slightly. The adsorption of CO₂ on the sorbent is relatively rapid.

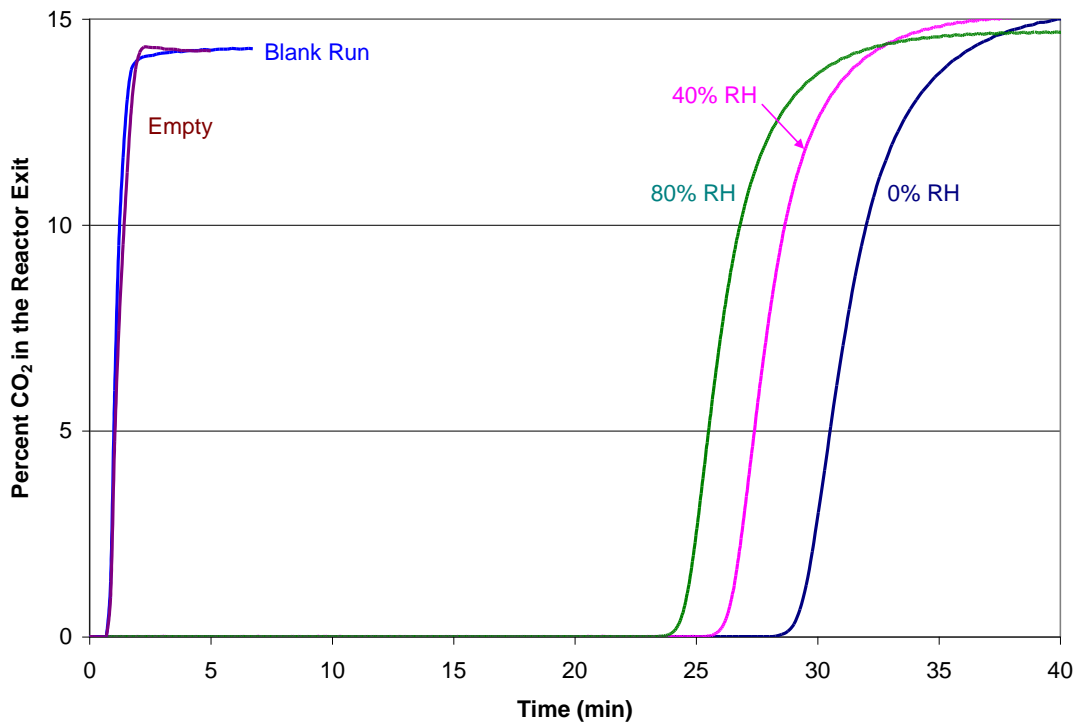


Figure IV-1. The breakthrough of CO₂ as a function of time at 25°C at various humidity levels.

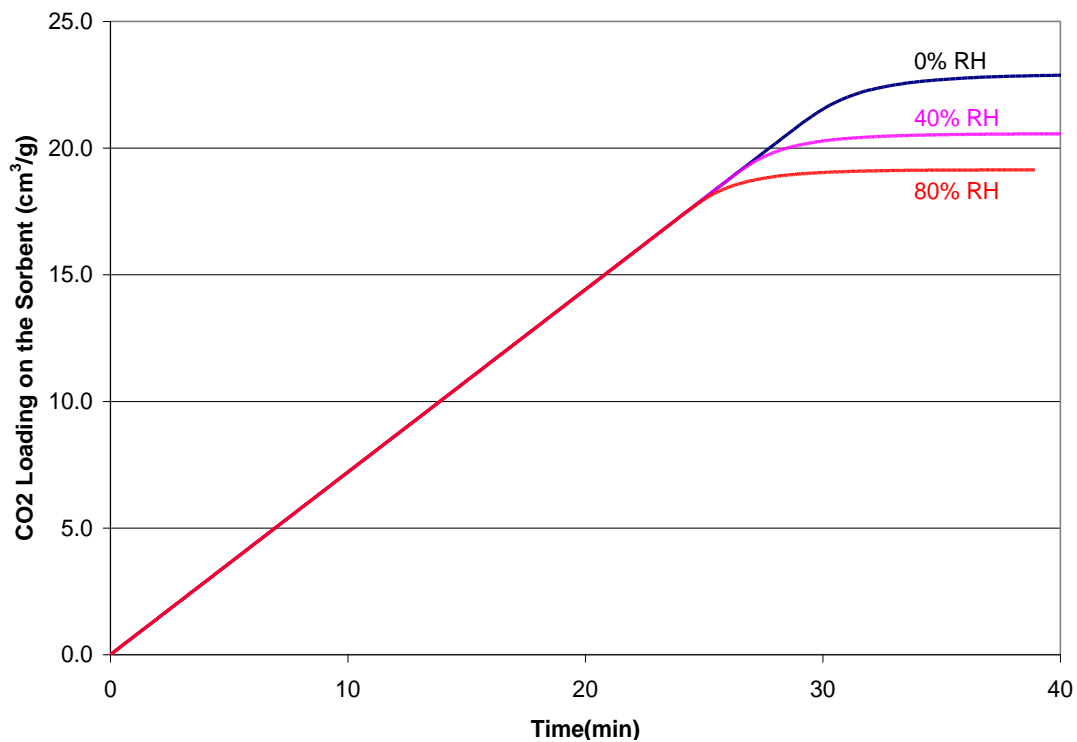


Figure IV-2. The calculated loading of CO₂ as a function of time at 25°C at various humidity levels.

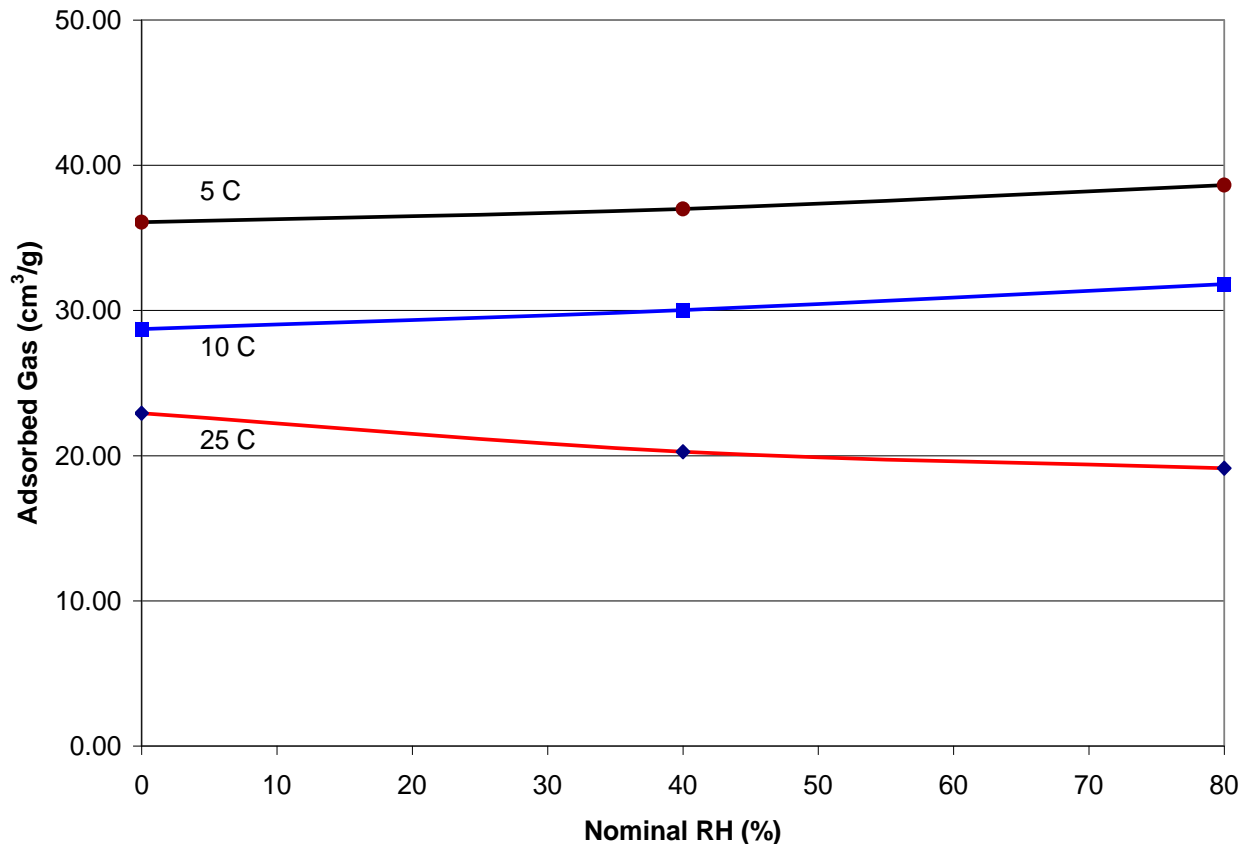


Figure IV-3. The calculated loading of CO₂ as a function of relative humidity at 5°, 15° and 25°C.

The fixed-bed reactor system was used also to determine the rate of CO₂ desorption from the sorbent. About 200 cm³/min of air containing 15% CO₂ and 80% RH moisture was passed through the bed to adsorb the CO₂ on the sorbent. After obtaining CO₂ breakthrough in the exit gas, air flow was replaced by a CO₂ gas stream and the sorbent bed was heated rapidly to desorption temperatures of 90 to 106° C. The CO₂ adsorbed on the sorbent is desorbed in a pure CO₂ atmosphere. The rate of CO₂ desorption was very rapid as shown in Figure IV-4. The CO₂ loading on the sorbent during regeneration at 90, 100, and 106°C is shown in Figure IV-5. These results indicate the desorption of CO₂ from the sorbent is not very sensitive to the regeneration temperature. This result is expected with a sorbent on which CO₂ is adsorbed and not chemically bound and the activation energy for desorption is low. These observations indicate that excessively high temperatures are not necessary to regenerate the sorbent. Low-grade or waste-heat is sufficient for the sorbent regeneration, and the use of such heat sources will not significantly penalize the efficiency of power generation due to CO₂ capture.

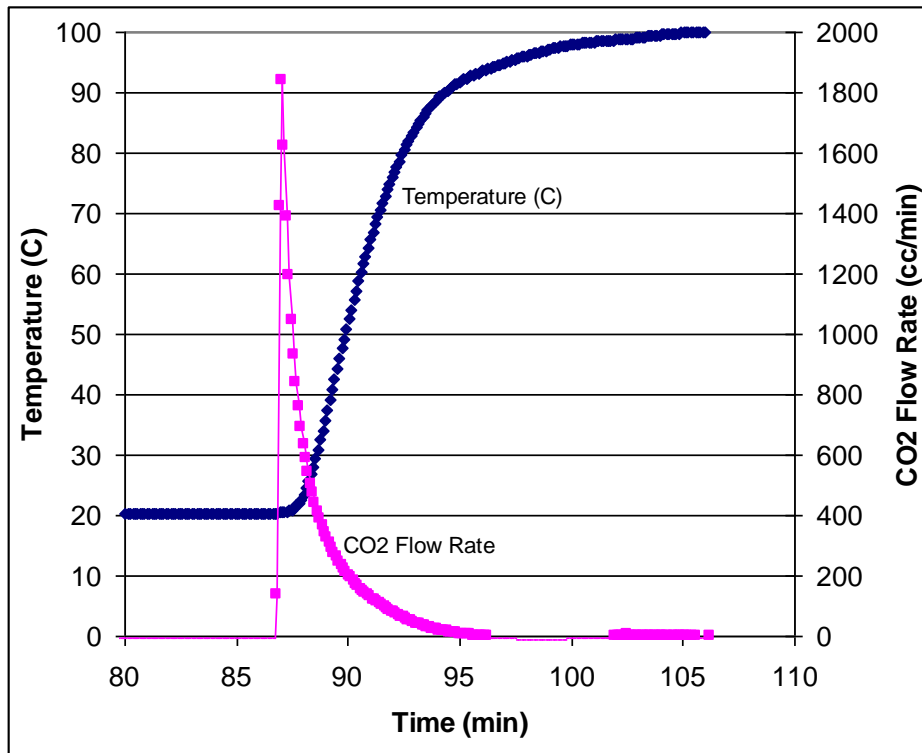


Figure IV-4. The rate of desorption of CO₂ from the ACS-1 sorbent as it is heated to the regeneration temperature.

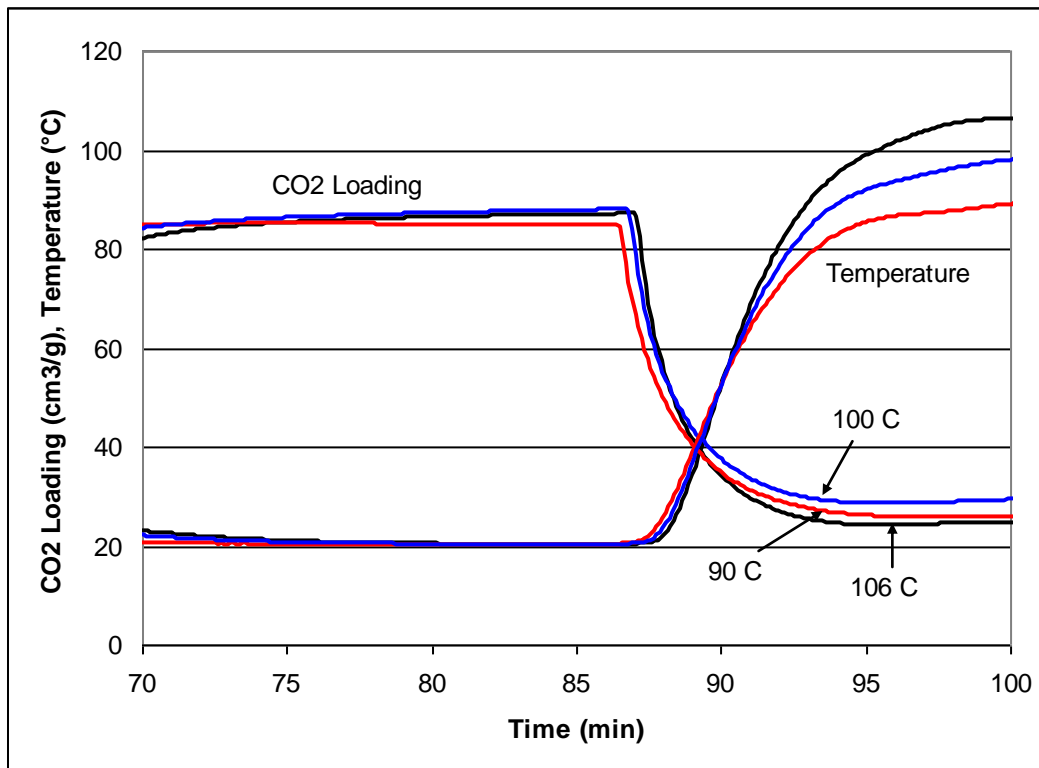


Figure IV-5. The CO₂ loading on the ACS-1 sorbent as it is heated to different regeneration temperatures.

In the CO₂ capture process, the sorbent is expected to undergo numerous adsorption and regeneration cycles, and degradation of the sorbent during such cyclic conditions will have serious impact on the efficiency of the process. Cyclic adsorption-desorption experiments were carried out to determine changes in the sorbent. Figure IV-6 illustrates the CO₂ loading of the sorbent as determined by TGA as the sorbent is cycled from 30 to 115° C and back to 30°C in a CO₂ atmosphere. The slight change in the absolute mass of the sorbent appears to be due to the instrumental drift. But the differences in the weight of the sorbent between each adsorption and desorption cycle are the same within experimental error. The CO₂ capacity of the sorbent did not vary during this cyclic treatment, indicating that the sorbent is extremely stable in this temperature range.

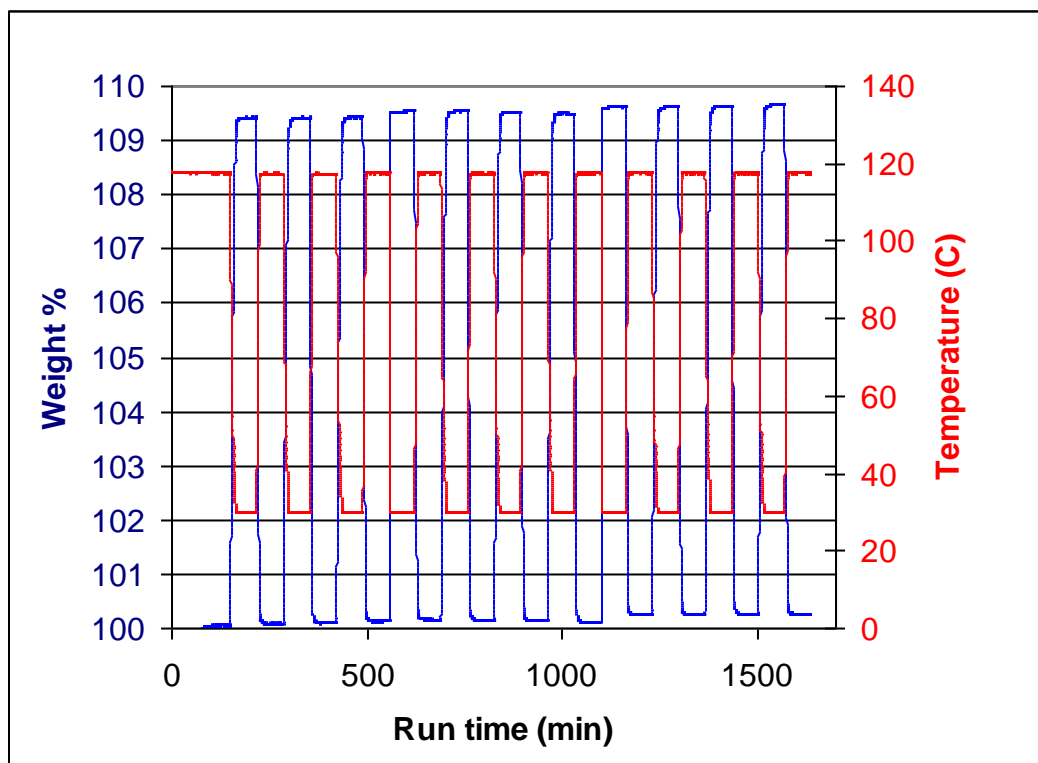


Figure IV-6. The CO₂ capacity of the ACS-3 sorbent during cycling at 30 and 115°C in a CO₂ atmosphere.

IV.2 IMPROVEMENTS TO THE SORBENT

ATMI made two additional sorbents (ACS2 and ACS3) improving the structural properties of the sorbent. The preparation method used to modify the sorbent is considered to be proprietary by ATMI. The surface areas of the modified sorbents, as measured with BET-CO₂ measurements, were significantly higher than that of the original sorbent. ACS-3 has a surface area that is 25% higher than that of ACS-1 (Figure IV-7). The CO₂ adsorption characteristics of these sorbents were determined by thermogravimetric analysis (TGA) at 30° and 110° C in a CO₂ gas stream. The difference in the wt% CO₂ adsorbed on the sorbents at these two temperatures is shown in Figure IV-8. The CO₂ capacity of the ACS-3 sorbent is significantly

(18%) higher than that of ACS-1 sorbent. These results suggest the CO₂ loading capacity can be improved by structural modification.

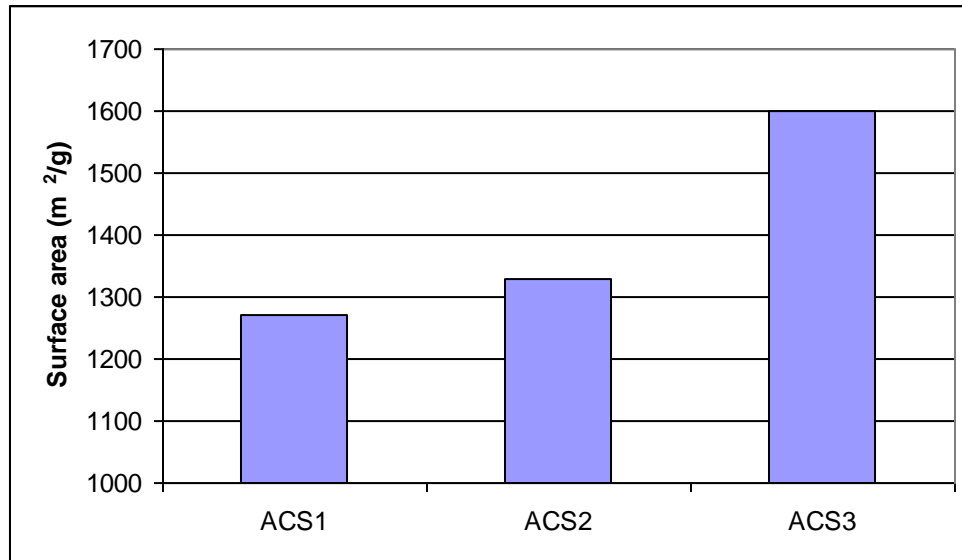


Figure IV-7. The surface area of the original and improved sorbents.

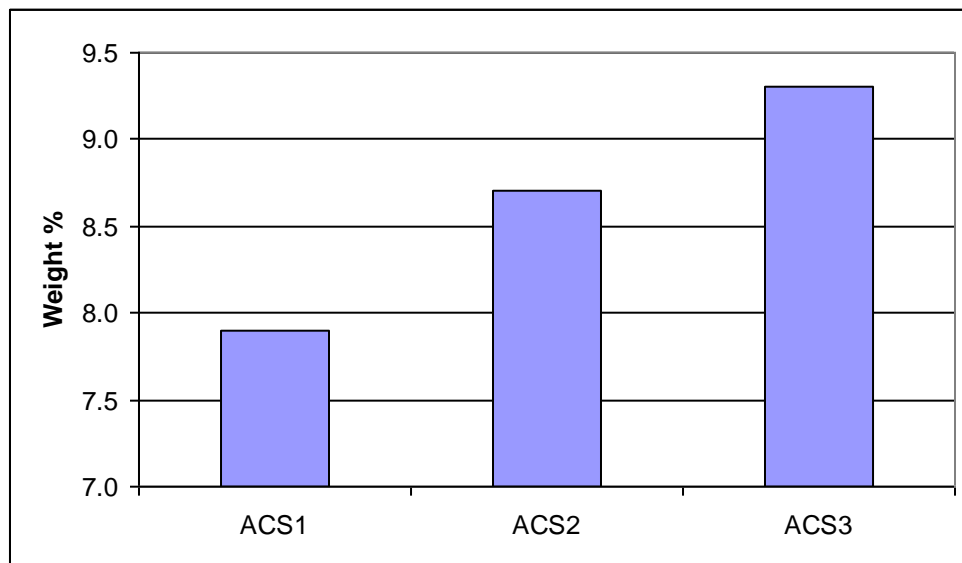


Figure IV-8. The difference in the CO₂ loading at 30° and 110°C of the ACS sorbents.

V. BENCH-SCALE PARAMETRIC TESTING

In this section, we describe the results of Task 6: Bench-scale parametric testing using a novel reactor design.

V.1 BENCH-SCALE REACTOR DESIGN

Reactor designs using a fixed- or fluidized-bed of sorbent granules have been proposed, but they result in a relatively high pressure drop for gas flow. Such a reactor design would increase the cost of CO₂ capture from a PC-fired boiler. A reactor design that allows a low pressure drop while preserving an efficient gas-solid contact is necessary for the present application.

We designed a special adsorption reactor that takes advantage of the unique high adsorption and desorption kinetics, high fluidity, and high attrition resistance of our carbon sorbent microbeads. The sorbent microbeads fall from the top to bottom of the reactor, as shown schematically in Figure V-1. The gas containing the CO₂ is flown upwards in a counter-current mode to maximize the rate and extent of absorption. A commercially available structural packing was chosen so that no special design of the packing is necessary. The selected structural packing is made of corrugated metal sheets on which sorbent microbeads fall down the reactor. Each segment of the packing contains crossing channels that distribute the solid and gas counter-flow along an inclined path. By placing successive packing segments in a staggered angular fashion, the flows are distributed effectively across the cross-section of the reactor. This structural packing provides a relatively low pressure drop compared to random packing. This design is somewhat similar to a standard liquid-gas absorber in which a liquid solvent flows down while gas flows upward.

This reactor design is suitable for rapid cycling of the sorbent because the carbon sorbent microbeads have rapid CO₂ adsorption and desorption kinetics and excellent attrition resistance. These characteristics will allow a compact reactor design that in turn will reduce the capital cost of the CO₂ capture system.

The reactor design also allows the heating of the sorbent by direct contact with steam. The carbon sorbent adsorbs CO₂ directly from the flue gas at near ambient temperature. The adsorbed CO₂ is then released by heating the sorbent with low pressure steam which is a readily available heat source in a coal-fired power plant. The desorbed CO₂ can be separated easily from the residual steam simply by condensing the steam.

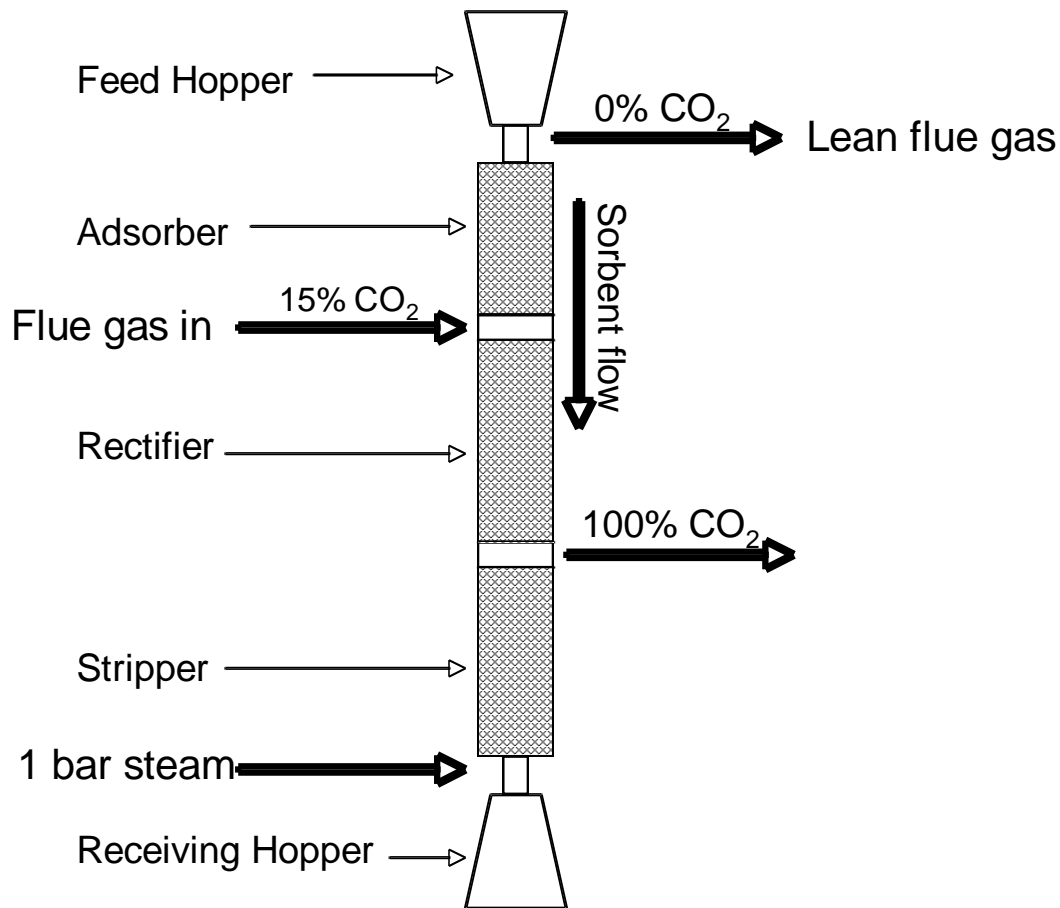


Figure V-1. Schematic diagram of the integrated absorber-stripper column.

V.2 ADSORBER BED FLOW DISTRIBUTION

Efficient adsorption of the CO_2 from the flue gas requires that the sorbent granules are uniformly distributed on the surface of the packing and intimately mixed with the counter flowing gas. The effectiveness of the packing in distributing the solid flow uniformly was demonstrated in a short length of the packing (4.5 inches) with a collimated inlet flow by observing the outlet flow (Figure V-2). We observed a remarkably uniform density of the granules leaving the reactor across the cross-section of the packing, as shown in the right half of the picture in Figure V-2.

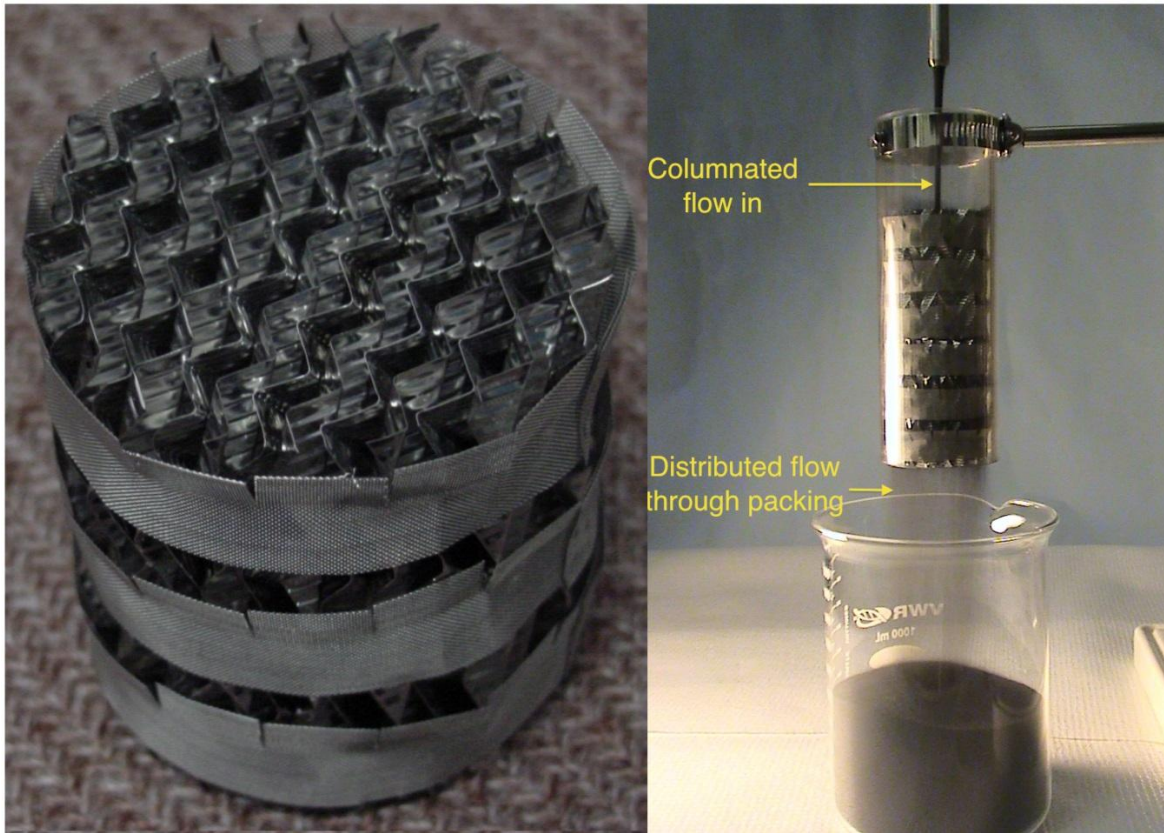


Figure V-2. Photograph of the structured packing used in the bench-scale reactor and a demonstration of the packing effectiveness at distributing the flow of sorbent granules.

V.3 PARAMETRIC TESTS IN A BENCH-SCALE SYSTEM

The bench-scale adsorber was used to determine: (1) gas and sorbent residence time; (2) pressure drop across the packing; and (3) CO₂ capture efficiency under varying operating conditions. The adsorber system is comprised of:

1. A feed gas manifold for introducing a simulated flue gas with independent control of CO₂ and air flow rates;
2. A sorbent feeder in which a batch of sorbent granules are gravity-fed from a reservoir into the top of the adsorber;
3. A 2-in-diameter by 3-ft-tall adsorption column containing a structural packing;
4. An IR-based CO₂ analyzer to measure the CO₂ concentration of the gas exiting the reactor.

Sorbent Residence Time: This cold flow setup was also used to measure the linear velocity of the descending granules by measuring the time lag between granules entering the top and exiting the bottom. From this data, we calculated that a solid residence time of about 5 s will be achieved in a bench-scale adsorber that is 3-ft tall. The linear velocity of sorbent granules was determined as a function of the counter-current gas velocity using a video-recording of the solid moving down the column. An example series of stills, extracted from the video, is shown in Figure V-3. The picture set on the left side is a schematic illustration, whereas the picture set on right side includes the actual photographs. Initially, the packing is free of any granules. After the introduction of the granules from the top, they move down the column and this solid front can be seen as a moving dark band. When this band of granules reaches the bottom of the bed, they fall out of the packing as a shower of particles, similar to a liquid shower.

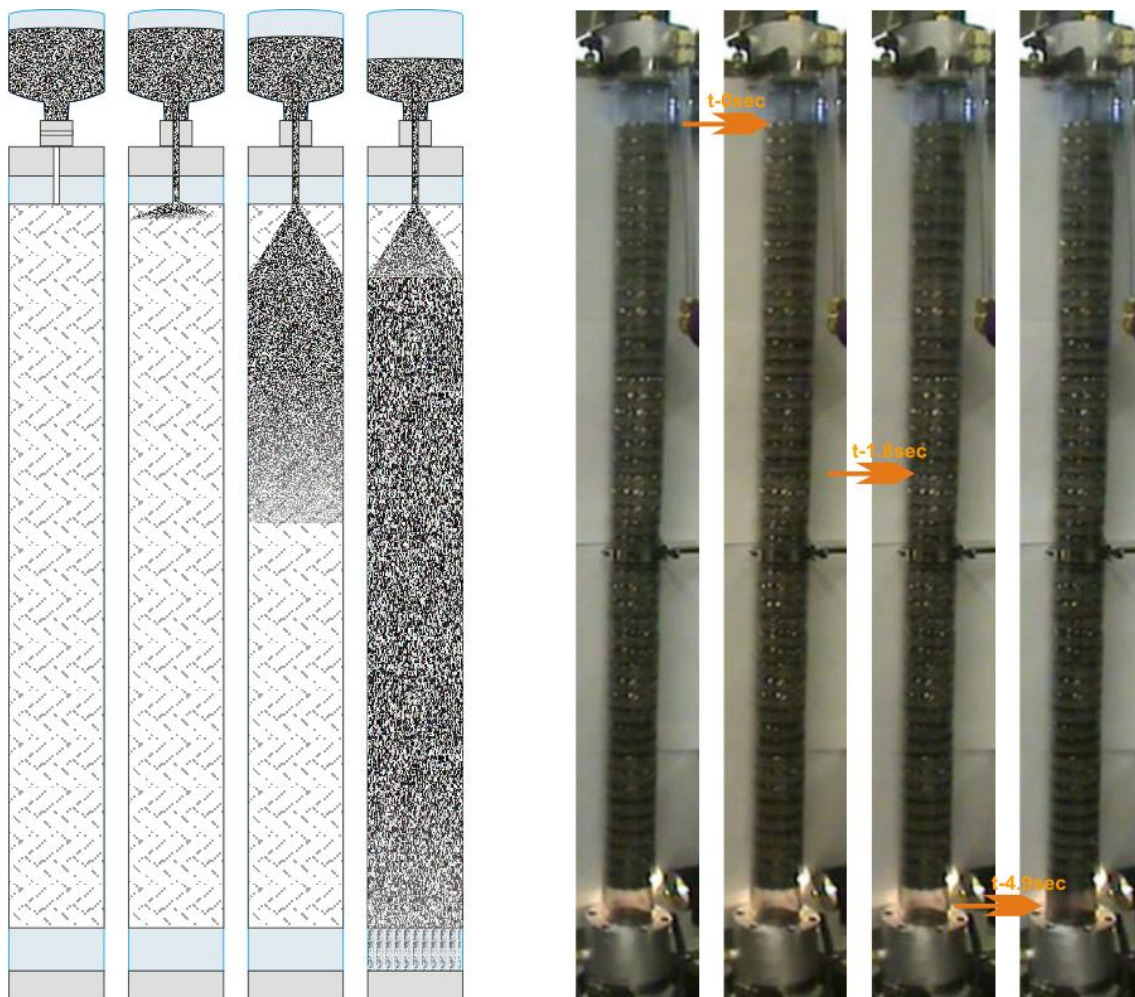


Figure V-3. Photographs of sorbent granules moving down the adsorption column.

The sorbent linear falling velocity was found to decrease as the velocity of the counter-current flow of air increases. This was expected, and it is a result of the air drag on the falling sorbent granules and a complicated interaction with the geometry of the system and the interaction among flows. The measured sorbent falling velocity varied from about 7 in/s to 3.8 in/s as the air velocity increased from 5 to 25 in/s (Figure V-4). This variation of the solid velocity will allow the solid and gas residence time to be controlled by appropriate choice of parameters such as reactor height, baffle design, and cross-section area for a given gas flow rate.

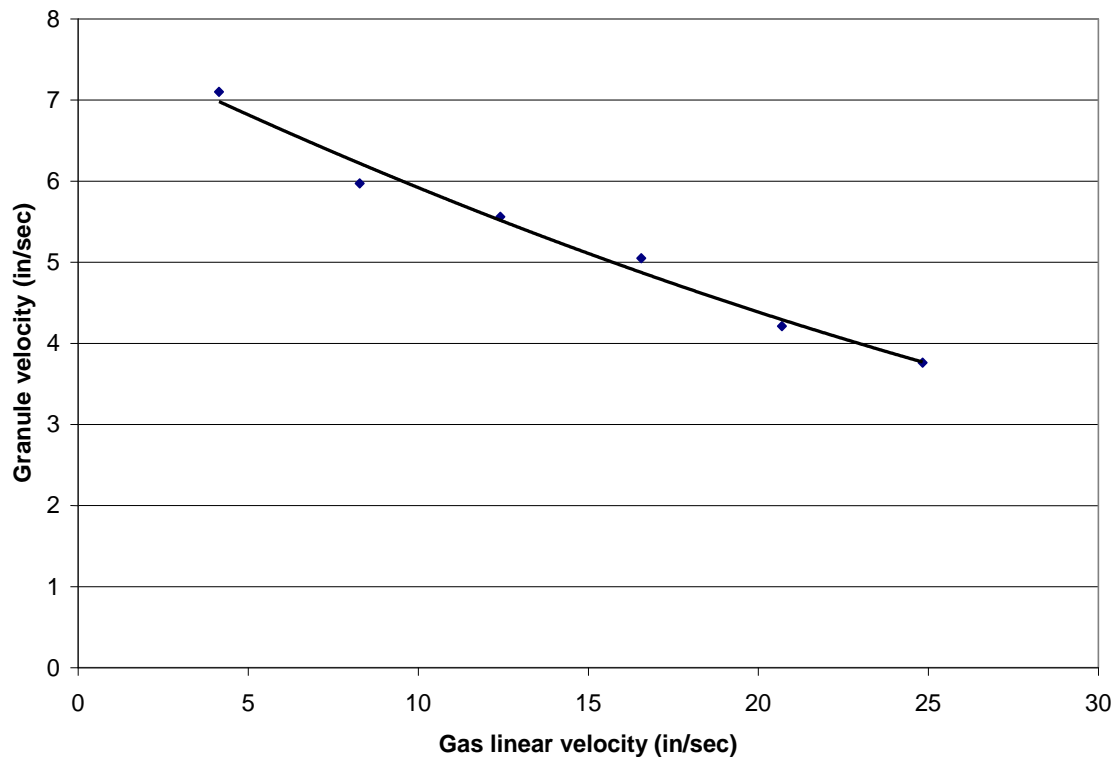


Figure V-4. Variation in sorbent linear velocity as a function of gas flow velocity.

Pressure Drop Measurements: Experiments were also performed to measure the pressure drop across the bed with and without solid flow. The measured pressure drop across the column as a function of air flow rate is shown in Figure V-5. As expected, the measured pressure drop increases with the gas flow and is somewhat higher with the counter-flow of sorbent granules. Even at an air velocity of 2.4 ft/s, the measured pressure drop is only 0.4 in H₂O/ft packing (0.014 psi/ft), a relatively low pressure drop. It is critically importance that this pressure drop is low because of the large volume of flue gas produced in a power plant. This is, therefore, a major benefit of this column design/sorbent approach.

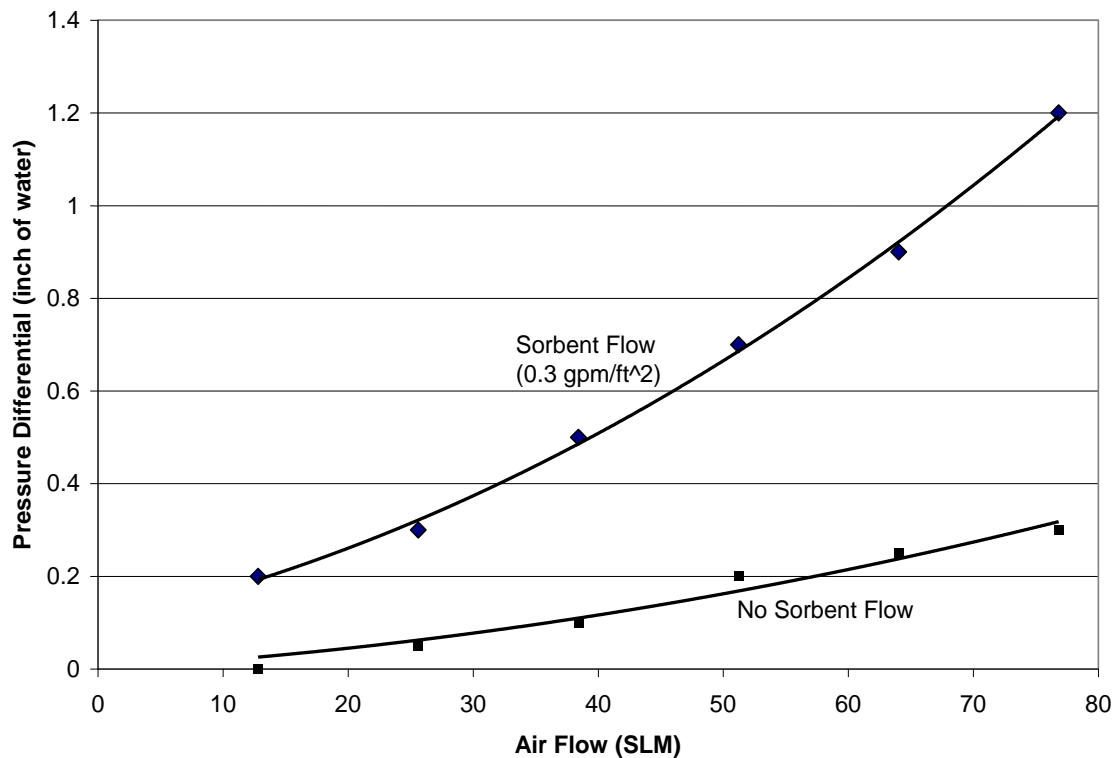


Figure V-5. Pressure drop across the adsorber column as a function of air flow rate.

Absorber Experiments: The CO₂ capture efficiency was measured as a function of the gas flow through the adsorber. In these tests, air containing 15% CO₂ was introduced initially from the bottom without a sorbent flow and allowing the outlet CO₂ concentration to stabilize at the feed gas value. The downward sorbent flow was then started, and the reduction in the outlet CO₂ concentration in the reactor exit gas was recorded. An example of the results obtained is shown in Figure V-6, in which the outlet CO₂ concentration is plotted as a function of time. In this example, more than 99% of the CO₂ was removed while the sorbent was flowing.

A series of adsorption runs were performed in which the simulated flue gas was maintained at 15% CO₂ while the total gas flow rate was increased. As gas feed rate was increased, a fraction of the CO₂ was not adsorbed and remained in the exit gas (Figure V-7).

The capture efficiency can be determined by integrating the exit CO₂ flow divided by the inlet flow. This efficiency is plotted as a function of gas flow rate in Figure V-8. The measured capture efficiency is greater than 99% for gas feed rates up to 19 SLM, above which the efficiency decreases. It can be calculated, from the previously reported adsorption isotherm data, that air stream containing 15% CO₂ at a feed rate of 19 SLM would saturate the sorbent in the reactor if all inlet CO₂ were adsorbed in the reactor. The data from these experiments confirm this prediction, indicating the adsorption isotherm data can be used in the reactor design. This capture efficiency was achieved in an adsorption column that is only 3-feet tall, reflecting the very rapid adsorption of CO₂ by this sorbent.

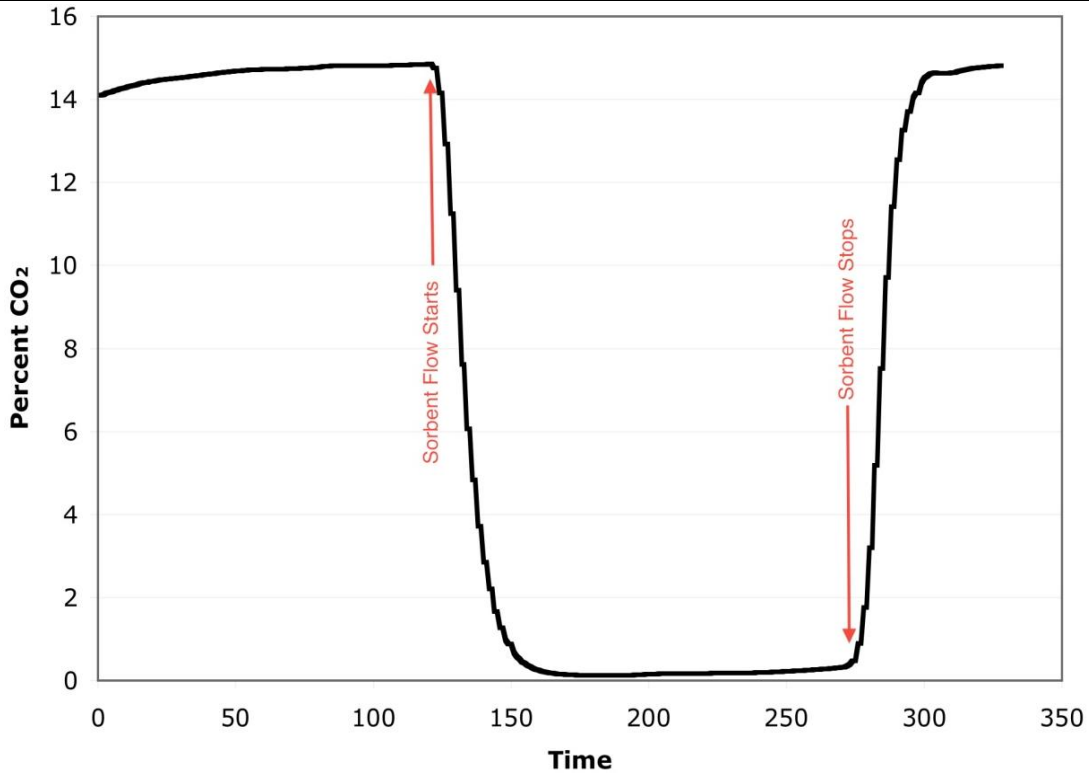


Figure V-6. Example adsorption run showing the removal of CO₂ while solid sorbent flows through the reactor. (Time in seconds)

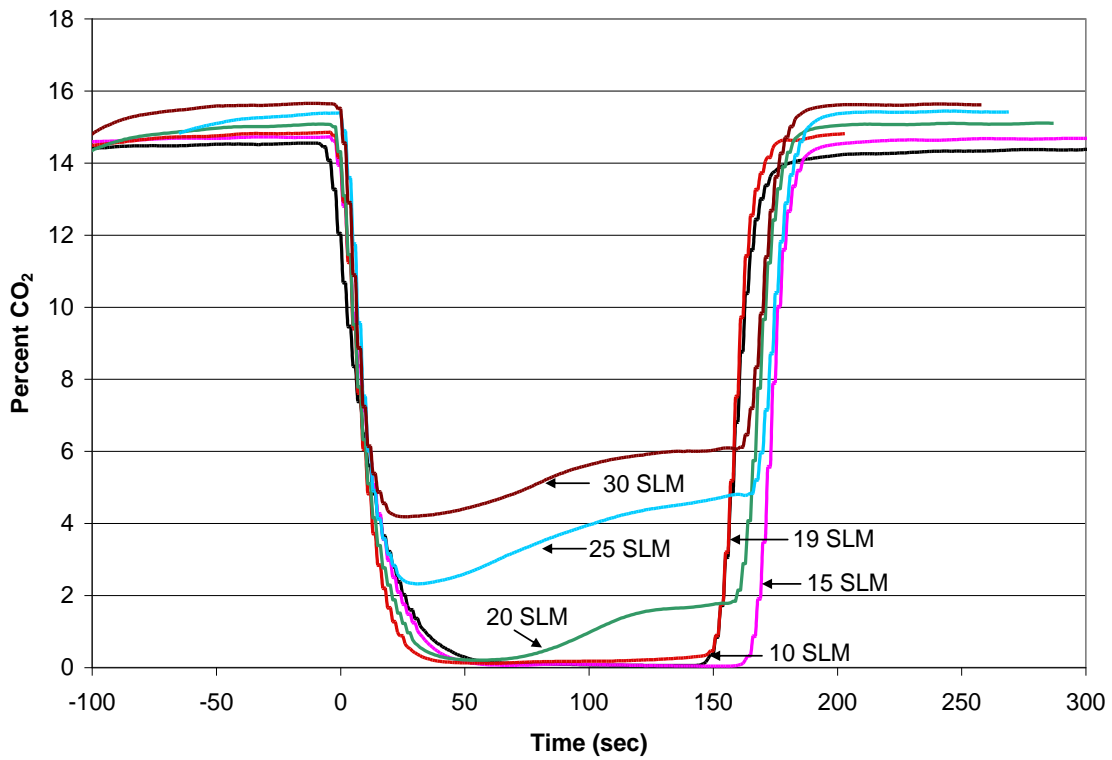


Figure V-7. The residual CO₂ concentration in the reactor exit gas at various gas flow rates.

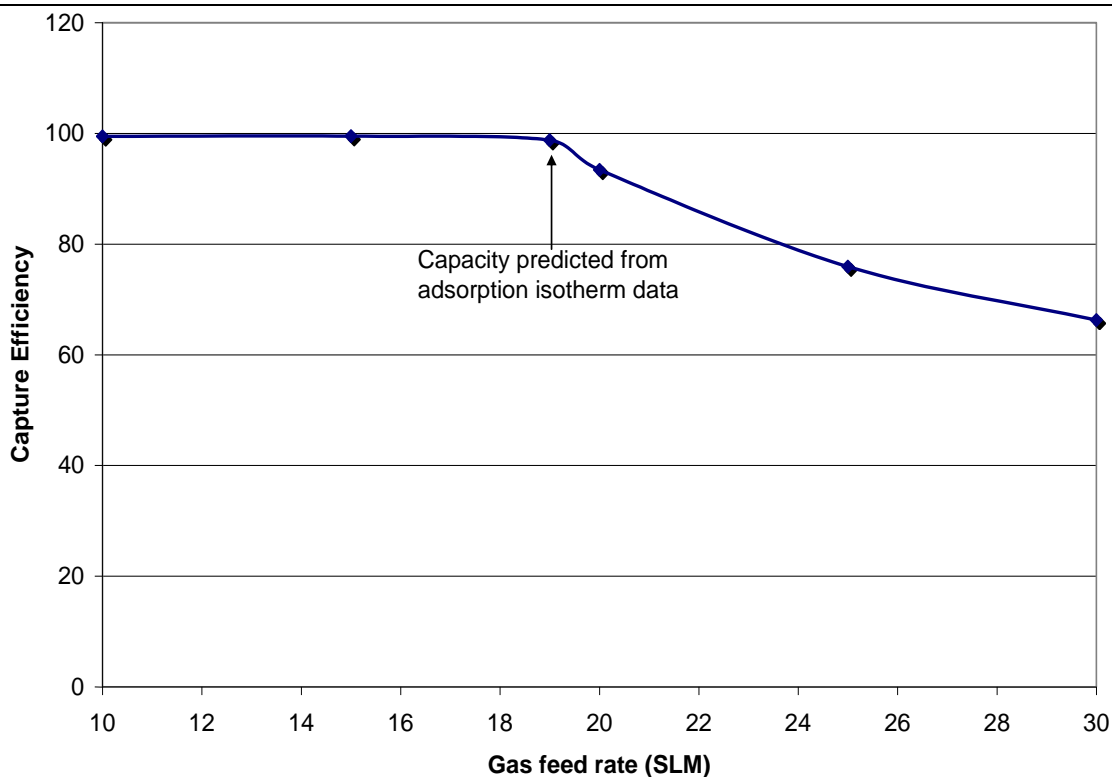


Figure V-8. Absorber section capture efficiency as a function of the simulated flue gas feed rate.

The sorption rate was also determined by a second series of adsorption experiments in which the inlet CO₂ flow rate is held constant while varying the air flow rate. In these tests, the inlet CO₂ concentration is varied. This series allowed the determination of CO₂ capture rate as a function of gas residence time for a fixed inlet CO₂ flow rate of 2.85 SLM. This value corresponds to an air stream containing 15% CO₂ flowing at a rate of 19 SLM, and the residence time will be 5.3 s. From the previous experiments, the sorbent will capture 100% of the feed CO₂ under these conditions. Figure V-9 shows the capture efficiency as a function of the CO₂ residence time in the adsorber. At a residence time longer than 5.3 s, 100% CO₂ was removed. A capture efficiency of 90% was observed at a residence time of 4.5 s. The capture efficiency decreases as the residence time becomes short, as expected.

In summary, the adsorber experiments showed that our carbon sorbent has excellent flow characteristics and can be used in a falling microbead reactor to completely adsorb CO₂ from a simulated flue gas stream. The microbead bed reactor offers a lower pressure drop for the gas flow than fixed- or fluidized-bed reactors and the low pressure drop reduces the operating cost for CO₂ capture. A commercially available stainless steel structural packing was found to be suitable to move the sorbent microbeads from top to bottom counter current to the gas flow, providing intimate contact between the gas and the solid.

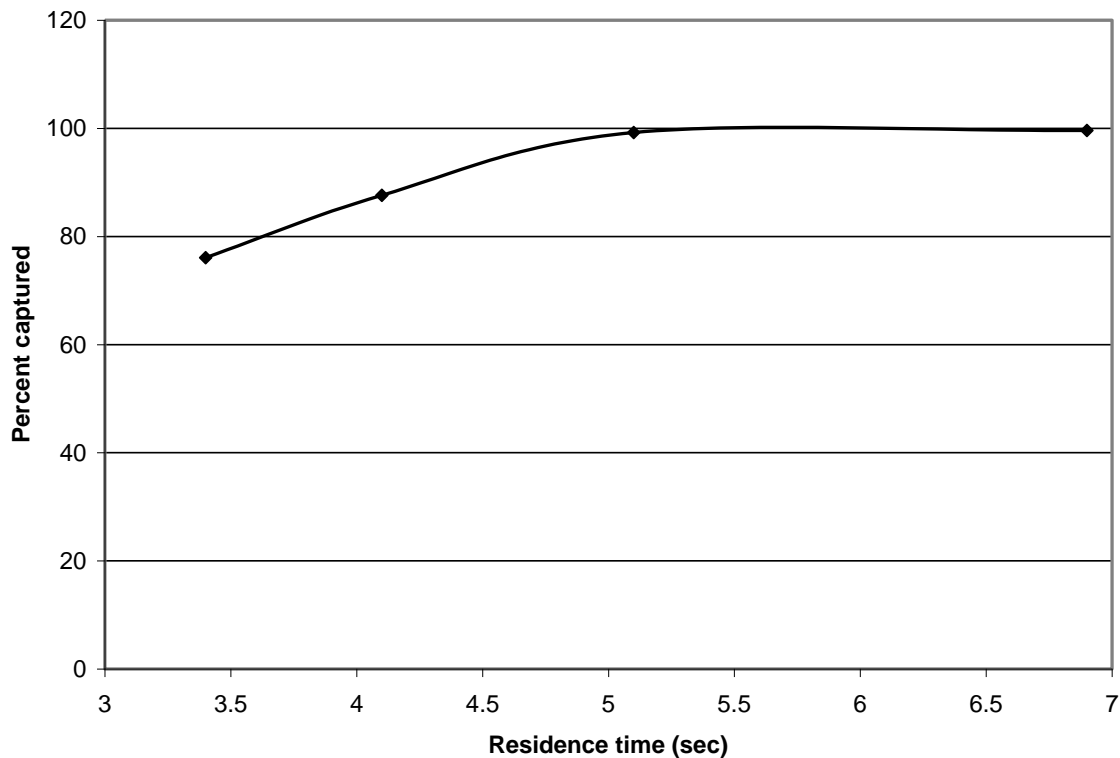


Figure V-9. Capture efficiency as a function of the CO₂ residence time in the adsorber.

Regeneration Experiments: Sorbent regeneration by using direct contact steam was tested in a 1-inch-diameter fixed bed reactor. The walls of the reactor were insulated to prevent steam condensation on the cold walls due to radial heat loss. A steam source that can meter up to 75 g/h of steam at 1 atm pressure was attached to the inlet manifold that allowed introduction of simulated flue gas, 100% steam, or a purge gas.

In the regeneration experiments, steam was introduced into the reactor at a rate of 13 g/h, and the CO₂ flow exiting the reactor was measured as a function of time. The CO₂ flow was integrated to calculate the amount of CO₂ desorbed from the bed. The sorbent microbeads remained dry and free-flowing until the steam breakthrough occurred. The steam was adsorbed into the micropores of the sorbent (displacing the adsorbed CO₂) preventing the formation of liquid water on the external surface of the granules.

Figure V-10 illustrates the CO₂ flow and the cumulative percentage of CO₂ desorbed. The data show an initial high desorption rate as the temperature of the bed increases with the initial exposure to the steam, followed by a steady desorption of CO₂ that is intentionally limited by the steam feed rate. CO₂ desorption continues until 90% of the CO₂ has been removed and steam breakthrough is observed.

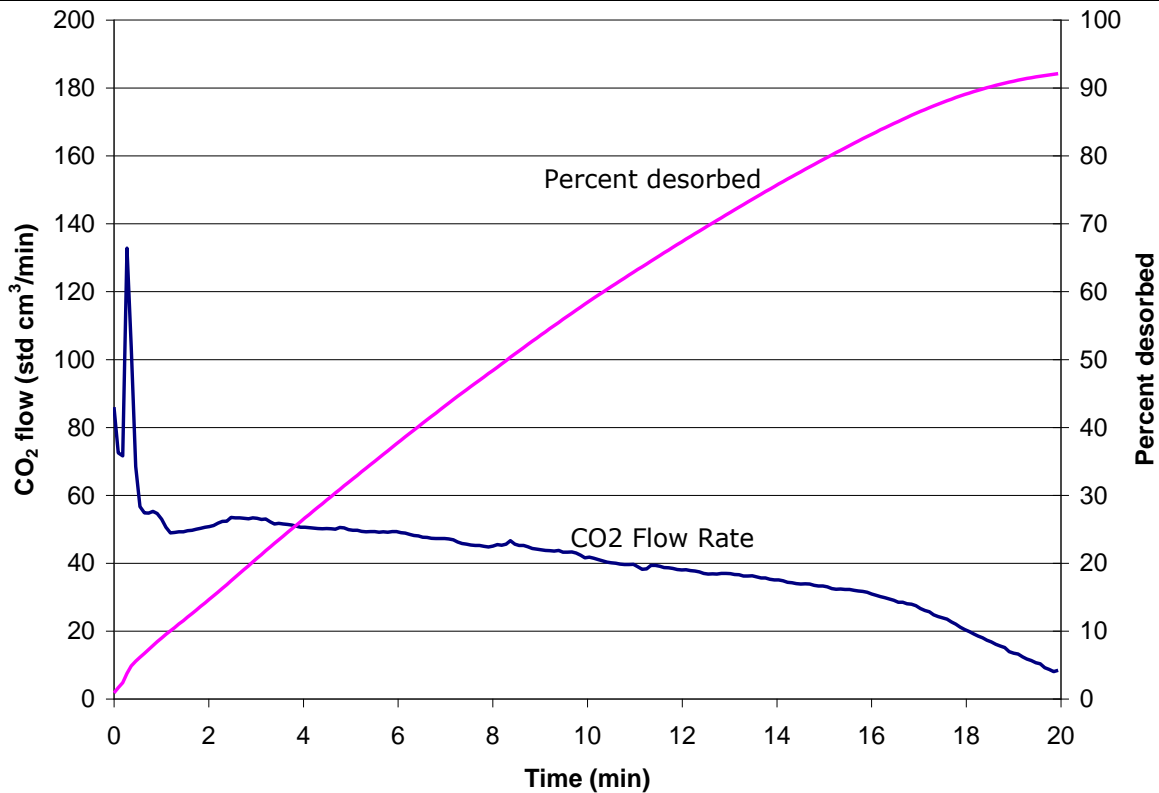


Figure V-10. Fixed bed desorption of CO₂ using direct contact heating with low-pressure steam.

The regeneration experiments showed that the adsorbed CO₂ can be rapidly desorbed by direct contact with low-pressure steam. During direct contact desorption, the temperature of the carbon sorbent rises due to the heat of adsorption of water vapor. The temperature rise is sufficient to raise the sorbent temperature to above the dew point of the steam, so the sorbent remains superficially dry and free flowing. At the elevated temperature, CO₂ is desorbed from the sorbent and any residual steam can be condensed out resulting in a pure CO₂ stream that can be sequestered.

V.4 DESIGN OF AN INTEGRATED ADSORBER-STRIPPER SYSTEM

The falling microbead reactor system enables the integration of adsorption and stripping of the CO₂ in a single vertical column (Figure V-11). The upper portion of the column functions as the absorber, whereas the CO₂ is stripped in the bottom section. The middle transition section separates the absorber and the stripper, allowing any adsorbed O₂ and N₂ to be removed before the sorbent enters the stripper section.

The sorbent microbeads fall from the top to the bottom of the column, passing first through the adsorber section, second through the transition section, and third through the stripper section. Simulated flue gas containing 15% CO₂ is fed in at the base of the adsorber section and exits, stripped of CO₂, at the top of the adsorber. As the sorbent cascades down the adsorber section, it adsorbs the counter-flowing CO₂ and a small fraction of the N₂, O₂ and other light components of the flue gas.

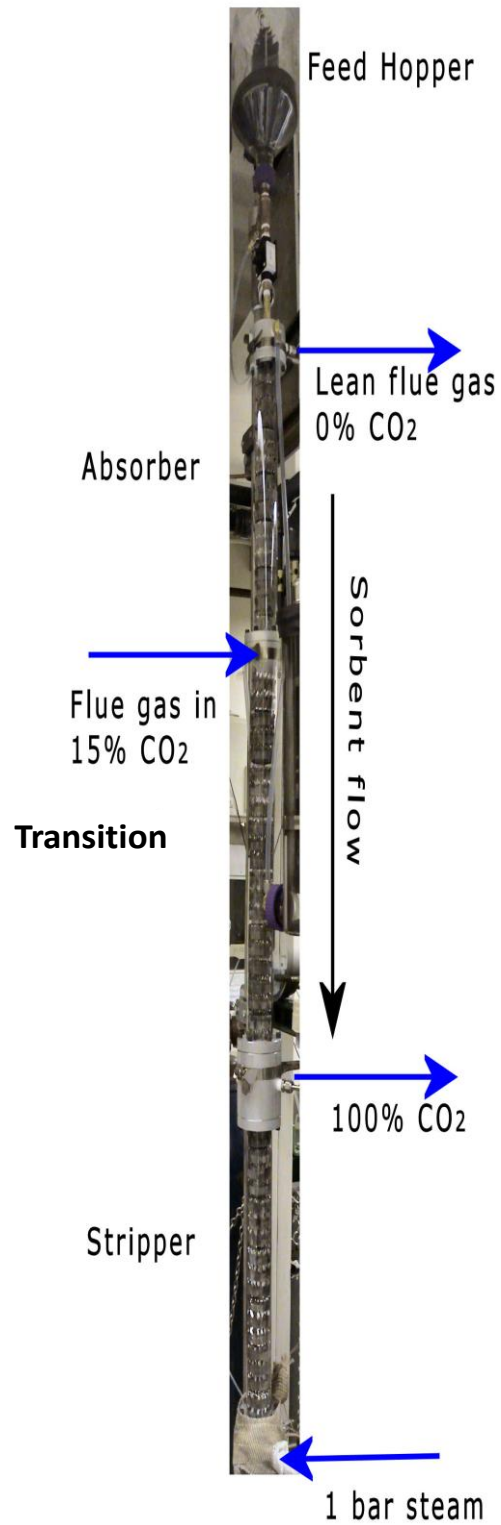


Figure V-11. Photograph of the integrated absorber-stripper system.

The transition section separates the absorber and stripper. In this section, the adsorbed N_2 and O_2 are desorbed and swept back into the adsorber section to be mixed with the CO_2 -lean flue gas stream. This is accomplished when the falling solid sorbent meets an upward flowing stream of pure CO_2 from the bottom stripper section. As the sorbent moves down the transition section, it encounters an increasing partial pressure of CO_2 and a decreasing partial pressure of the light gases. This causes the sorbent to adsorb more CO_2 and to desorb the N_2 and O_2 . At the base of the transition section, the sorbent is saturated with pure CO_2 .

The stripper operates by contacting the sorbent with steam at 1 bar of pressure. The steam is adsorbed, causing the sorbent temperature to rise, resulting in desorption of CO_2 . The steam also acts to reduce the partial pressure of CO_2 , enhancing additional removal of CO_2 . The desorbed CO_2 flows up out of the stripper, where it is extracted as the product stream of pure CO_2 .

V.5 OPERATION OF THE INTEGRATED ADSORBER-STRIPPER SYSTEM

The operation of the integrated system starts with establishing the gas flow rates for the particular experiment. The sorbent feed rate and the steam injection rate were fixed, and the flow rate of simulated flue gas and the CO_2 product stream were varied. Initially, the gas flow was continued until the column was purged and both output gas streams had a stable composition at the concentration of the simulated flue gas (15% CO_2). The sorbent flow was then started and when the cascading sorbent filled the column, the steam flow was started. The compositions of the two product streams were monitored, and the experiment was continued until a stable CO_2 composition in the product streams was established. The experiment was terminated by stopping the steam feed, allowing the sorbent to adsorb the remaining steam, and then stopping the sorbent flow.

Figure V-12 illustrates the composition of the gas leaving the absorber in a typical run. After the introduction of the sorbent, the CO_2 concentration in the absorber exit gas decreased rapidly from 14.5% to 0.3%. This decrease, after accounting for the change in the volumetric flow of the gas, corresponds to 98% CO_2 capture from the feed gas.

The corresponding composition trace of the CO_2 -rich stream from the stripper is shown in Figure V-13. On the introduction of steam into the stripper, CO_2 is desorbed from the sorbent. The CO_2 concentration in the stripper exit gas increases and attains > 90% value after about a minute. Under steady-state conditions, the CO_2 purity achieved in this run was 97%.

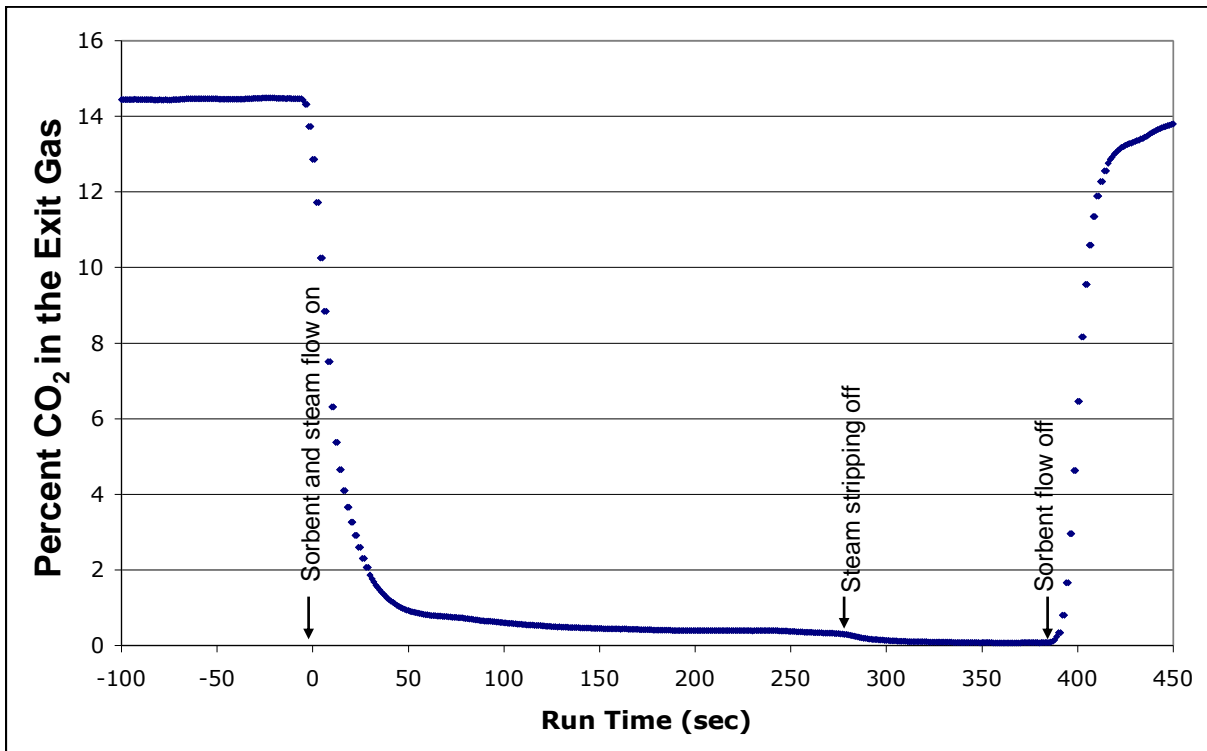


Figure V-12. CO₂ concentration in the absorber exit gas stream.

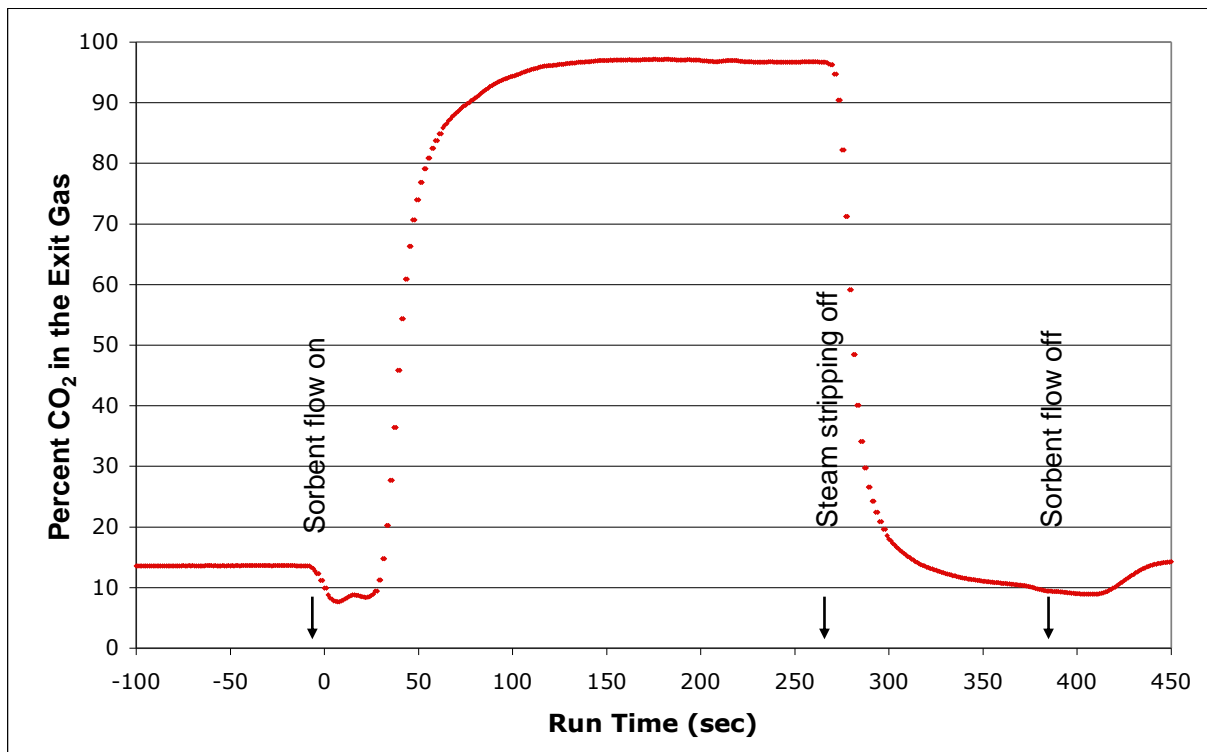


Figure V-13. CO₂ concentration in the stripper exit gas.

In the absorber section, the capture efficiency increases to 100% after the steam to the stripper is stopped (Figure V-12). This result is due to the complete absorption of CO₂ by the sorbent. When the steam is flowing into the stripper, the desorbed CO₂ passes mainly through the stripper exit. A fraction of the CO₂ also passes through the transition section to be captured by the sorbent.

The continuous operation of the steam stripper requires that the solid sorbent continues to be free-flowing, even in a high steam environment. This operation is possible because the sorbent temperature rises above the dew point of the steam as steam is adsorbed. To show this in the current column, a temperature probe was placed in the solid stream, near the location of steam injection at the base of the stripper segment. The steam is injected at a pressure of 1 bar, so the dew point is 100°C. As can be seen in Figure V-14, the temperature at that location rises initially to 110°C and stabilizes at 105°C, well above the dew point.

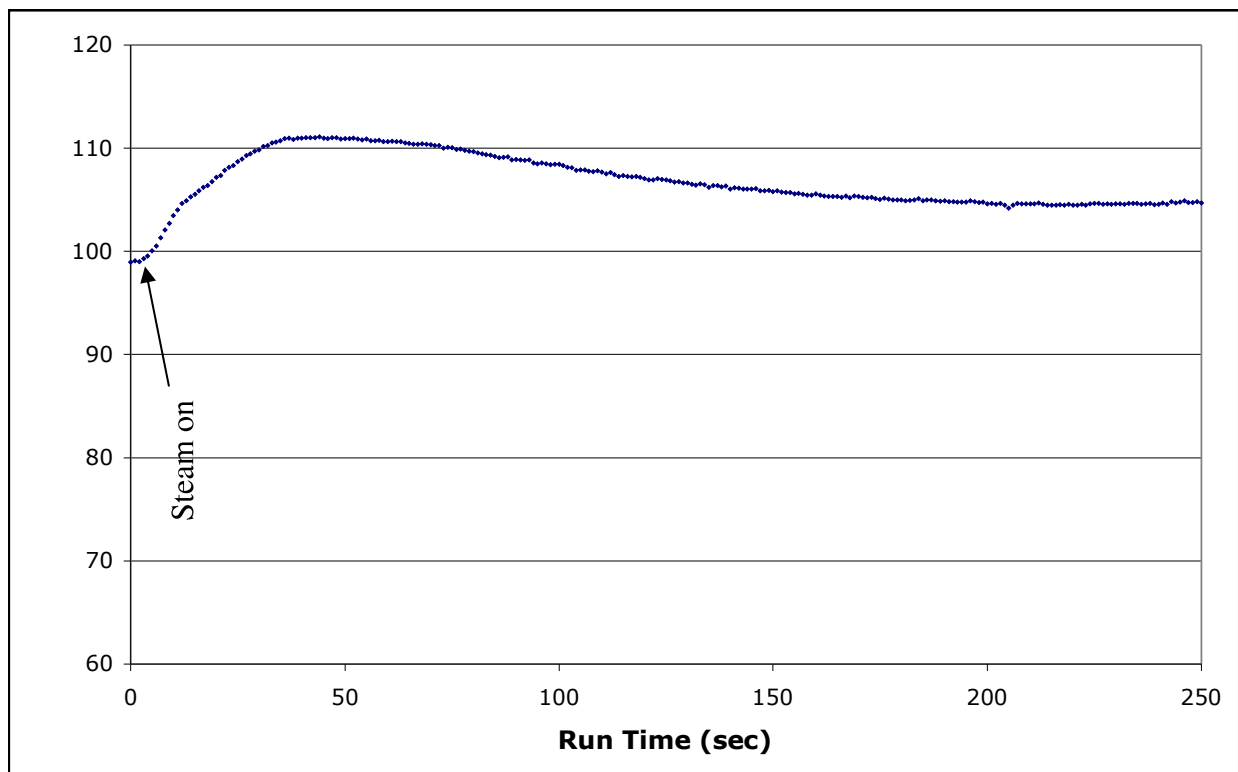


Figure V-14. Temperature rise during steam injection.

V.6 RESULTS FROM THE INTEGRATED SYSTEM

The integrated reactor system was operated to determine optimum conditions necessary to capture CO₂ from a simulated flue gas and provide a pure CO₂ gas stream that can be sequestered. The process variables include simulated flue gas flow, sorbent flow, steam flow, the exit gas flow rates. In this series of tests, the sorbent and steam flows were fixed. The residual

CO₂ in the absorber exit gas and the purity of CO₂ in the stripper exit gas are affected by both the feed gas rate and the stripper exit gas rate.

The integrated reactor was characterized by varying the input flow rate of the simulated flue gas and the output flow rate of the rich gas stream. When the stripper exit gas flow is low, more CO₂ is entering the reactor through the feed gas than is flowing out in the stripper gas. In that case, the remaining CO₂ must exit with the absorber exit gas stream. Under these conditions, the CO₂ purity is high but the capture efficiency is reduced.

When the stripper exit gas flow rate is too high, then there is not enough CO₂ entering the column to produce a pure CO₂ stream and some of the feed air exits at the stripper exit port. Then the capture efficiency is high, but the purity is low. When the stripper exit gas flow matches the input flow of CO₂ contained in the flue gas, then both high purity and high capture efficiency are achieved. High purity and high capture efficiency can only be achieved if all three segments of the column are operating efficiently. The system was operated from efficient to inefficient mode by increasing the incoming simulated flue gas flow rate. As the flow rate is increased, the gas residence time in each reactor segment is reduced until there is not enough time for the components to be separated. The optimal operating point is that where the gas flow is as high as possible to get high throughput and still have efficient separation of the CO₂.

Figures V-15 and V-16 show the measured product purity and capture efficiency for a series of runs with a gas residence time of 7 seconds. As can be seen from these two figures, high purity is achieved at low CO₂ output flow, and high capture efficiency is achieved at high CO₂ output flow. In this series, at the optimum flow rate (product/feed ratio = 1), 97% purity and 98% capture efficiency were observed.

The results shown in Figures V-15 and V-16 show that gas residence time of 7 s is enough to efficiently separate CO₂ from flue gas. However, higher feed gas flow rates or a shorter residence time would allow even higher productivity and therefore decreased cost of CO₂ capture. The capture efficiency and CO₂ purity were determined by increasing the feed gas flow until the column could no longer efficiently separate CO₂ from the feed gas. The results are summarized in Figure V-17. For each gas residence time, an optimum capture efficiency was determined while still maintaining high CO₂ purity. From these data, it can be seen that the minimum residence time is 6 seconds for the current set of process conditions. Such data is useful in the design of pilot-scale reactors.

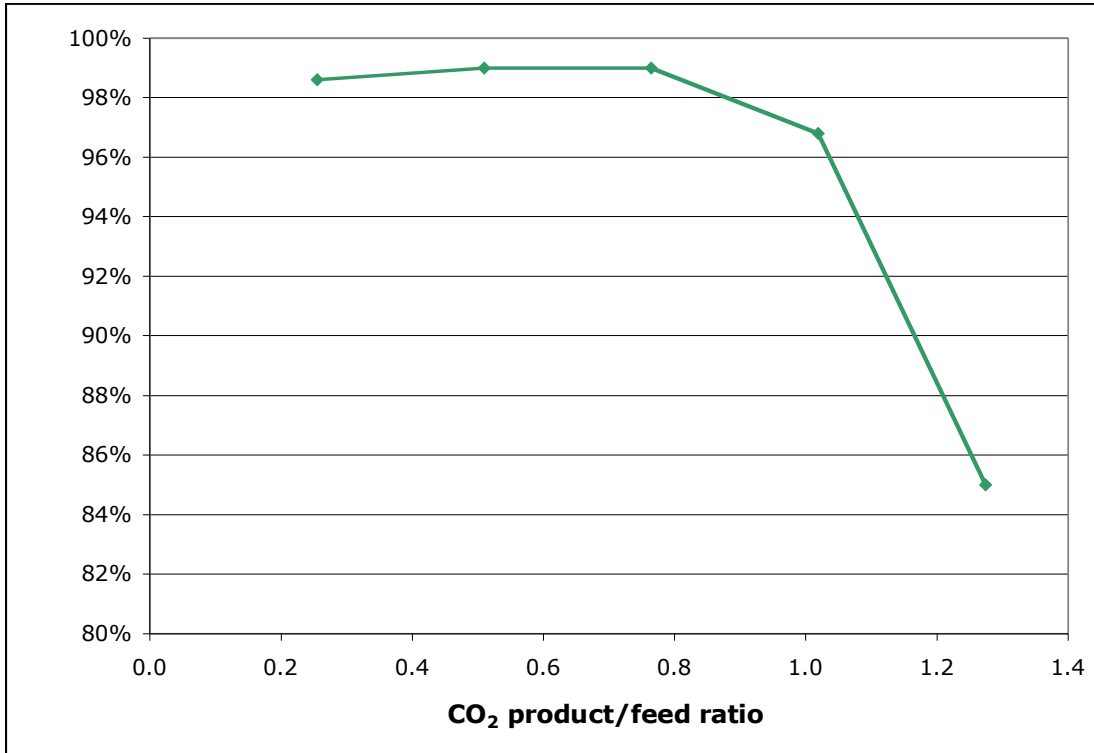


Figure V-15. Product purity vs output flow rate.

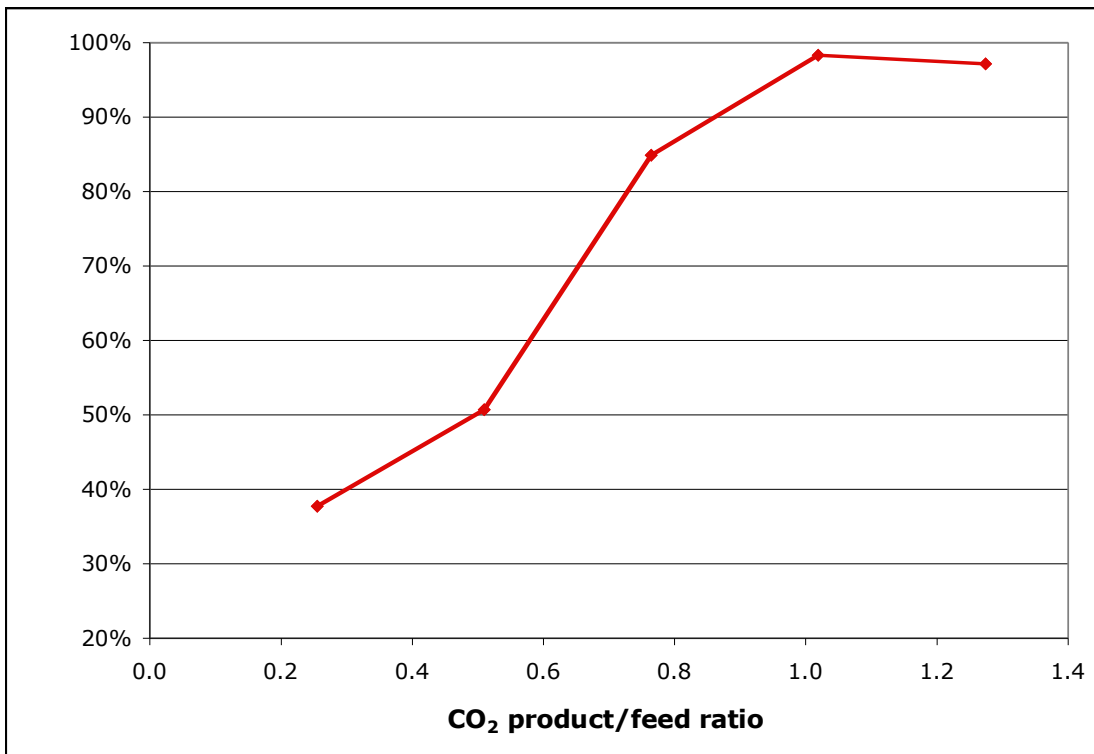


Figure V-16. Capture efficiency vs output flow rate.

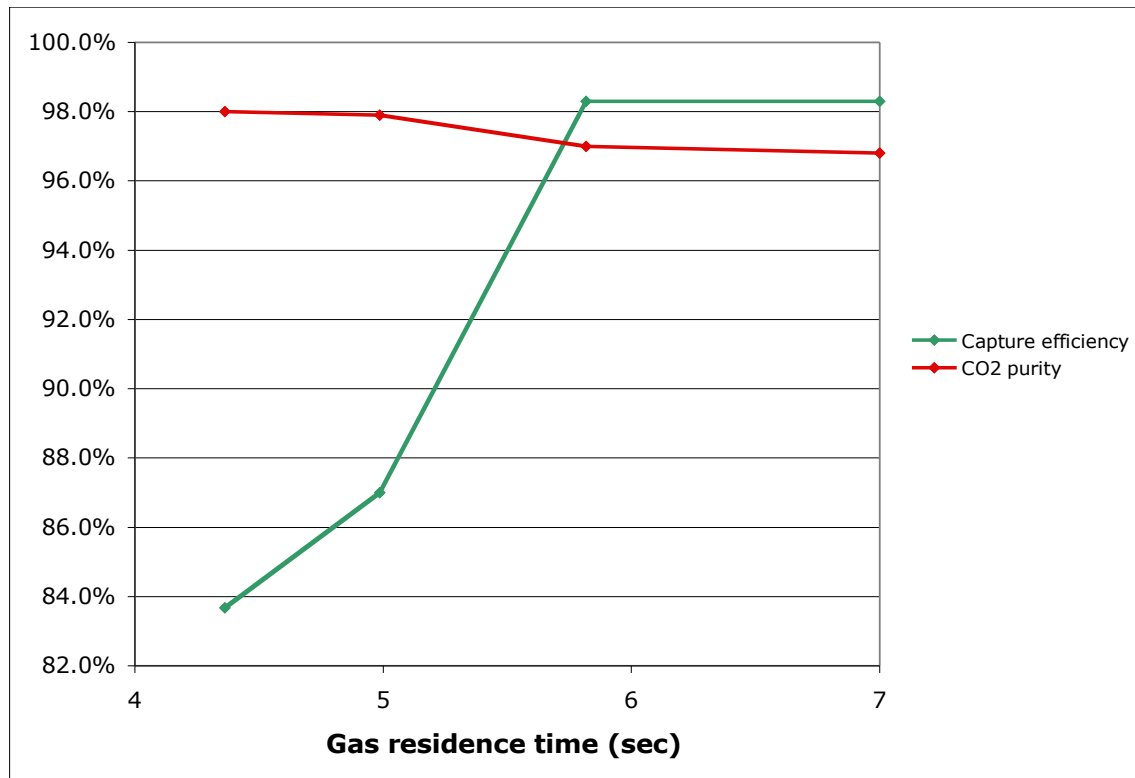


Figure V-17. Optimal purity and efficiency vs gas residence time in the absorber.

V.7 DESIGN OF A LARGE BENCH-SCALE INTEGRATED SYSTEM

We designed a large bench-scale integrated absorber-stripper system that will allow us to determine the steam consumption more reliably than in the small bench-scale system. This system will have a column of 6-inch ID compared to the previous 2-inch diameter bench-scale system. Both the diameter and the height of various sections have been increased so that it can process about 10 times more gas flow. We added a dehydration section to remove the moisture that is absorbed on the sorbent during the steam stripping. The regenerated sorbent is collected at the bottom section and is transported to the top of the absorber by a pneumatic lift.

Figures V-18 and V-19 are a schematic diagram and a photograph, respectively, of the bench-scale system. The upper portion of the column functions as the absorber, whereas the CO₂ is stripped in the middle section. Moisture absorbed during steam stripping is removed from the sorbent at the bottom section. Transition sections separate the absorber, stripper, and the dehydrator, allowing minimal intrusion between various gas streams.

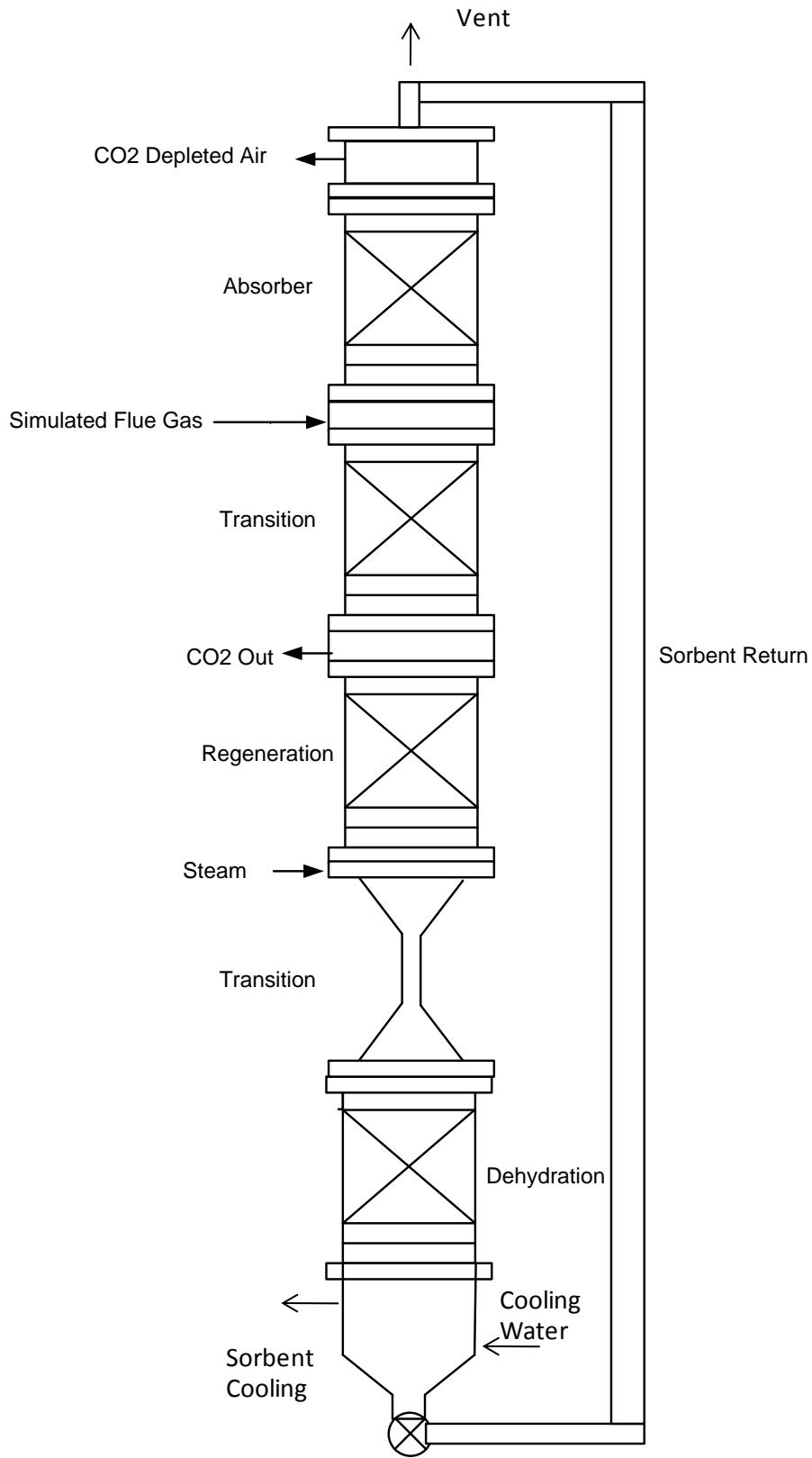


Figure V-18. Schematic diagram of the large bench-scale integrated absorber-stripper column.

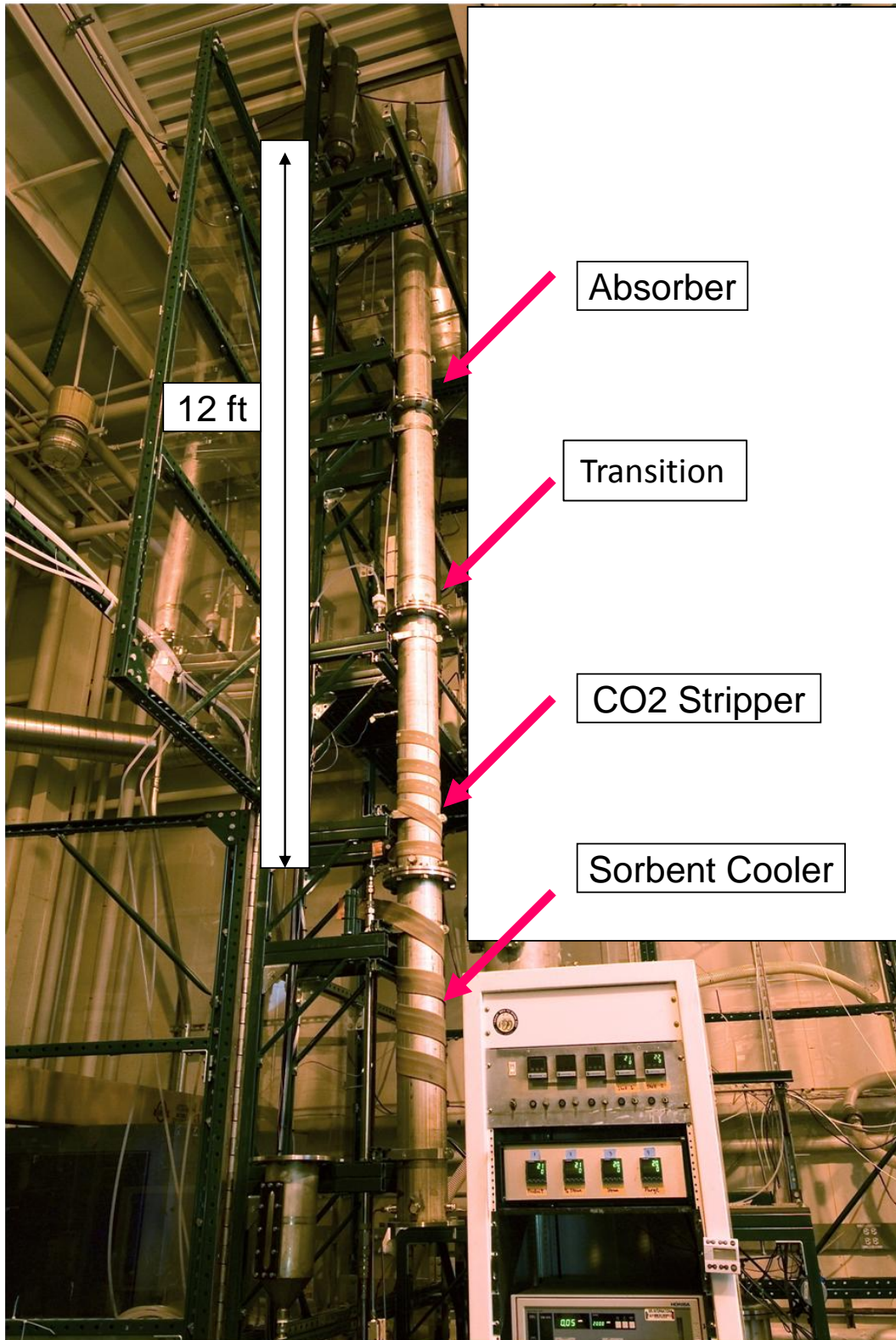


Figure V-19. Photograph of the 6-in-diameter x 20-ft-tall integrated system.

Long-term testing was performed in a 6-in-diameter by 24-ft- tall integrated system. Ambient air containing 15% CO₂ was introduced into the absorber at a rate of 50 SLPM. This up-flowing gas stream contacts the sorbent microbeads flowing down the absorber column, and CO₂ is absorbed by the sorbent. The sorbent continues to flow down, by gravity, to the stripper section (with a transition section between absorber and stripper), where it is heated by steam flowing directly into the stripper to ~ 110°C. CO₂ is desorbed from the sorbent and flows out of the stripper. The stripper walls are heated externally to 110° C to prevent condensation on the walls. The sorbent flows down from the stripper to the dehydrator in which the adsorbed water is removed by a stream of up-flowing air. This dehydration step cools the sorbent from 110°C to 60°C. The dehydrator walls are also electrically heated externally. In a commercial reactor, the evolved moisture will be condensed to recover the water. Further sorbent cooling is accomplished at the bottom of the column in a heat exchanger, in which cold water is passed through a coil. The sorbent microbeads, cooled to 30°C, are withdrawn using a screw feeder and lifted pneumatically to the top of the absorber for further CO₂ absorption. Note that the sorbent flows down by gravity in this system except for the return of the sorbent to the top of the absorber. This feature minimizes energy consumption and reduces or eliminates attrition of the sorbent microbeads.

During the initial operation of the system, some parameters were varied to determine the response of the system to changes in process variables. Several operational issues were identified and resolved. The major issues were: uneven rate of steam injection, obstruction in the screw feeder, incomplete cooling of the solid sorbent microbeads, and incomplete dehydration of the sorbent before recirculation. The adsorption and desorption kinetics were found to be slower than the design rates which was caused by the use of relatively large diameter carbon microbeads compared to the sorbent used in the 2-in bench-scale system.

V.8 INITIAL OPERATION OF THE LARGE BENCH-SCALE SYSTEM

Several tests were conducted during this series of runs. The duration of these runs varied from 1 to 4 h depending on system performance. These tests showed that the removal of the adsorbed steam in the sorbent and the cooling of the sorbent after steam stripping are influenced by the operational parameters of the system. Minor modifications were made to the system based on the results of these tests to achieve stable performance.

Run 1: During operation, CO₂ product concentration reached ~ 70%. Capture efficiency was not stable and oscillated between 40% and 70% due to condensation in the product stream entering the CO₂ flow meter. During operation, the sorbent temperature rose steadily.

Run 2: A cooling coil was added to the bottom hopper. With reduced product flow rate and reduced air purge in the steam recycler, about 85% CO₂ concentration and 50% capture efficiency were achieved (Figure V-20). The capture efficiency degraded with time as the sorbent temperature rose in the adsorption segment. The cooling coils were not as efficient as expected.

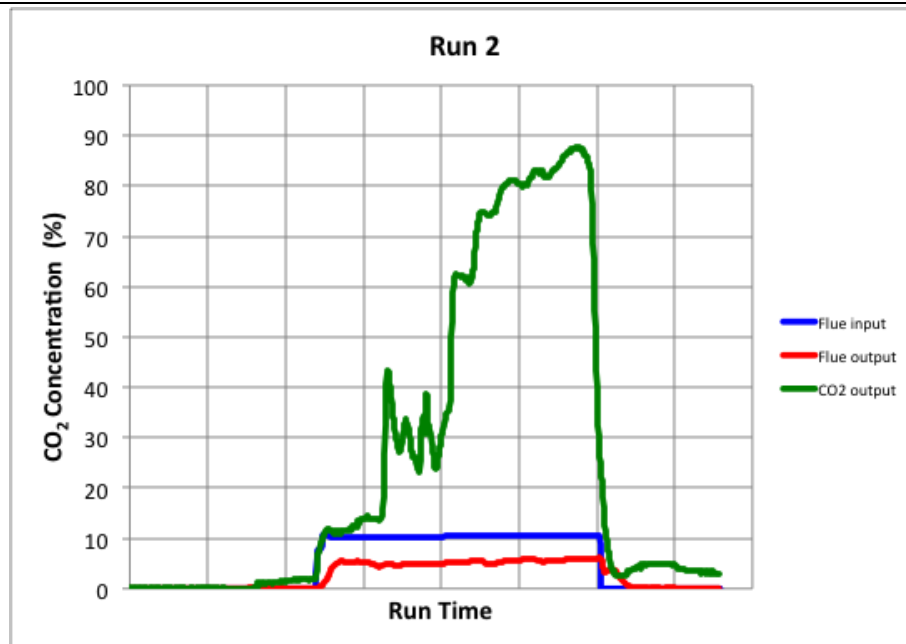


Figure V-20. System performance during Run 2.

Run 3: Results from this run showed that increased product CO₂ purity can be obtained with an increased air purge. The sorbent cooling was more efficient, but steam recycling was less efficient with the air purge at the base of the hopper. The temperature at the steam input location decreased during the run, implying that the sorbent is slowly becoming saturated with moisture and is not adsorbing enough steam to heat up to design temperature. Therefore, it was determined that an increased dehydration of the sorbent was required before it was recirculated back to the adsorber.

Run 4: Both the capture efficiency and product purity initially were better than in Run 3, but the solid flow became unstable due to moisture condensation in the base of the hopper. Near the end of the run, the capture efficiency was comparable to that of Run 2, but CO₂ purity was lower than that in Run 2. Condensation in the hopper indicated that moisture is not effectively being removed from the sorbent, and that the cold wall of the hopper is causing condensation.

Run 5: In this run, the simulated flue gas input rate and the solid recirculation rate were reduced to decrease the heat load to the system. We increased the residence time of the sorbent in the hopper to allow better desorption of moisture. The sorbent recirculation became stable; however, the sorbent was still not completely cooled before recirculation, so capture efficiency and CO₂ purity degraded during the run (Figure V-21).



Figure V-21. Performance of the system in Run 5.

Runs 6 and 7: The system was operated without external heating of the steam-stripping and steam-recycling segments. This configuration reduced the heat load on the solid and prevented the solid temperature from rising during the run. Both runs had significant problems with sorbent flow due to water condensation on the walls.

Run 8: The sorbent dehydrator and cooling sections were modified to improve their performance. Parametric tests with the air flow through the dehydrator showed that when the air flow through the dehydration segment is too high, evolved steam causes the sorbent microbeads to fluidize, dumping all the sorbent through the down-comer tube. The tests also showed insufficient cooling of the sorbent.

Runs 9 through 12: The dehydrator and the sorbent cooling section operations were optimized. At the end of this series of runs, we achieved a stable capture efficiency and product CO₂ purity with smooth flow of the sorbent through the integrated system.

Run 13: The air purge rate, steam feed rate, dehydration air flow rate, and sorbent feed rate were varied, and the conditions were determined for obtaining 60% capture efficiency and 75% CO₂ purity. No operational problems were identified that will limit continuous operation, allowing the system to operate under a consistent set of operating conditions. This optimization allowed the operation of the system for a cumulative 25 hours of operation to complete the first 50 h of operation with the integrated system (Figure V-22).

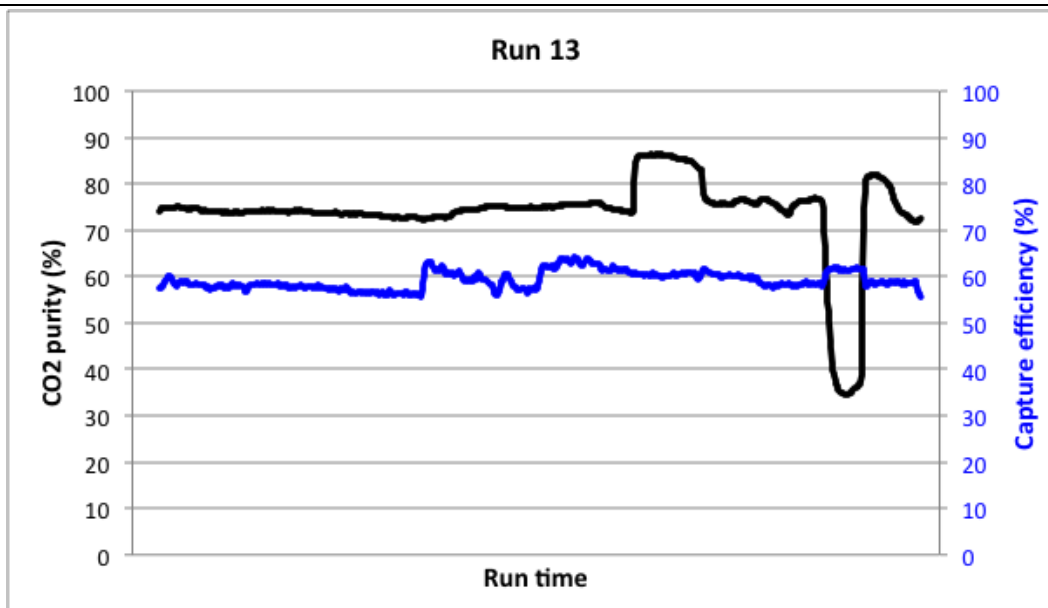


Figure V-22. Results of Run 13 showing stable operation without loss of capture efficiency.

V.9 STABLE OPERATION OF THE BENCH-SCALE SYSTEM

During the second 25 h of operation, the system was operated under a set of constant conditions to determine if there was any degradation of the performance with time. These runs were performed during normal working hours, and the system was kept idle during the evening and nighttime. During any particular run, a stable performance was obtained for ~ 30 adsorption/desorption cycles. The sorbent was not changed for the entire series of runs (52 h total), and the microbeads did not show any mechanical or chemical degradation. Figure V-23 shows the results from the final 25 h of cumulative operation in this series. The capture efficiency and the CO₂ purity achieved are ~ 35% and ~ 65%, respectively. This series of runs represents about 250 cycles of adsorption and desorption for the sorbent. From these data, the sorbent adsorption and desorption characteristics were concluded to be stable, and the sorbent was not adversely affected by repeated heating and cooling, contact with steam, or reaction with CO₂.

Based on the results of these tests, three issues (sorbent microbead diameter, incomplete dehydration of the sorbent after steam stripping of CO₂, and incomplete cooling of the sorbent before recirculation) were identified to be the cause of the capture efficiency and CO₂ purity to be less than that achieved in the 2-in bench-scale reactor system. First, the sorbent microbeads that were manufactured for the 6-in reactor have a larger diameter (0.5 mm vs. 0.2 mm) than those used in the 2-in reactor. This large sorbent size was chosen to allow larger linear gas velocity without sorbent entrainment.

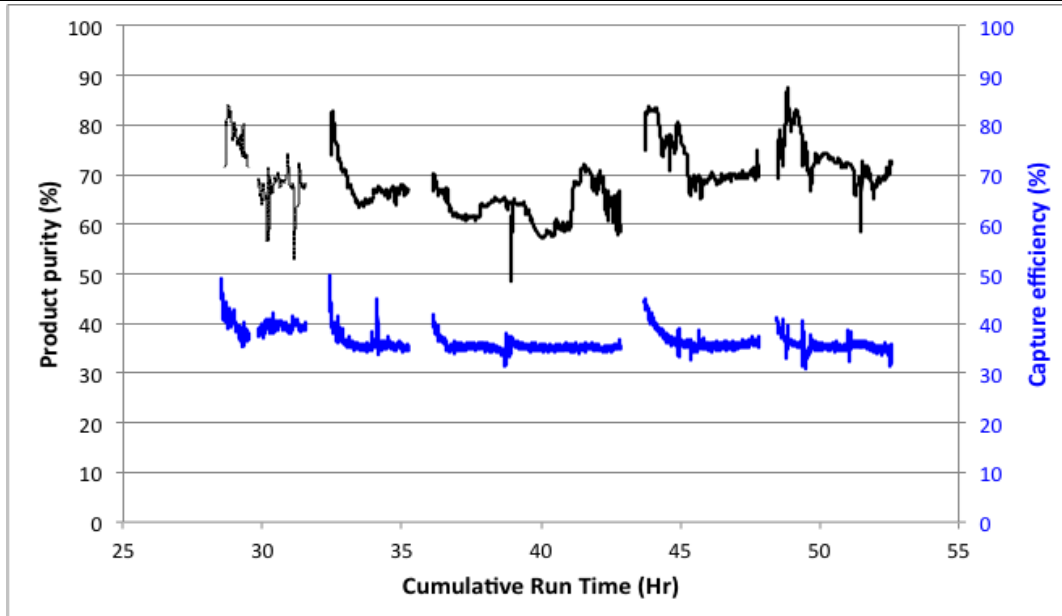


Figure V-23. CO₂ product purity and capture efficiency during 50-h test of the integrated system.

Increased air linear velocity is desirable because it increases the throughput of the column and therefore decreases the system capital cost. However, we found that the adsorption and desorption kinetics are pore diffusion limited, so the increased granule diameter resulted in incomplete capture of the CO₂ with the limited height of the adsorber column. Another batch of sorbent was obtained with a smaller granule size, and it was tested this sorbent in the 6-in column. As shown in Figure V-24, the CO₂ purity improved from 60-70% to 80-90%, and the capture efficiency increased from 35% to 60%. The remaining two issues are incomplete dehydration of the sorbent after steam stripping of CO₂ and incomplete cooling of the sorbent before recirculation. The limited modifications we made during the 50-h test series demonstrated that the performance improved with improved dehydration and sorbent cooling.

At the conclusion of the 50-h test series, the fines collected in the exhaust filter were retrieved and characterized. If the sorbent microbeads lose mass due to attrition, fines are generated and carried out with the flue exhaust. Therefore, the mass of fines collected gives a measure of the attrition rate of the sorbent. The mass of fines was 0.2% of the mass of sorbent. If those fines were created by attrition, then that would represent a lifetime of more than 3 years. Microscopic examination of the fines showed that more than 95% are intact spherical microbeads as manufactured (Figure V-25). No rough surfaces indicative of fracture were readily apparent. Therefore, the actual attrition rate is much less than just estimated. In that case, the mechanical attrition rate is so small that it is irrelevant and will not contribute to the cost of CO₂ capture in this process.

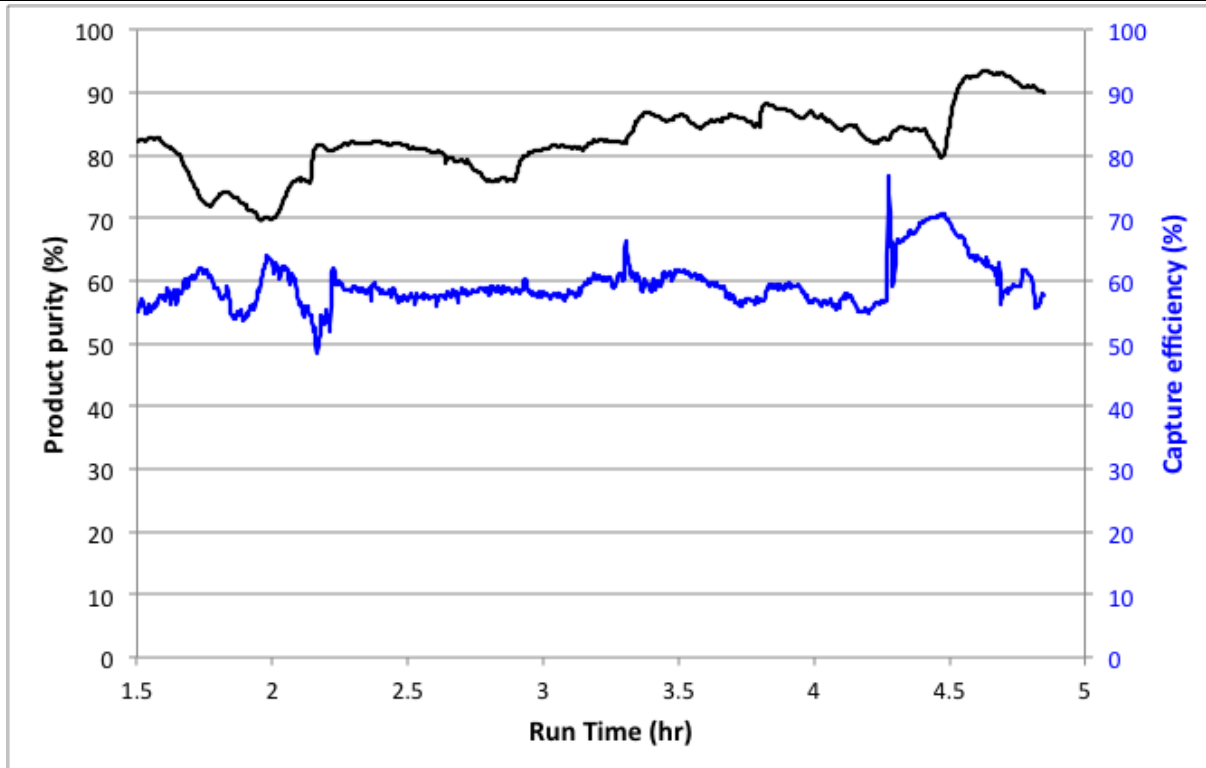


Figure V-24. CO₂ product purity and capture efficiency using reduced granule size sorbent.

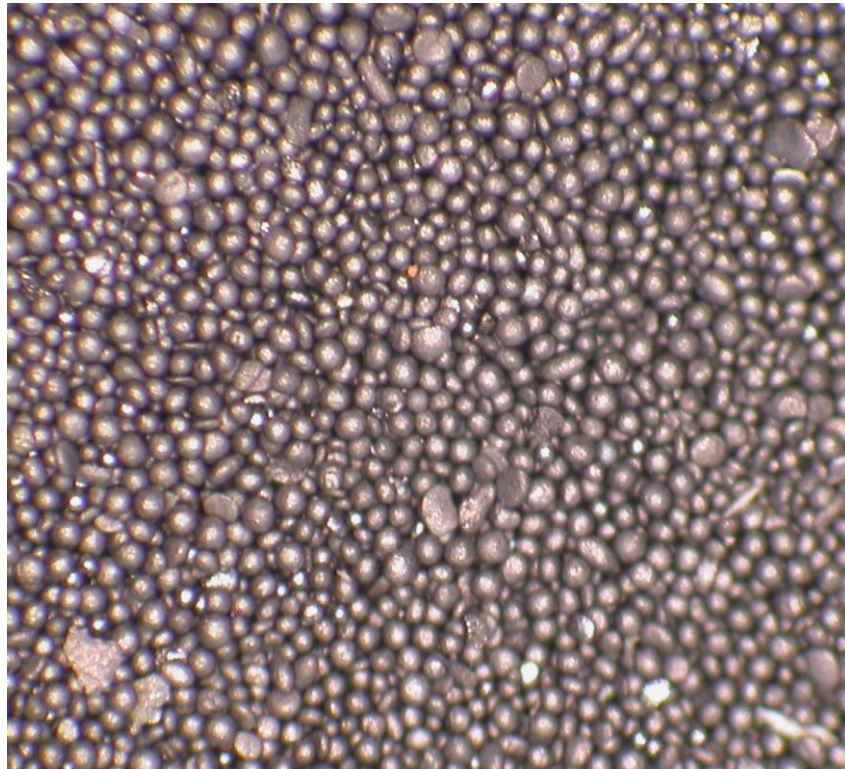


Figure V-25. Photograph of fines recovered from exhaust filter at end of 50-h test series.

V.10 LONG-TERM TESTING

Long-term tests were conducted with the integrated bench-scale system after minor modification of the system and the operating procedure. About 1,000 cycles of absorption and regeneration were completed at a total operational time of 210 h. The system was operated intermittently with test durations varying from 8 to 30 h with the system usually shut down overnight. The same batch of sorbent microbeads was used in these tests.

Figures V-26 and V-27 illustrate the CO₂ capture efficiency in the absorber and the CO₂ purity of the stripper exit gas. About 80% of the CO₂ was absorbed in the absorber section. The capture efficiency can be improved further to >90% by increasing the height of the absorber. A tall absorber was not feasible because of the height limitation in the building. As the process develops further, the absorber can be made taller, especially at an outdoor location near a PC-fired power plant.

The product gas leaving the stripper contained mostly CO₂ at a concentration of ~80% v/v. The remainder of the gas is mainly air that is not removed in the transition section, again due to the height limitation of the current transition section. If both absorber and transition sections are made taller than the current unit, we expect to produce a CO₂ stream with about 98% purity.

In general, the operation of the system became more efficient as the test proceeded, presumably due to the experience gained in the operation of the system. Only one operator was needed to monitor the operation.

The CO₂ absorption isotherms of the sorbent microbeads were measured with the fresh microbeads after the 1,000-cycle tests to determine whether the CO₂ adsorption characteristics of the sorbent had changed (Figure V-28). The adsorption isotherms were nearly identical, indicating that the sorbent did not degrade during the long-term test.

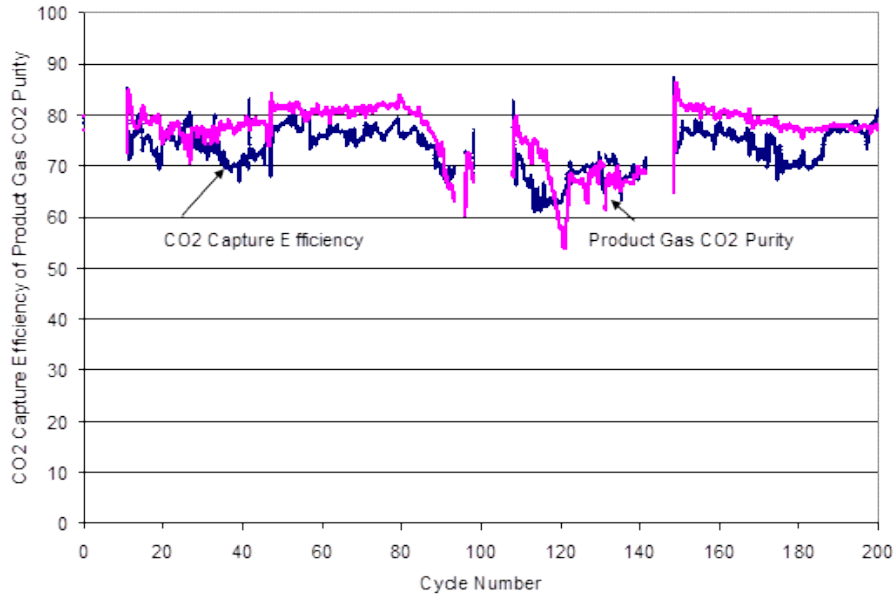


Figure V-26. Efficiency of CO₂ capture and purity of the product gas leaving the stripper in the first 200 cycles.

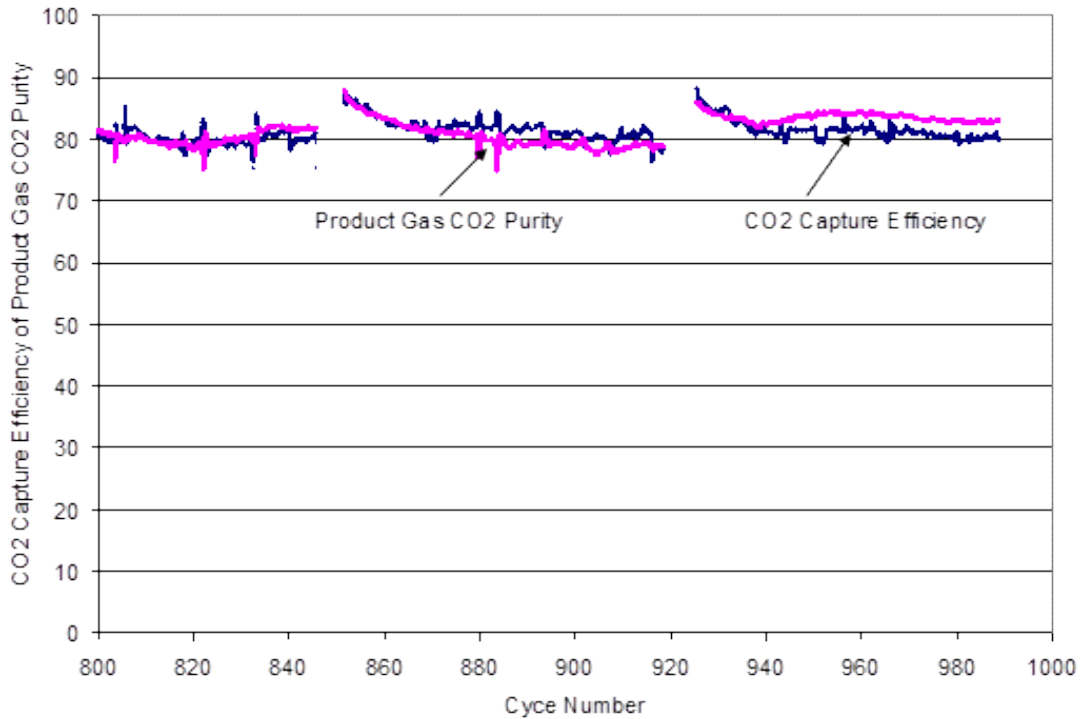


Figure V-27. Efficiency of CO₂ capture and purity of the product gas leaving the stripper in 800 to 1,000 cycles.

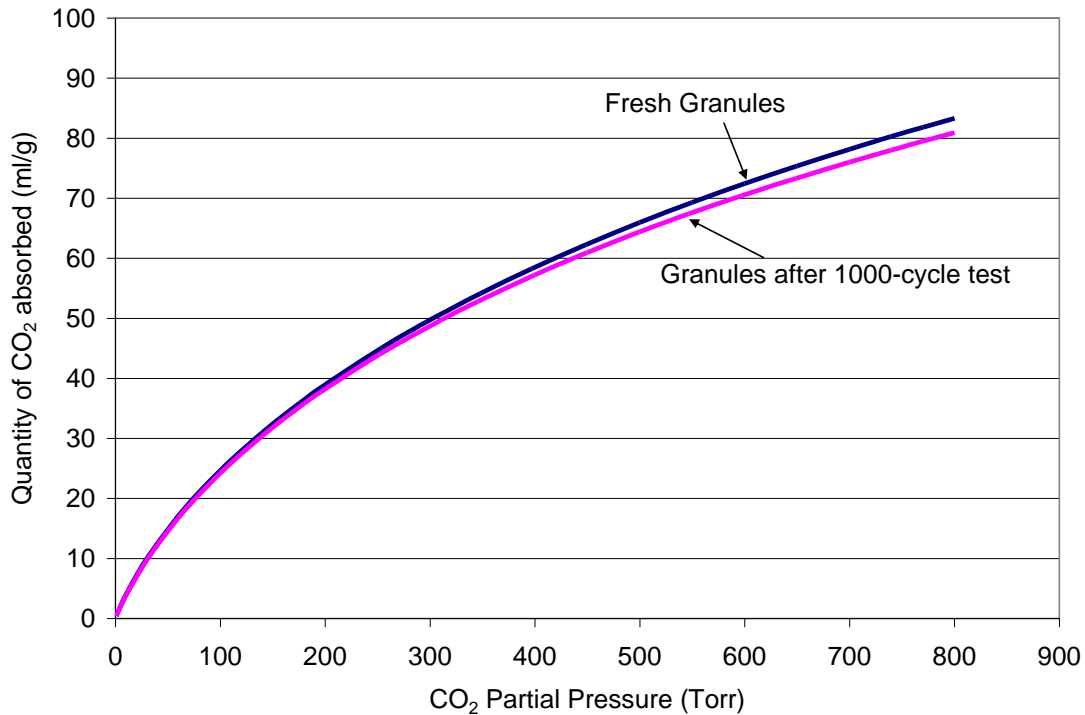


Figure V-28. CO₂ absorption isotherms of the sorbent before and after the 1,000-cycle test.

As noted previously, the CO₂ capture efficiency in the integrated 6-in reactor was about 80%, primarily due to the short height of the absorber section. A secondary reason for the decreased absorption efficiency was that the sorbent microbeads fed to the absorber were at a slightly higher temperature of ~ 35 to 40°C, primarily due to an inefficient sorbent cooler. The sorbent cooler unit was modified to improve its efficiency. The hot sorbent microbeads from the stripper section were dehydrated and cooled to ~ 25 to 30°C in a water-cooled heat exchanger. The adsorber height was also increased by 15% when the new sorbent cooler was installed. These changes allowed achievement of 95% CO₂ capture efficiency with a high purity gas that was ~ 98% CO₂ leaving the stripper (Figure V-29). Note that the data were obtained with the same sorbent microbeads that were tested for 1,000 cycles.



Figure V-29. Steady-state CO₂ capture efficiency and product gas CO₂ purity after improvements.

VI. FIELD TEST OF THE ADVANCED CARBON SORBENT PROCESS

Based on the successful results of the long-term tests, it was decided to test the process with the flue gas stream from an operating coal combustor. The field tests were conducted at the University of Toledo (UT) in Toledo, OH. The field test was performed with the same bench-scale unit used for the long-term (1,000 h) tests. The heights of the adsorber and the transition units were increased to take advantage of the outdoor location.

VI.1 INSTALLATION OF THE INTEGRATED REACTOR SYSTEM AT THE UNIVERSITY OF TOLEDO

The UT campus has three coal-fired steam boilers to provide steam and power to its Health Science Campus. The stoker boilers have a capacity of 100,000 lb/h steam and use low-sulfur coals as the fuel. One such boiler was operated between the middle of January 2012 and February 2012 at a rate of 15,000 lb/h of steam. The flue gas from the boiler is sent to an electrostatic precipitator and then to a chimney. No flue gas desulfurization or nitrogen oxide control was practiced by the boiler facility. UT allowed SRI to use a slip stream of the flue gas from the coal-fired boiler to field-test the CO₂ capture using the advanced carbon sorbent.

The 6-in-diameter, 45-ft-tall integrated reactor assembly was installed next to the flue gas chimney of the steam boiler (Figure VI-1). The installation was completed in ~ 2 weeks. This short duration was feasible with the excellent help of the UT Facilities staff and the dedication of SRI technical staff.

A schematic diagram of the integrated assembly is shown in Figure VI-2. From top down, the assembly consists of: (1) exhaust gas vent filter, (2) sorbent feed inlet, (3) adsorber, (4) flue gas inlet, (5) transition section, (6) product gas outlet, (7) stripper, (8) rotary valve, (9) dehydrator and sorbent cooling section, and (10) screw feeder for re-circulating the sorbent microbeads to the top of the adsorber. Photographs of some of these units are shown in Figures VI-3 through VI-6.

VI.2 OPERATION OF THE SYSTEM WITH THE FLUE GAS AT THE UNIVERSITY OF TOLEDO

The UT Energy Center's stoker-fired coal boiler was operated from January 16, 2012 to provide supplemental steam to the University Medical Center. About 200 liters/min (STP) of the flue gas from the chimney was diverted to the bench-scale system to capture the CO₂ present in the flue gas. The flue gas from the boiler contained about 4.5% CO₂ and 60 ppm SO₂. We believe that the low value of the CO₂ concentration is due to the stoker boiler operating with considerable excess air. The flue gas stream was cooled, and SO₂ present in the gas was removed in the sodium bicarbonate desulfurization unit. The gas was then passed through the adsorber to capture the CO₂ present in it. Table VI-1 summarizes the nominal values of the parameters used in the field test at the UT boiler site.



Figure VI-1. The integrated reactor installed at the University of Toledo boiler site.

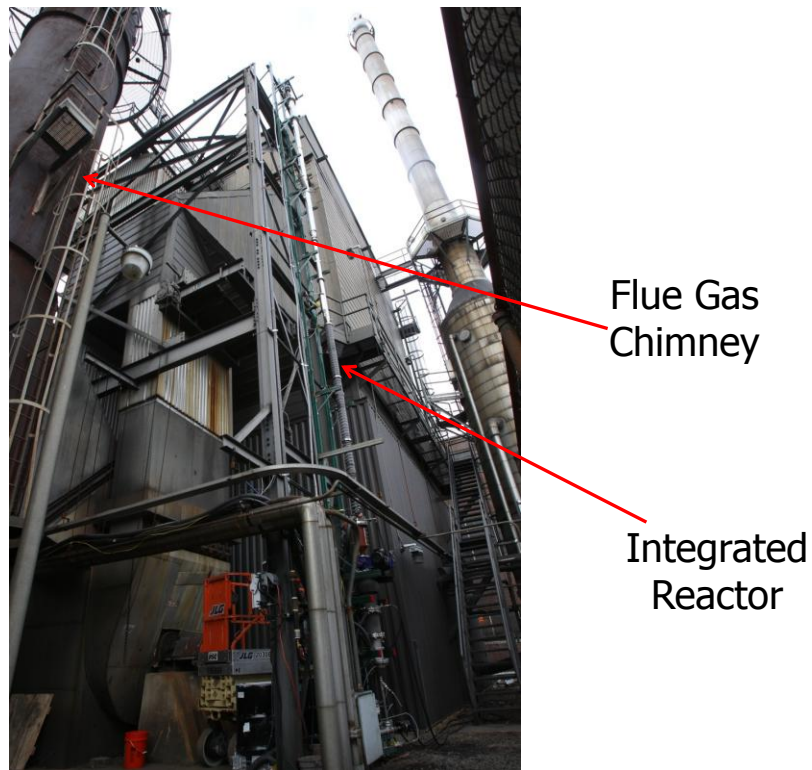


Figure VI-3. A photograph of the of the integrated reactor assembly.

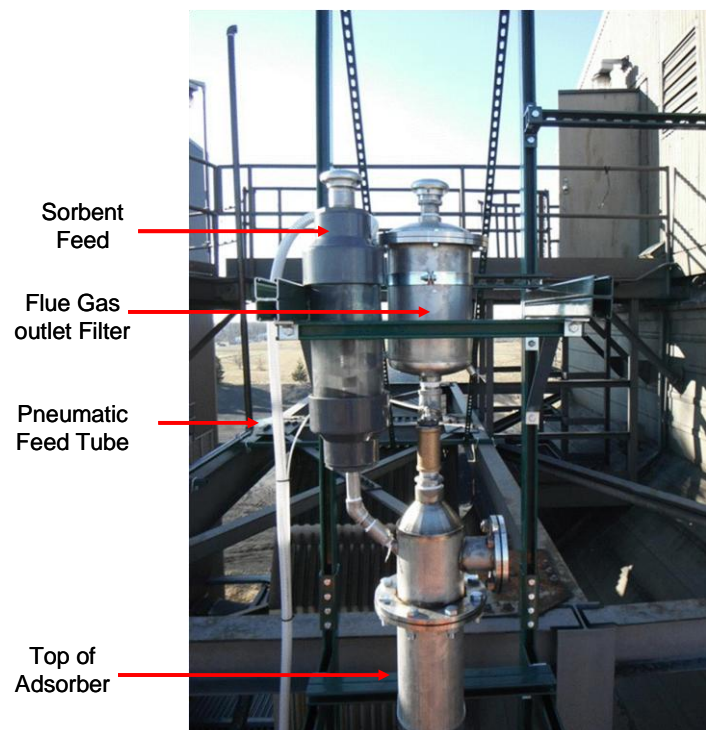


Figure VI-4. A photograph of the sorbent inlet and flue gas outlet sections.

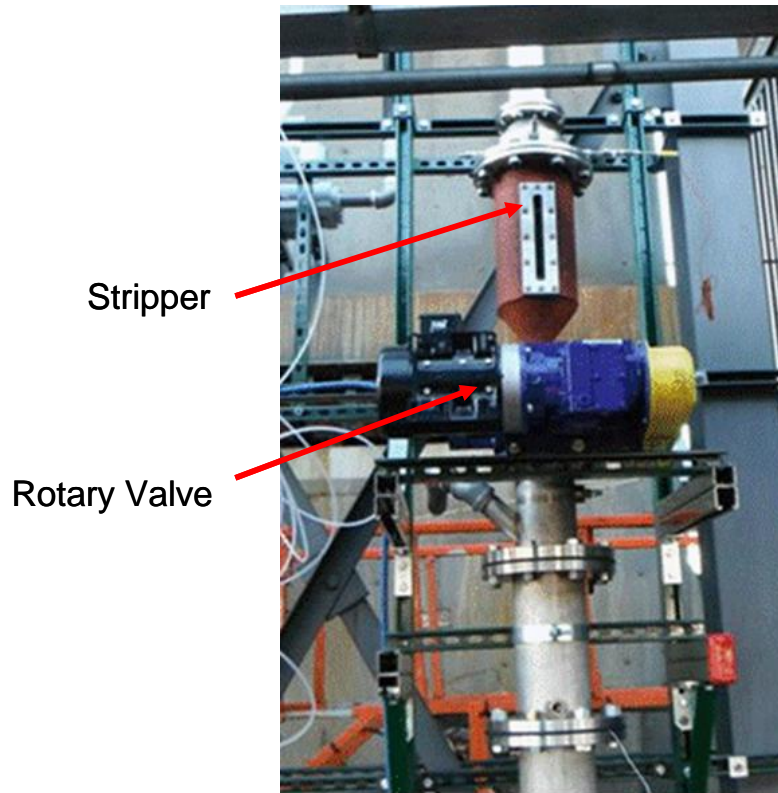


Figure VI-5. A photograph of the stripper and rotary valve sections.

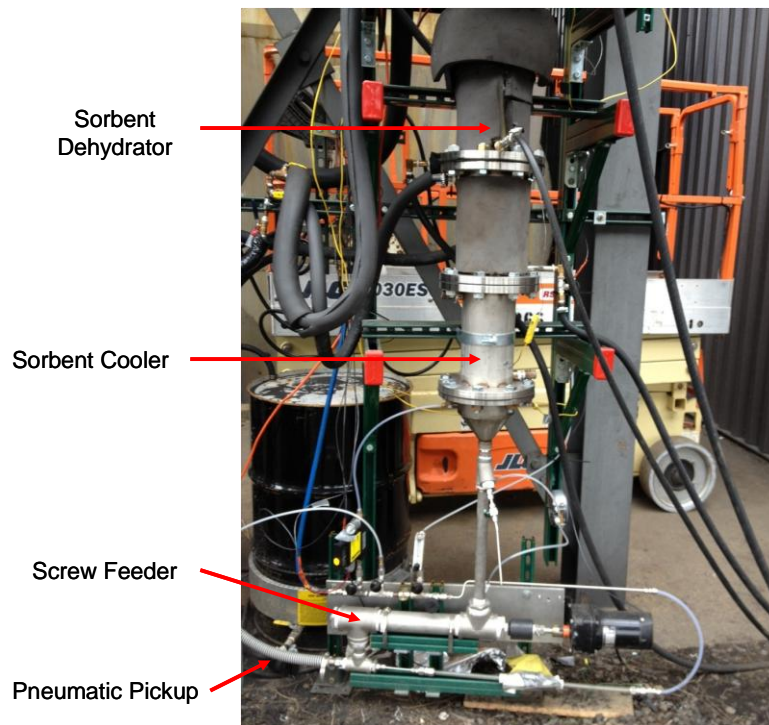


Figure VI-6. A photograph of the sorbent dehydrator, cooler, screw feeder, and pneumatic recycle sections.

Table VI-1 . Process Parameters and Their Values Used in the Field Test at the University of Toledo

Parameter	Unit	Nominal Value
Column diameter	cm	15
Column height	meters	15
Flue gas flow rate	liters/min (STP)	200 to 240
CO ₂ level in the flue gas	%	4.5 to 4.7
SO ₂ level in the flue gas	ppm	60
CO ₂ level at the adsorber inlet	%	4.5 to 4.7
SO ₂ level at the adsorber inlet	ppm	<5
CO ₂ level at the adsorber exit	%	0.05 to 0.6
Pressure drop in the adsorber	inch water column	0.4
Sorbent flow rate	kg/min	1 to 1.2
Absorber temperature	degrees Celsius	5 to 15
Stripper temperature	degrees Celsius	100 to 120
CO ₂ product flow	liters/min (STP)	7 to 9
Dehydrator temperature	degrees Celsius	100 to 120
Cold Sorbent temperature	degrees Celsius	25 to 35

Figure VI-7 represents the performance of the integrated system when operated with the flue gas stream from the UT boiler. As mentioned previously, the percentage of CO₂ in the inlet gas was at 4.7%. The percentage CO₂ capture as measured from the adsorber inlet and outlet gases varied from 85 to 90%. Initially, the percentage CO₂ in the stripper outlet was about 82%, and that value increased to 90% as the operation progressed.

Figure VI-8 represents the performance of the system after about 100 h of operation. With increased operational experience, a stable performance was obtained with both the percentage of CO₂ capture in the adsorber and the purity of CO₂ in the stripper outlet. During this operational period, an 85% to 95% CO₂ capture efficiency and a CO₂ product gas purity of ~ 100% were achieved. Note that a decrease in the CO₂ purity was observed during an interruption of the steam to the stripper. When the operation was resumed, the CO₂ purity value resumed to the original value indicating the robust nature of the system.

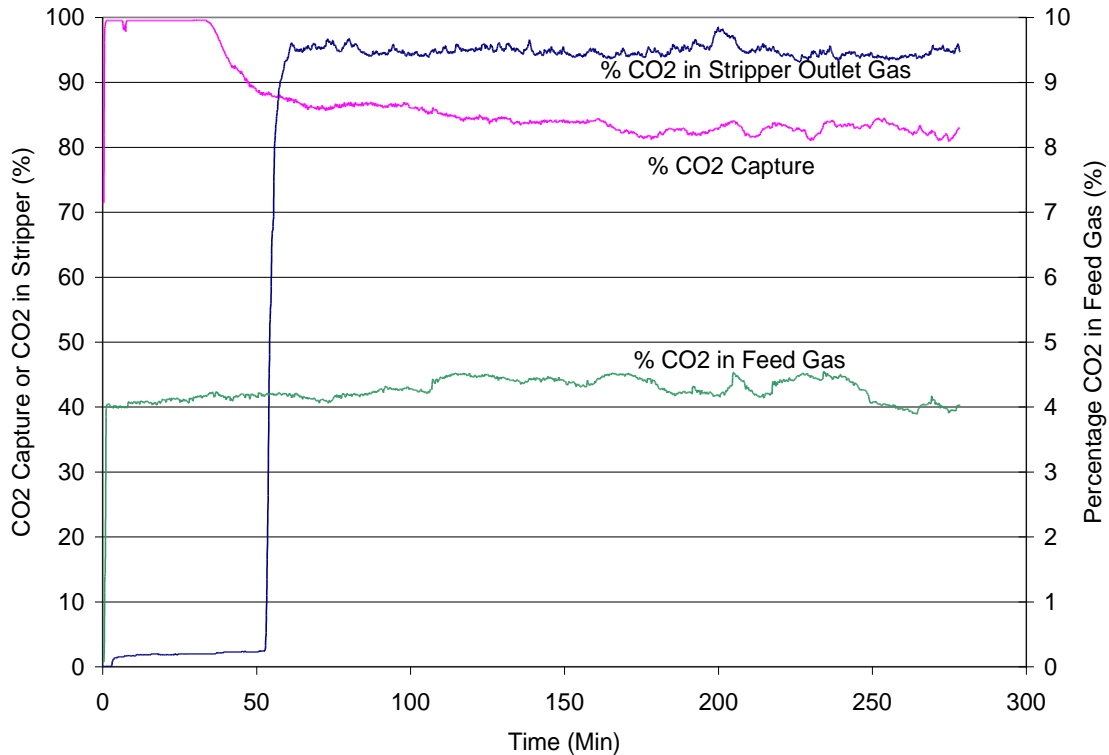


Figure VI-7. Percentage of CO₂ capture and the CO₂ purity of the stripper gas.

The UT steam boiler was shut down on February 18, 2012, and we terminated the field tests after 135 h of testing. The field unit was operated during the daytime for about 8 to 10 h. During the test period, the flue gas flow and solid circulation were maintained without any significant problem. The major difficulty encountered was maintaining the temperatures of the stripper and the dehydrator, especially in the cold weather encountered in Ohio in the middle of winter. When the external heating of the walls of the stripper and the dehydrator were implemented along with additional insulation, a reliable performance was obtained. The performance of the integrated system is shown in Figure VI-8 illustrating both high CO₂ capture efficiency and CO₂ product gas purity. The results observed in the field test at Toledo, OH with a flue gas containing only 4.5% CO₂ is consistent with the data obtained with a simulated air-15% CO₂ mixture used at SRI campus at Menlo Park, CA.

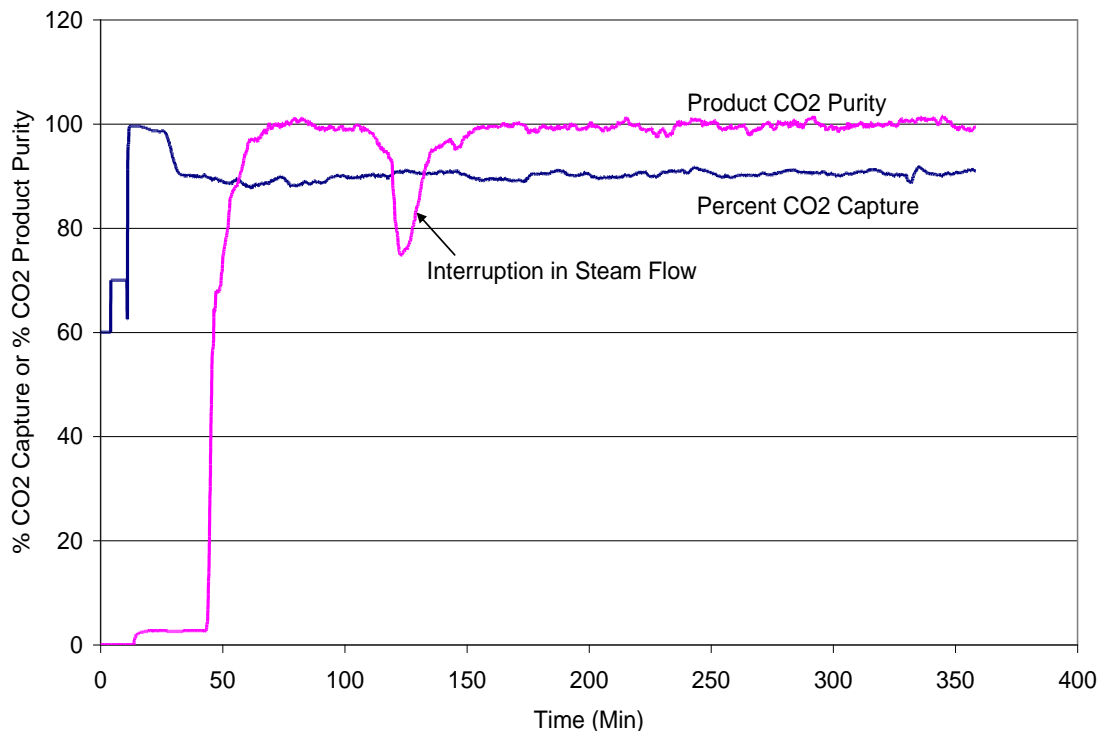


Figure VI-8. A plot of the CO₂ capture efficiency and product gas purity in the field test after 100 h of operation.

In the field test, the sorbent microbeads were circulated for about 7,000 cycles of adsorption and stripping. We measured the CO₂ adsorption isotherm of the sorbent after such long testing and compared it with the isotherm obtained with the fresh sorbent. As shown in Figure VI-9, the CO₂ adsorption capacity did not change significantly during the field test. In fact, the CO₂ adsorption capacity appears to be slightly higher after the field test than with the fresh sorbent.

VI.3 ANALYSIS OF THE SORBENT AFTER THE FIELD TEST AT THE UNIVERSITY OF TOLEDO

The sorbent samples from the field test were analyzed to determine any accumulation of flue gas components such as mercury, chlorine, sulfur, and nitrogen compounds. These analyses were performed at the ATMI laboratories and included:

- CO₂ isotherms
- Thermogravimetric analysis in vacuum
- Trace metals analyses plus S, Cl, Hg
- Organic/vapor/gases adsorbed.

The results of these analyses are described below:

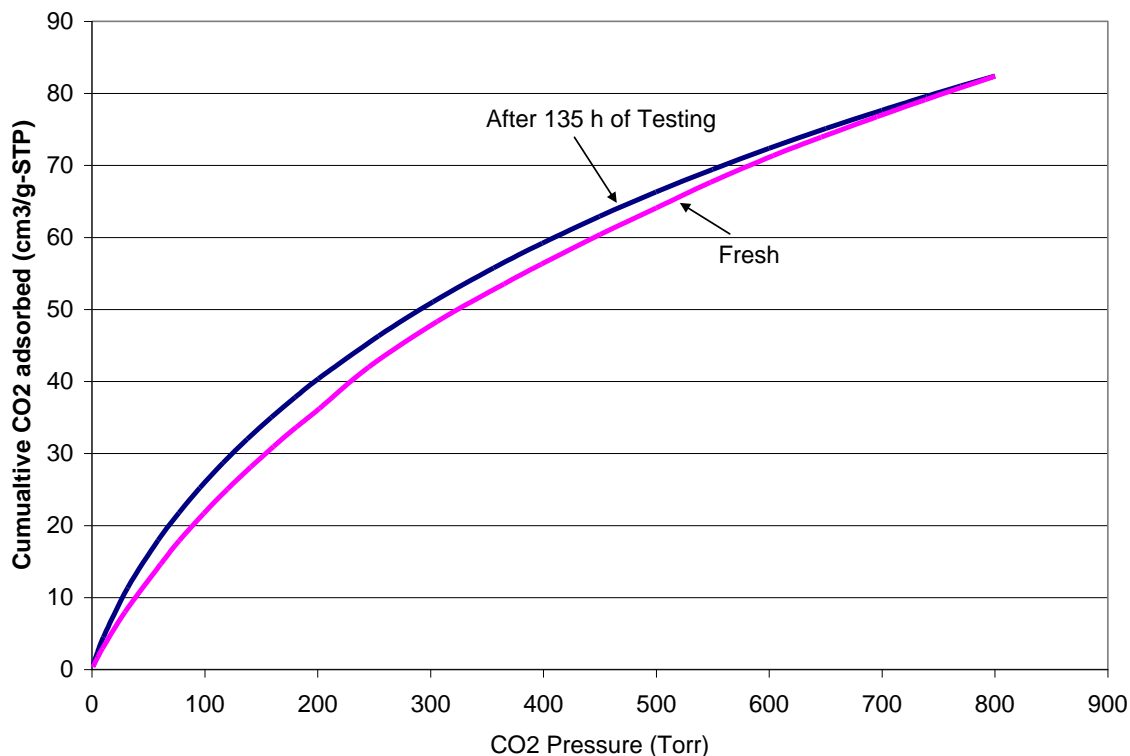


Figure VI-9. CO₂ adsorption isotherms before and after the field test.

The CO₂ adsorption isotherms of the fresh and used sorbents were obtained by measuring the equilibrium amount of CO₂ adsorbed as a function of CO₂ pressure at 273 K. As shown in Figure VI-10, the CO₂ adsorption capacity did not change significantly during the field test. In fact, the CO₂ adsorption capacity appears to be slightly higher after the field test than with the fresh sorbent. These results are similar to those obtained at SRI and described previously.

The sorbent from the field test was heated under vacuum in a thermogravimetric analyzer. The sample was heated to about 200°C, and the weight loss as a function of temperature was measured. As shown in Figure V-40, three regions of weight loss can be observed. The initial rapid weight loss at 20°C is likely to be due to the release of adsorbed air from the sample as it was kept in air for a number of days before the analysis. As the sample is heated, a second weight loss was observed in the temperature range 20° to 60° C; this weight loss was due to desorption of CO₂ from the sample. As the sample was heated further, adsorbed water was desorbed. The weight gain observed during cooling is due to the buoyancy effect.

Table VI-2 compares the concentration of several inorganic elements between the fresh and field-tested samples. Only Fe was found in significantly higher concentration in the used sample than in the fresh sample. The iron contamination is due to aerosol of rust in the flue gas from the iron pipe carrying the flue gas from the chimney to the adsorber. In fact, we collected rust-contaminated condensate solution at the bottom of the flue-gas inlet pipe. Small amounts of accumulation of S and Hg were also observed, presumably from the flue gas.

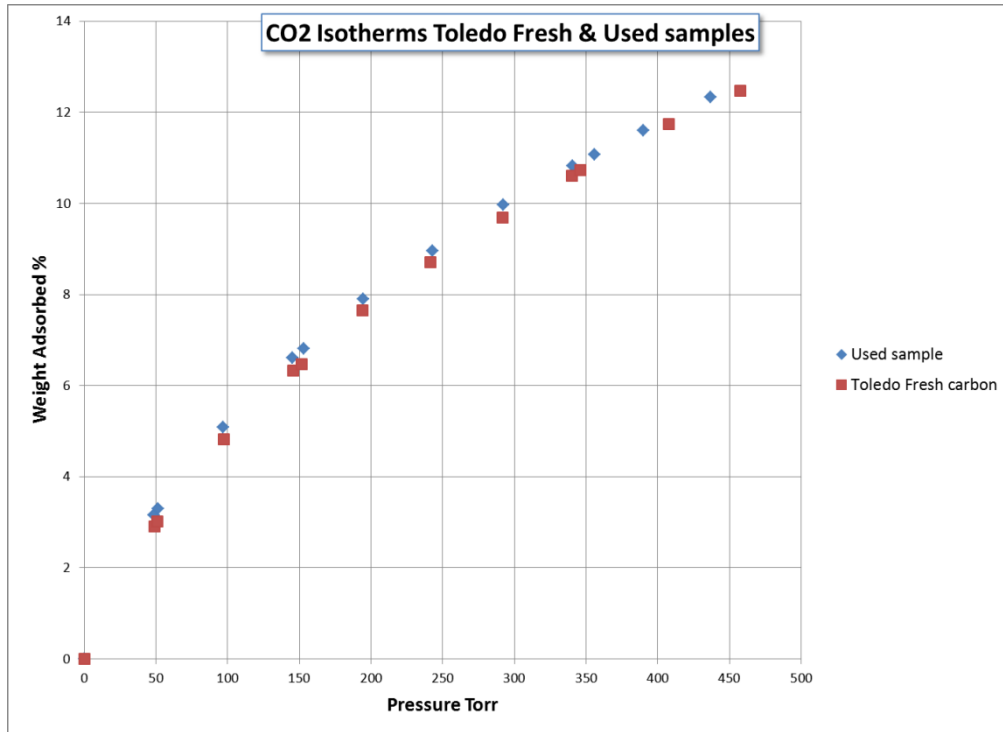


Figure VI-10. Comparison of the CO₂ adsorption characteristics of freshly and field-tested sorbents.

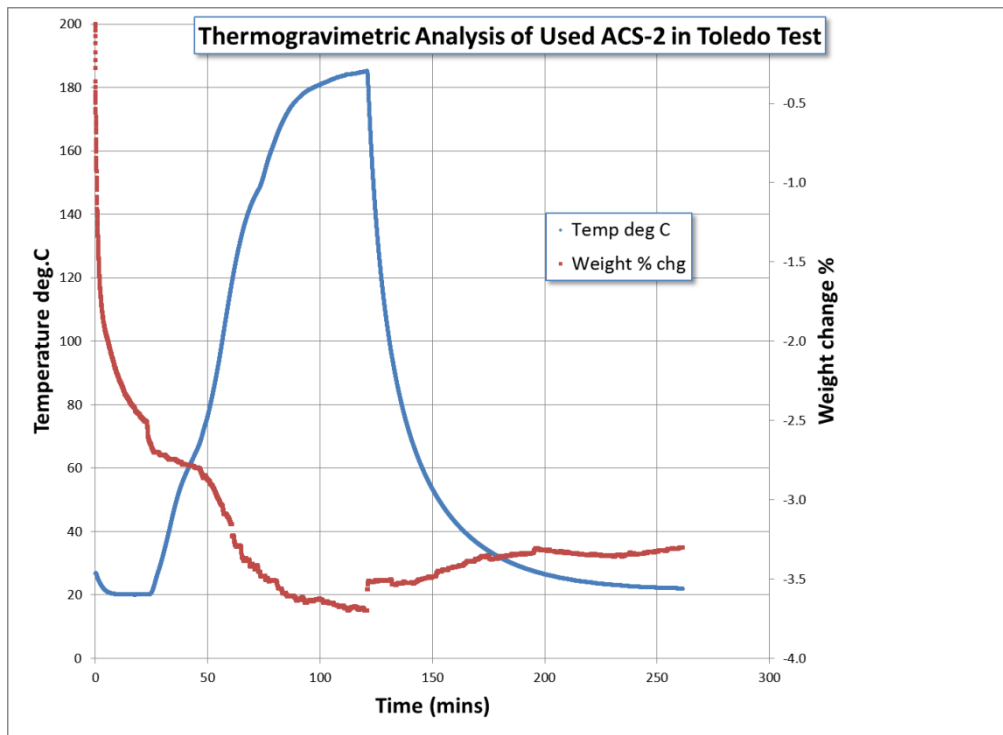


Figure VI-11. Thermogravimetric analysis of the sorbent after the field test.

Table VI-2. Comparison of Inorganic Elements in the Fresh and Field Test Sorbents

Element	Fresh	Used
	ppm	ppm
Na	102	95
P	80	66
K	74	6
Ca	41	41
Mn	<2	24
Fe	<2	1234
Zn	<2	15
Cl	468	611
S	19	132
Hg	<0.06	0.31

Table VI-3 lists the amount of several organic compounds found in the field test sample. The amounts of these organic compounds are extremely low. A small amount of NO was also adsorbed in the sample, due to the presence of NO in the flue gas. No active NO_x control was practiced with the flue gas in the field test. The accumulation of the sulfur and nitrogen oxides in the sorbent did not change its CO₂ adsorption characteristics, as evidenced from the nearly identical adsorption isotherm of fresh and field-test samples.

Table VI-3. Comparison of Adsorbed Gases in the Fresh and Field Test Sorbents

Contaminant	Fresh	Used
	ppb	ppm
Acetone	3.24	9.02
NO	N.D.	3210
CO₂	N.D.	758
Methylbutane	N.D.	19.6
Methylisocyanide	N.D.	67.1
Pentane	N.D.	30.1
Benzene	N.D.	40
Acetic Acid	N.D.	284

VI.4 FIELD TEST AT THE UNIVERSITY OF TOLEDO

The tests at UT used the flue gas stream from a stoker-fired steam boiler. These demonstrated the preliminary viability of operation with a real flue gas. The process was also tested using the flue gas from a PC-fired power plant at the National Carbon Capture Center (NCCC), Wilsonville, AL. The system used at the NCCC was designed to handle a flue gas flow that is about 10 times higher than that used at the National Carbon Capture Center.

The system that was installed at the NCCC was of square cross-section reactors rather than the cylindrical cross section used at Toledo. The square cross section will allow simple fabrication using sheet metals in a fashion similar to that of building ventilation ducts. Such a construction is feasible, because no liquid is used inside the reactor and no significant pressure difference exists between the inside and the outside of the reactor. Furthermore, the structural packing of square cross section is substantially cheaper than that for round cross sections. The adsorber of this field test unit was designed to be a 1.5-ft-square, 10-ft-tall column that will handle a flue gas stream of 70 cfm (~250 tons CO₂/year, or 40 kWe). Several of the components from the previous field test were reused.

Table VI-4. Design Parameters and Their Values Used in the Field Test at NCCC

Parameter	Unit	Nominal Value
Adsorber column size (square)	cm	46
Adsorber column size height	meters	2.5
Stripper column size (square)	cm	30
Stripper column height	meters	2.5
Total height of the system	Meters	15
Flue gas flow rate	liters/min (STP)	1000 to 2000
CO ₂ level in the flue gas	%	4.5 to 12
SO ₂ level in the flue gas	ppm	<10
Pressure drop in the adsorber	inch water column	0.4
Sorbent flow rate	kg/min	12
Absorber temperature	degrees Celsius	20 to 30
Stripper temperature	degrees Celsius	100 to 120
CO ₂ product flow	liters/min (STP)	100 to 200
Dehydrator temperature	degrees Celsius	40 to 120
Cold Sorbent temperature	degrees Celsius	25 to 35

During this quarter, we have been designing parts and procuring equipment for the test at the NCCC. We worked with NCCC personnel to identify utilities needed for the test, and structural requirements for the column. A schematic of the piping and instrumentation diagram (P&ID) is shown in Figure VI-12. Figures VI-13 and VI-14 are the schematic diagrams of the

integrated adsorber-stripper column and the structure to support the column, respectively. A certified Alabama engineer designed the support frame for the reactor to withstand 90 mph wind.

The heat exchangers with custom-designed coil arrangement were used to improve the heat transfer efficiency between the sorbent microbeads and the gas stream. The heat exchangers were used to: (1) pre-heat the carbon microbeads as they move down the column from the transition zone to the stripper; (2) reduce the temperature of the microbeads by evaporative cooling as they move down the column through the dehydrator section; and (3) cool the microbeads further in the cooling section before they are lifted back to the top of the column. A photograph of a heat exchanger is shown in Figure VI-15.

The flow of the sorbent microbeads is controlled at: (1) the entrance to the adsorber at the top; and (2) a point between the bottom of the stripper and top of the dehydrator. In the earlier field test, a rotary valve was used for the control, and it was found that the microbeads were being crushed by the rotor. Instead, a pinch valve was used in which the size of the opening was controlled. Such valves are used to control the flow of slurries. A photograph of the pinch valve is shown in Figure VI-16.

A bed of carbon microbeads is maintained at various sections to prevent gas back flow between the sections. The bed of microbeads is created in a hopper, and the height of the bed will allow sufficient pressure drop for preventing gas flow. This hopper was designed so a radar sensor can be used to measure the level of solids. The signal from the sensor controls the pinch valve at the bottom of the hopper to maintain a desired bed height

The adsorber, transition, and the stripper sections of the system were filled with structural packing to allow uniform distribution of the sorbent within the column. The structural packing was procured from Sulzer, Ltd. Figure VI-17 is the photograph of the structural packing placed inside the column.

The system used Class I, Division 2, code-compliant motors, sensors, and controllers to comply with the NCCC requirements. The controllers were mounted inside a Class I, Division 2, code-compliant enclosures (Figure VI-18). The right-hand side enclosure contains the pressure gauges and temperature controllers for the heat trace. The heat trace keeps the stripper and hopper above the dehydrator above the dew point so that water condensation may not occur in those regions. The enclosure on the left hand of Figure VI-18 contains the variable frequency controllers for the blower motor and the screw feed motors. This arrangement allows control of the equipment without opening the enclosure.

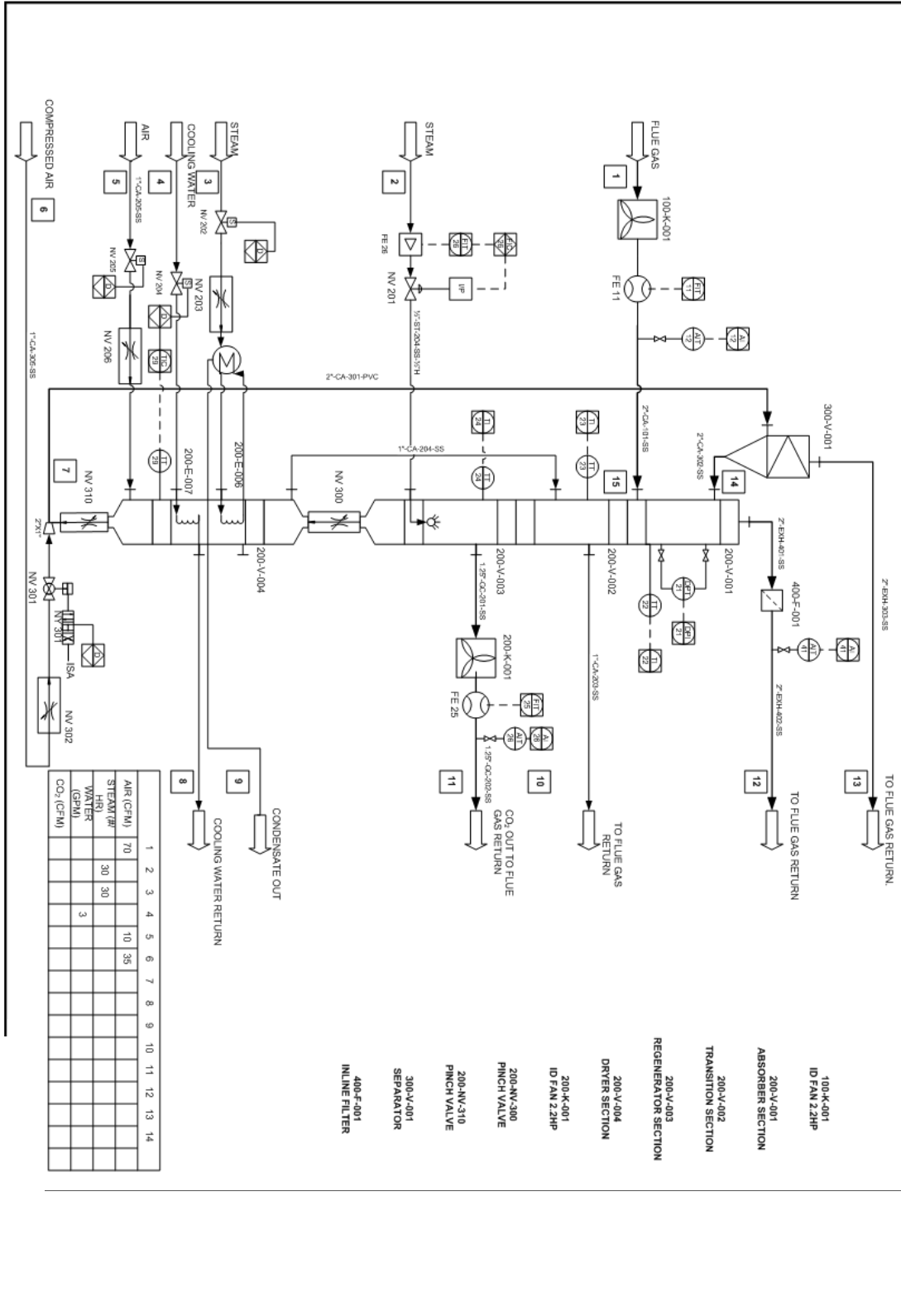


Figure VI-12. Piping and instrumentation diagram of the system installed at NCCC.

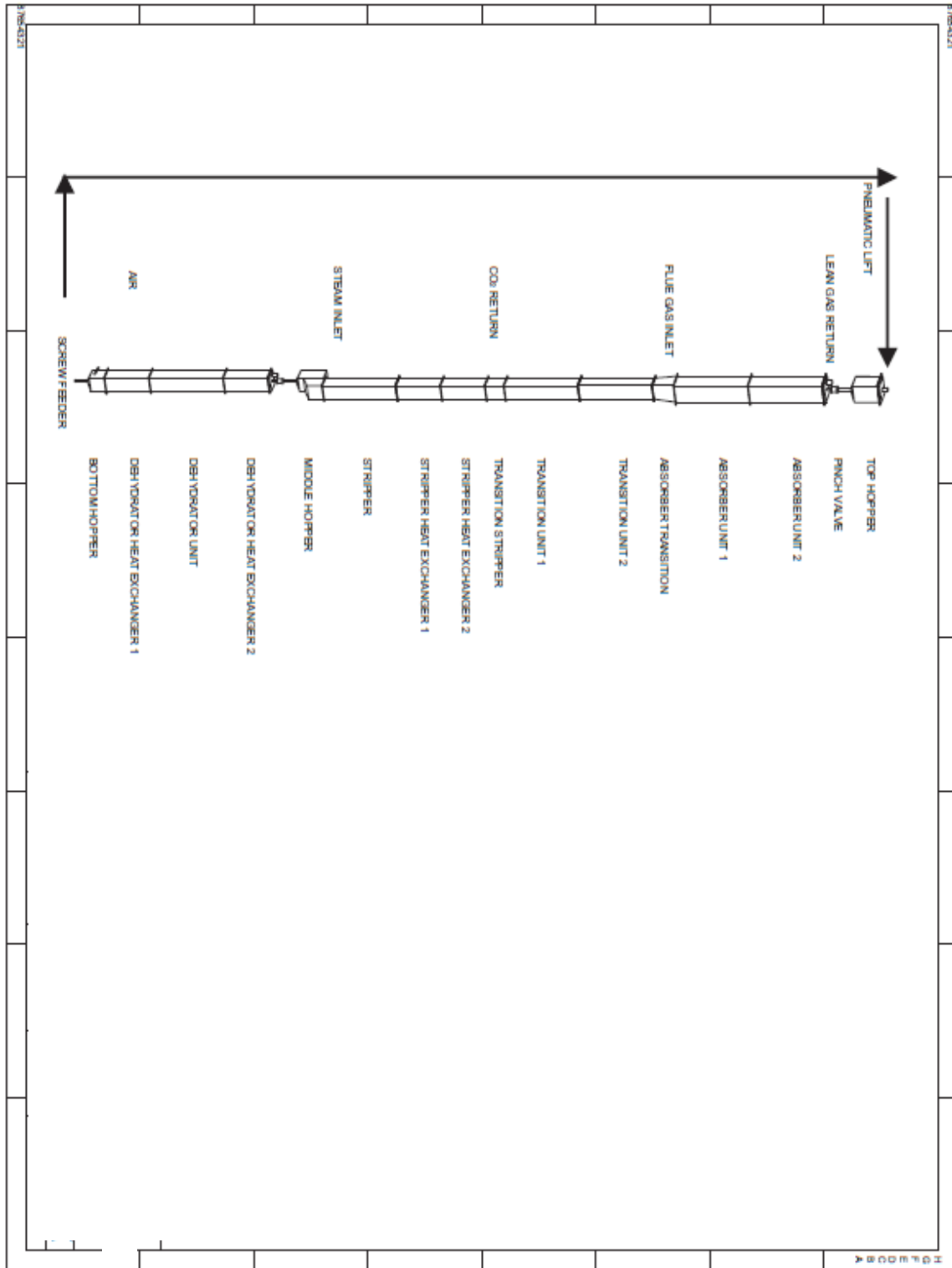


Figure VI-13. Schematic of the integrated adsorber-stripper column.



Figure VI-15. Photograph of a heat exchanger for recovering thermal energy from the sorbent granules.



Figure VI-16. Pneumatically operated sorbent flow control valve (pinch valve design).

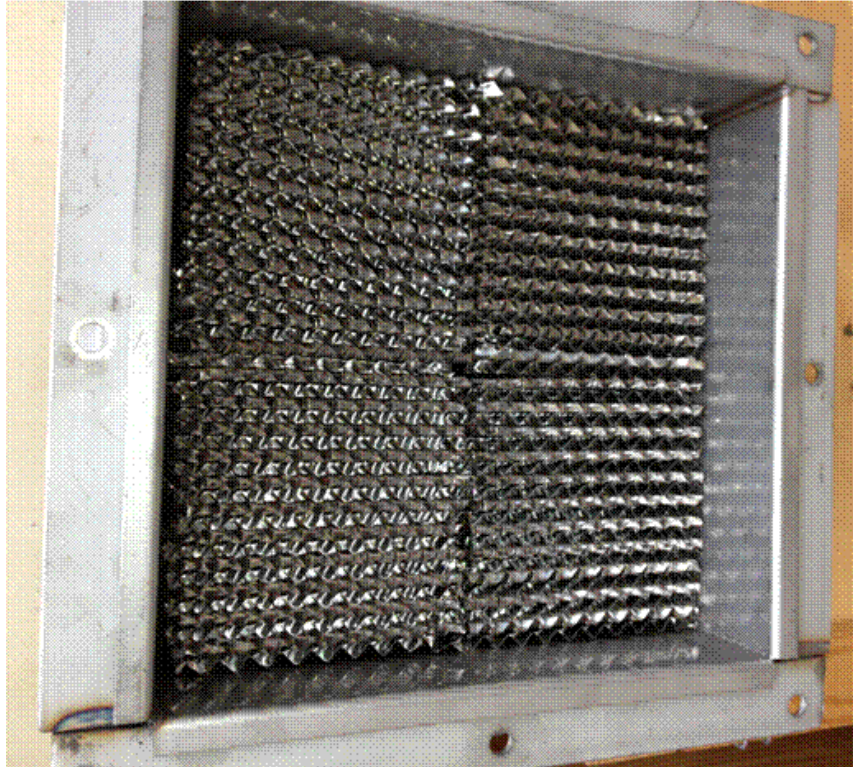


Figure VI-17. Photograph of the inside of the column filled with structural packing.

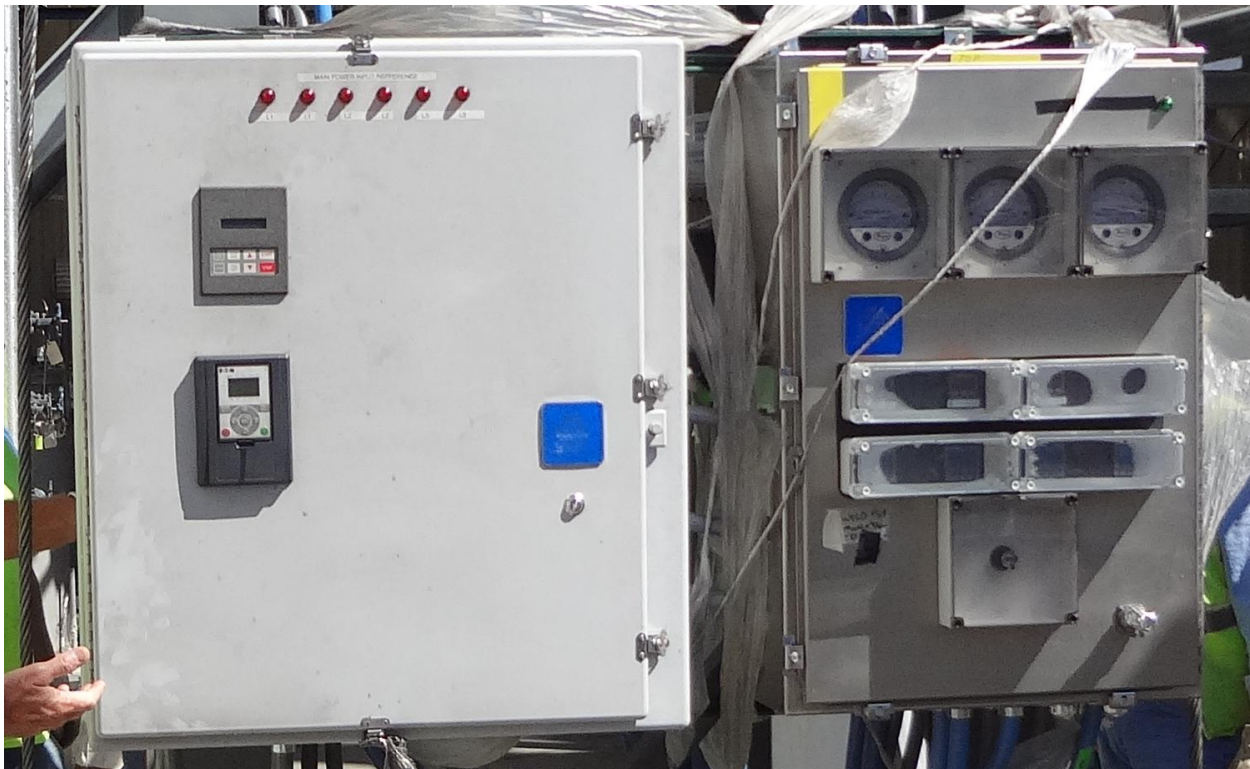


Figure VI-18. Photograph of the code-compliant enclosures.

Several instruments are incorporated in the system to measure pressure, flow, and temperature at various locations. The operation of differential pressure gauges, various types of flow meters, and temperature sensors were checked at SRI before shipment to NCCC. The signals from the instruments were found to be linear with changes in the process parameters, as shown in Figures VI-19 through VI-22.

Figure VI-23 illustrates the assembled skid on the floor ready for transportation, and it is being lifted by the crane. The crane placed the skid on a flat-bed truck (Figure VI-24). The truck delivered the skid to the NCCC site without incident

A drawing and a dummy base plate was provided to the NCCC staff for installing anchor bolts on which the skid was to be attached. A licensed Alabama engineer designed a lift plan for lifting the skid from the truck and placing it inside the foundation. We arranged for two cranes (rental) to be available when the truck arrived at the NCCC site.

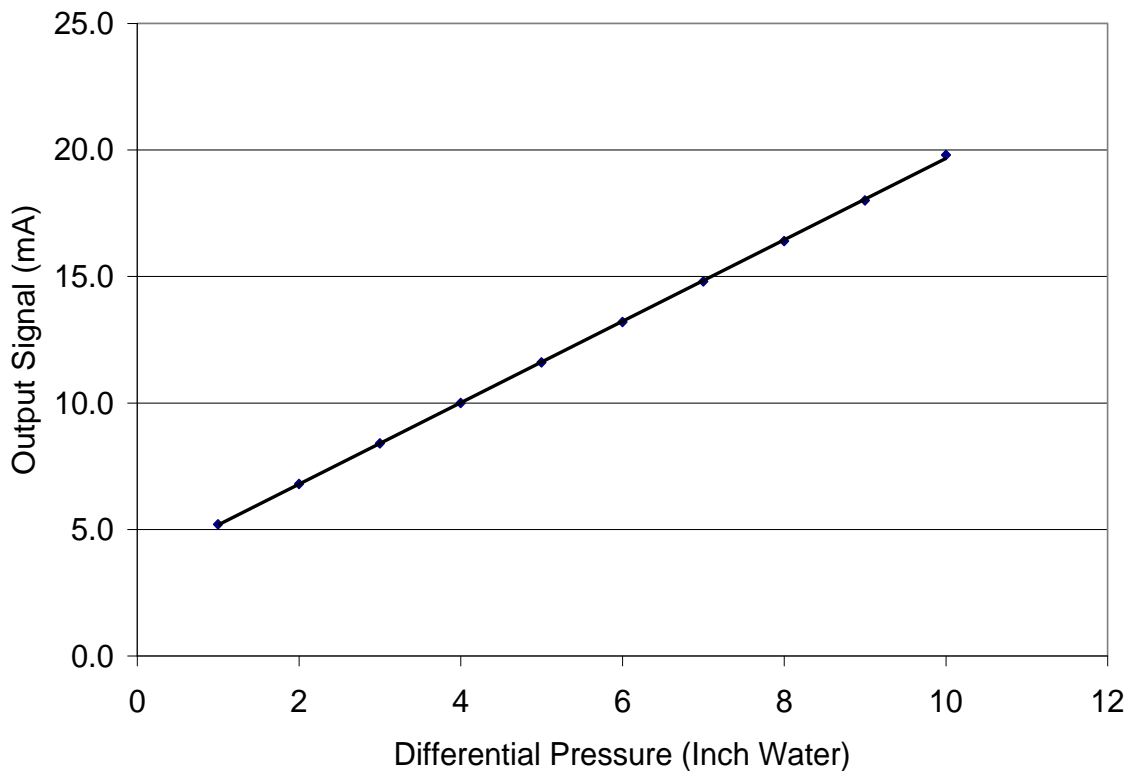


Figure VI-19. Operational verification of a differential pressure gauge.

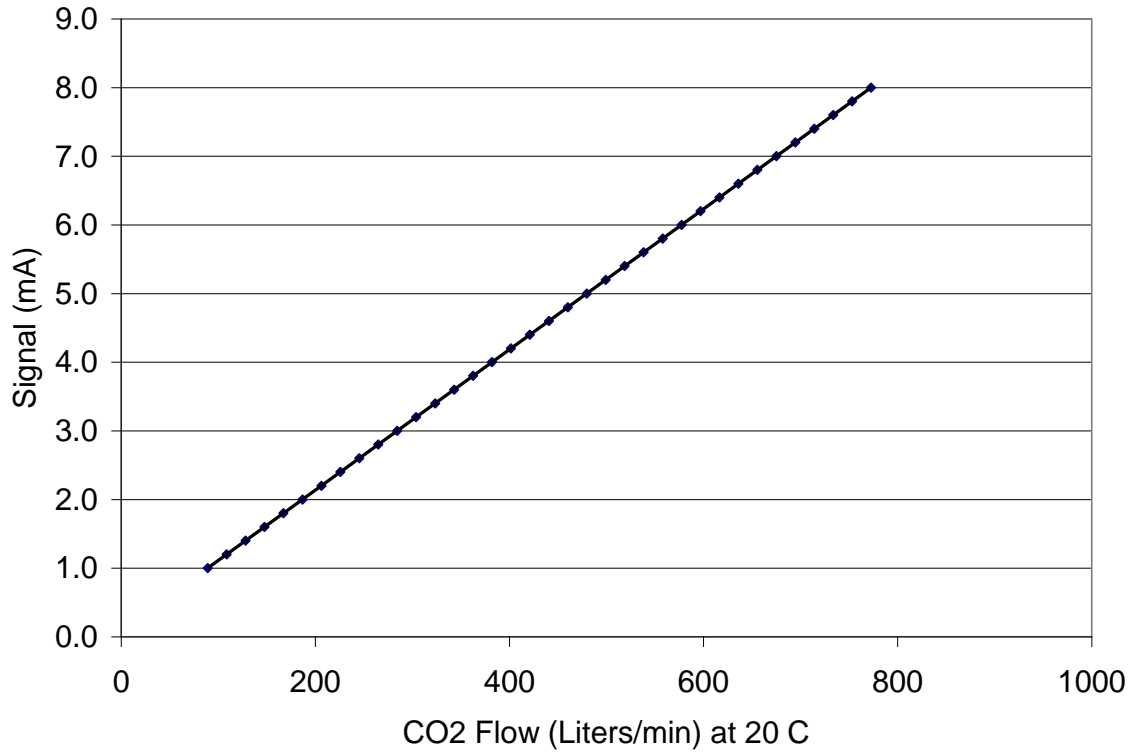


Figure VI-20. Operational verification of the CO₂ flow meter sensor.

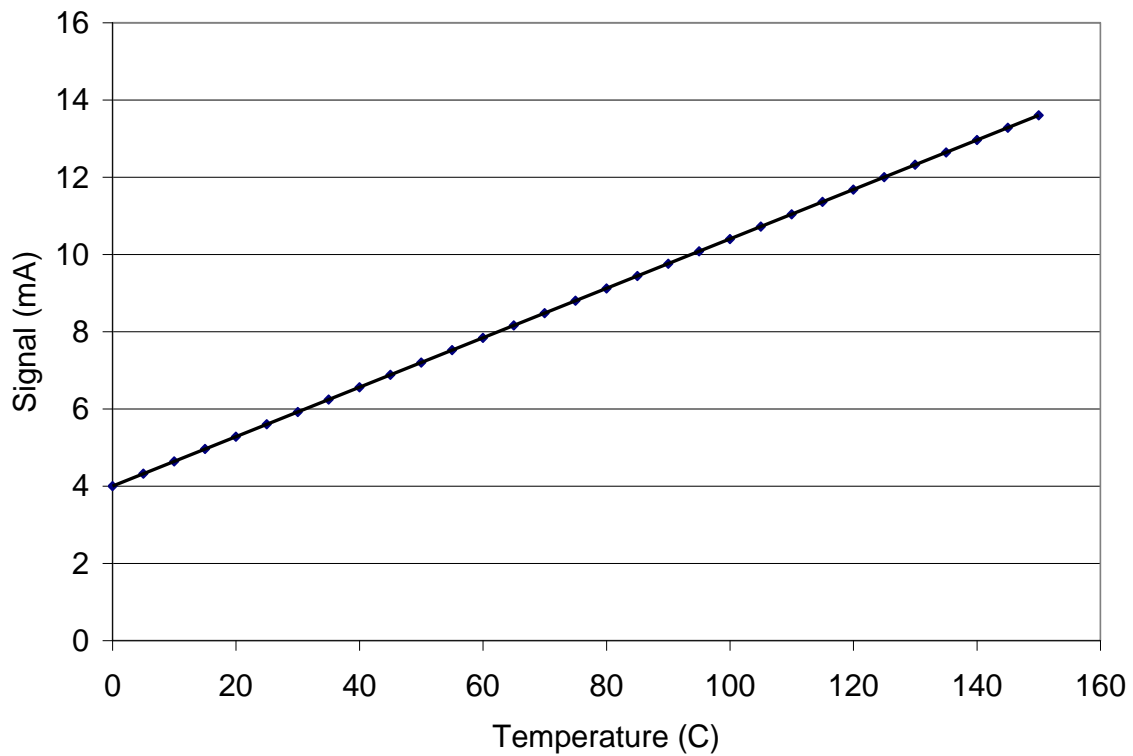


Figure VI-21. Operational verification of the temperature sensor.

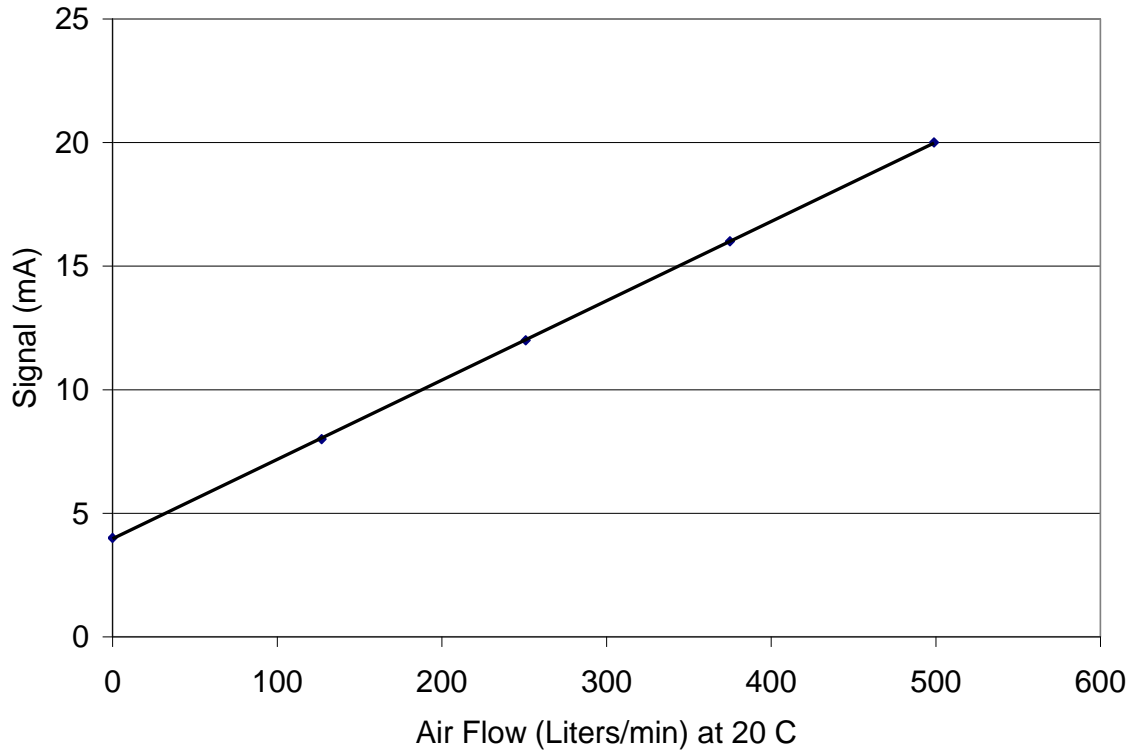


Figure VI-22. Operational verification of air flow meter.

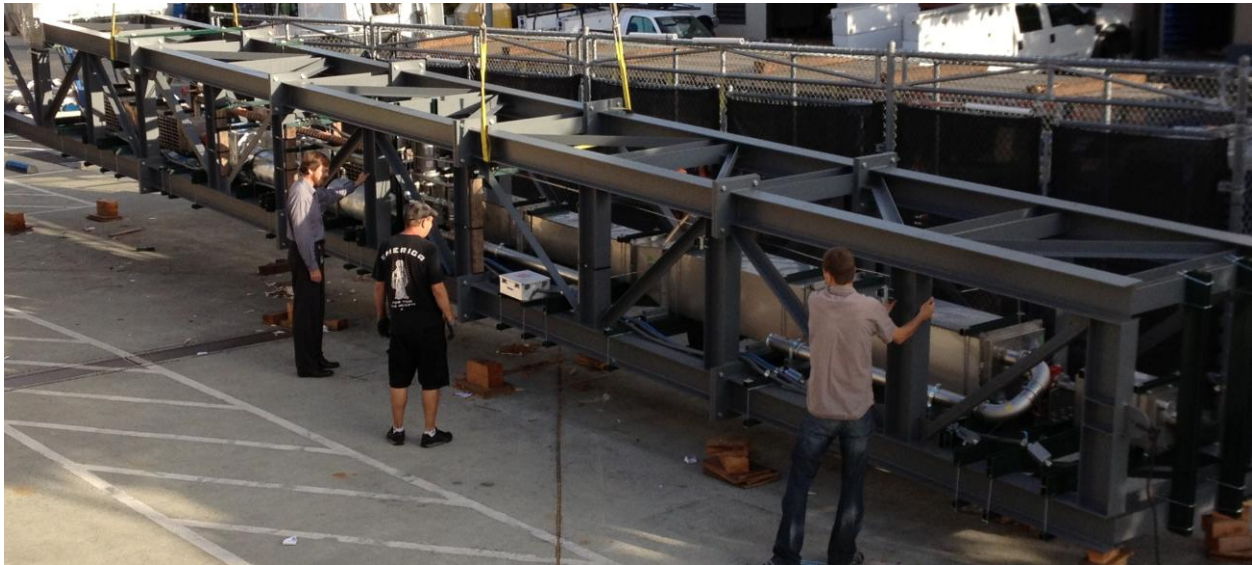


Figure VI-23. The skid is being lifted from the assembly floor to the truck by a crane.



Figure VI-24. Skid to demonstrate CO₂ capture by carbon sorbent is on the truck to transport it to National Carbon Capture Center.

The skid was transported successfully from SRI campus at Menlo Park, CA to the NCCC site, Wilsonville, AL. The unit was lifted from the horizontal position in the truck using two cranes to a vertical position (Figure VI-25). It was swung over the existing structure and was anchored on the concrete platform at the selected site (Figure VI-26).

After installation, shake-down runs were performed with the system. Corrective actions were taken to prevent both gas and sorbent particles leaks from the reactor. The pneumatic lift design was changed to allow lifting of the required rate of sorbent from the bottom of the sorbent cooler to the top of the adsorber. This change in the design required an increase in the diameter of the lift tube and a higher flow rate of lift air than the original design and so the disengagement section at the top of the adsorber was modified also.

Figure VI-27 shows some results during the initial runs. The data shows a CO₂ capture efficiency of ~65% and a CO₂ product gas purity approaching 65%. In previous operations both at SRI and the University of Toledo, the CO₂ product gas purity takes certain period of time to achieve high values.



Figure VI-25. The skid lifted from the truck at the NCCC installation.

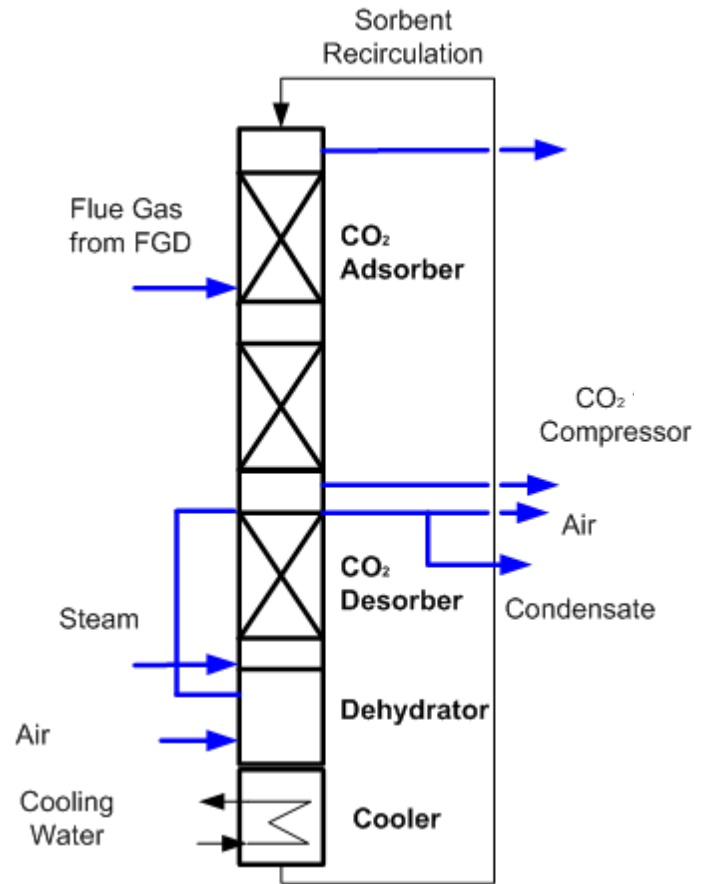
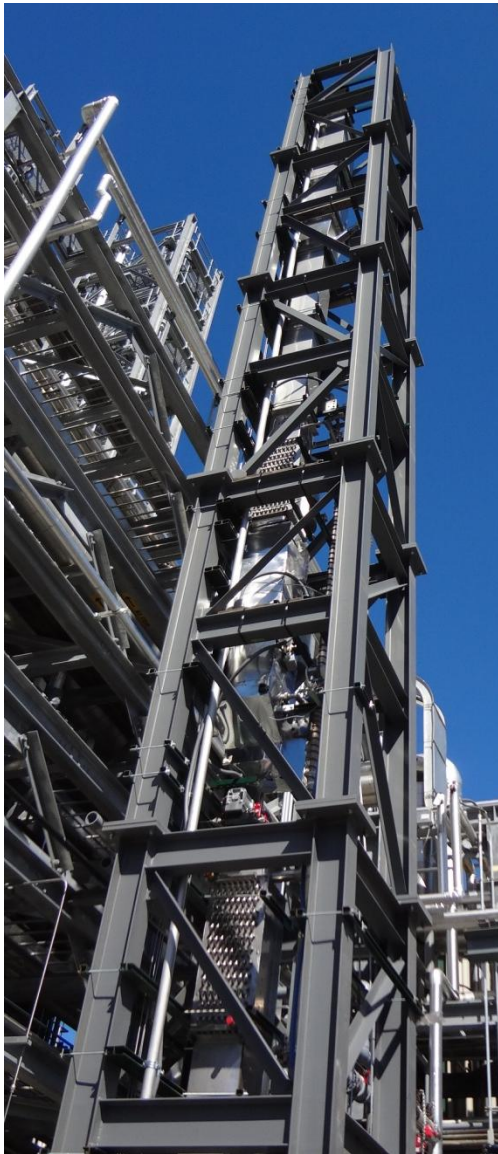


Figure VI-26. The skid installed at the NCCC site.

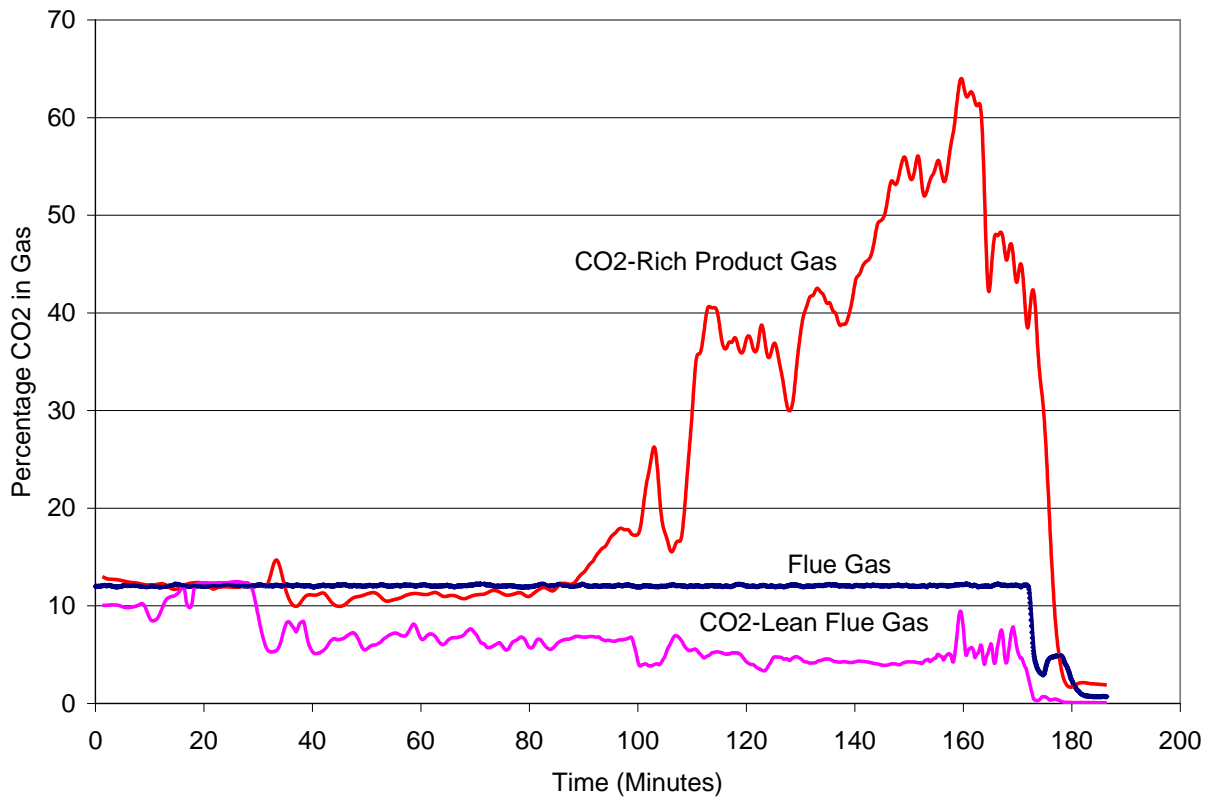


Figure VI-27. CO₂ composition of the feed flue gas, adsorber exit gas and rich product gas during the initial runs at the NCCC site.

VII. PRELIMINARY PROCESS EVALUATIONS

Preliminary process evaluation was performed on the capture of CO₂ from PC-fired flue gases using the advanced carbon sorbents. Initially, the power plant and CO₂ capture process model was validated with publically available data. The NETL report, “Cost and Performance Baseline for Fossil Energy Plants” [Klara, 2007], was used as the bench mark. Specifically, the performance of the SRI model was compared against the NETL’s supercritical pulverized coal cases (Cases 11-12). The results of NETL’s Case 11 (No CO₂ capture) and Case 12 (CO₂ capture using Econamine solvent) are shown along with the SRI’s results (Table 1). For both the capture and non-capture cases, the SRI’s estimated levelized cost of electricity (LCOE) agrees with the NETL estimated costs to within 1%, which is an excellent validation of the model. The model is then used to estimate the performance of carbon sorbents for CO₂ capture.

Table VII-1. Comparison of SRI Modeling Results with NETL Published Results on Supercritical Pulverized Coal-Fired Power Plants

	NETL		SRI	
	No	Yes	No	Yes
CO₂ Capture				
Gross Power Output (kW)	580,260	663,445	581,034	679,911
Auxiliary Power Requirement (kW)	30,110	117,450	31,016	129,485
Net Power Output (kW)	550,150	545,995	550,018	550,426
Net Plant HHV Efficiency (%)	39.1%	27.2%	38.9%	27.1%
Net Plant HHV Heat Rate (Btu/kW-hr)	8,721	12,534	8,859	12,590
Coal Flowrate (lb/hr)	411,282	586,627	414,000	594,000
CO ₂ Emissions (lb/MWh)	1,773	254	1,790	252
Total Plant Cost (\$ x 1000)	866,391	1,567,073	872,118	1,586,765
Total Plant Cost (\$/kW)	1,575	2,870	1,586	2,883
LCOE (¢/kWh)	6.33	11.48	6.40	11.58

VII.1 MODEL VALIDATION

Two software tools were used for the process modeling effort. The primary simulations were performed in Steam-Pro 19, while Aspen Plus 2006 is used to verify certain results and investigate issues that are outside the scope of Steam Pro. Steam-Pro is a simulation program specifically for modeling Rankine cycle PC power plants. The Steam-Pro software package is marketed by Thermoflow, Inc., the leading thermal engineering software provider for the power industry. Aspen Plus is a leading process modeling tool for conceptual design and optimization and is offered by AspenTech.

Case 1. No CO₂ Capture:

The baseline power plant is a supercritical 550 MWe PC-fired plant. An overview of the power plant is shown below in Figure VII-1. Pulverized Illinois #6 coal is fed into the boiler, where it is combusted in the presence of air. The hot gases pass over the heat exchangers and then to NO_x and SO_x removal steps. First the flue gas passes through the Selective Catalyst Reduction (SCR), where NO_x is reduced with NH₃ to N₂ and H₂O. The gases then pass into a baghouse, where fabric filters are used to remove the fly ash. The final flue gas processing step is the flue gas desulfurization (FGD) unit, where the SO₂ is reacted with limestone and air to form gypsum. Upon leaving the FGD unit, the flue gas is sent through the stack and vented to the atmosphere. The steam cycle begins with the cool water leaving the steam turbine condenser. The water then passes through a series of feed water heaters before entering the boiler, where heat exchangers are used to produce superheated steam. The superheated steam turns the steam turbines, which in turn power the generator. After the steam is cooled and decompressed through the steam turbines, it is fed to the condenser to complete the cycle.

The process assumptions of the SRI model are shown below in Table VII-2 and are compared with the assumptions described in the NETL report. The process conditions such as pressure drops, slurry weight percentages, operating temperatures, and fan efficiencies are matched.

The capital and operating costs of the various units were taken from the NETL report but assumed to vary linearly with the increasing or decreasing size of the particular unit in consideration. This assumption is valid for small changes in the unit size. For example, the total plant cost associated with the supercritical PC boiler in the NETL report is \$280.7 million. This cost is for a coal feed rate of 411,282 lb/hr. The SRI model estimates a coal feed rate of 417,600 lb/hr, and therefore the boiler capital cost is increased by \$4.3 million to \$285.0 million. Similarly, a 1.5% increase in coal flow rate results in a 1.5% increase in the capital cost of the boiler and all the other unit operations that are dependent on the coal flow rate.

Table VII-3 provides a detailed summary of both process and cost results. In this table, the total plant cost includes the steam turbine costs. The net efficiency of the SRI power plant is slightly lower than the NETL plant due to certain minor assumptions within the Steam-Pro program. This lower efficiency causes a slight increase in the cost of electricity. In spite of these differences, the agreement between our model and the NETL model is extremely good.

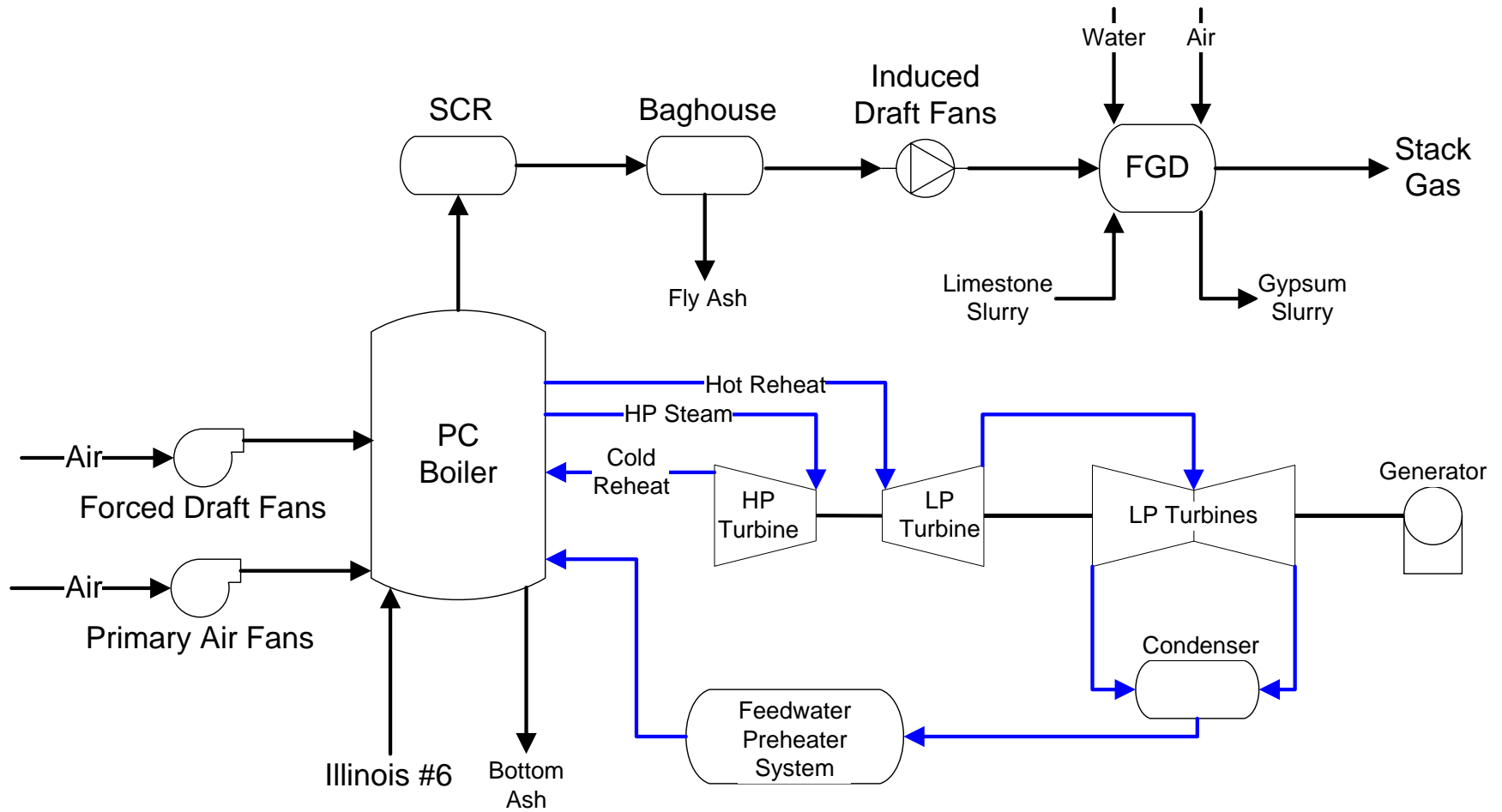


Figure VII-1. Process flow diagram of a PC power plant without CO₂ capture.

Table VII-2. Process Assumptions of a Supercritical Power Plant with No-CO₂ Capture

	SRI Supercritical Power Plant	NETL Supercritical Power Plant
Net Power Output, MW	550	550
Steam Cycle, (psig, °F, °F)	3500,1100,1100	3500,1100,1100
Coal	Illinois #6	Illinois #6
Condenser pressure, mmHg	50.8	50.8
Cooling water to condenser, °F	67.5	60
Cooling water from condenser, °F	94.5	80
Stack Temperature, °F	131.0	135.0
SO ₂ Control	Wet Limestone Forced Oxidation	Wet Limestone Forced Oxidation
FGD Efficiency, % SO ₂ Removal	98.0	98.0
NOx Control	Low NOx Burners w/OFA and SCR	Low NOx Burners w/OFA and SCR
SCR Efficiency, % NOx Removal	86.0	86.0
Ammonia Slip, ppmv	2.0	2.0
Particulate Control	Fabric Filter	Fabric Filter
Fabric Filter Efficiency, % Ash Removal	99.8	99.8
Mercury Control	Co-Benefit Capture	Co-Benefit Capture
Mercury Removal Efficiency, %	90.0	90.0
CO ₂ Capture, %	N/A	N/A

Table VII-3. Comparison of NETL and SRI Results for the Case with No-CO₂ Capture

	NETL	SRI
	No	No
CO₂ Capture		
Gross Power Output (kW)	580,260	581,034
Auxiliary Power Requirement (kW)	30,110	31,016
Net Power Output (kW)	550,150	550,018
Net Plant HHV Efficiency (%)	39.1%	38.9%
Net Plant HHV Heat Rate (Btu/kW-hr)	8,721	8,859
Coal Flowrate (lb/hr)	411,282	414,000
CO ₂ Emissions (lb/MWh)	1,773	1,790
Total Plant Cost (\$ x 1000)	866,391	872,118
Total Plant Cost (\$/kW)	1,575	1,586
LCOE (¢/kWh)	6.33	6.40

Case 2: CO₂ Capture with Econamine FG+

The baseline CO₂ capture technology is Flour's Econamine FG+ in a 550 MWe supercritical power plant. An overview of the power plant is shown below in Figure VII-2. As in Case 1, the pulverized Illinois #6 coal is fed into the boiler, where it is combusted in the presence of air. The hot gases pass over the heat exchangers and is then subjected to SCR and FGD processes for the removal of NO_x and SO₂. Upon leaving the FGD unit, the flue gas is sent to the Econamine process, where 90% of the CO₂ is absorbed by the amine solution and compressed for sequestration. The remainder of the flue gas leaves the Econamine absorber and is vented to the atmosphere through the stack.

The steam cycle begins with the cool water leaving the condenser. The water then passes through a series of feed water heaters before entering the boiler, where heat exchangers are used to produce superheated steam. The superheated steam turns the steam turbines, which in turn power the generator. A portion of the low-pressure stream is not passed through the turbine but is used to regenerate the Econamine solution. After the steam has passed through the turbines, it is combined with the Econamine steam condensate and fed to the condenser to complete the cycle.

The process assumptions of the SRI model are shown below in Table VII-4. As in the earlier case, process conditions such as pressure drops, slurry weight percentages, operating temperatures, and fan efficiencies are matched. The capital and operating cost assumptions were also taken from the NETL report but varied linearly with the increasing or decreasing size of the particular unit in consideration. The net power of the plant with CO₂ capture was kept at the same value as the plant with no CO₂ capture. Additional fuel was used to generate additional steam and electricity to compensate for the increased electrical and steam requirements.

Table VII-5 provides a detailed summary of both process and cost results. Again, the net efficiency of the SRI power plant is slightly lower than the NETL plant due to certain assumptions within the Steam-Pro program. Excellent agreement is observed between the SRI and NETL models.

The process models predict that the capture of CO₂ using the Econamine process results in more than 80% increase in the LCOE, a significantly higher increase than stated in the DOE goals. This large increase in LCOE for CO₂ capture is due to an 80% increase in the capital cost due to the increased size of the equipment to produce the same net power, a 4-fold increase in the auxiliary power requirements, and large steam requirement for solvent regeneration. CO₂ compression, solvent pumping, and additional cooling water circulation also add to the increased auxiliary power requirements.

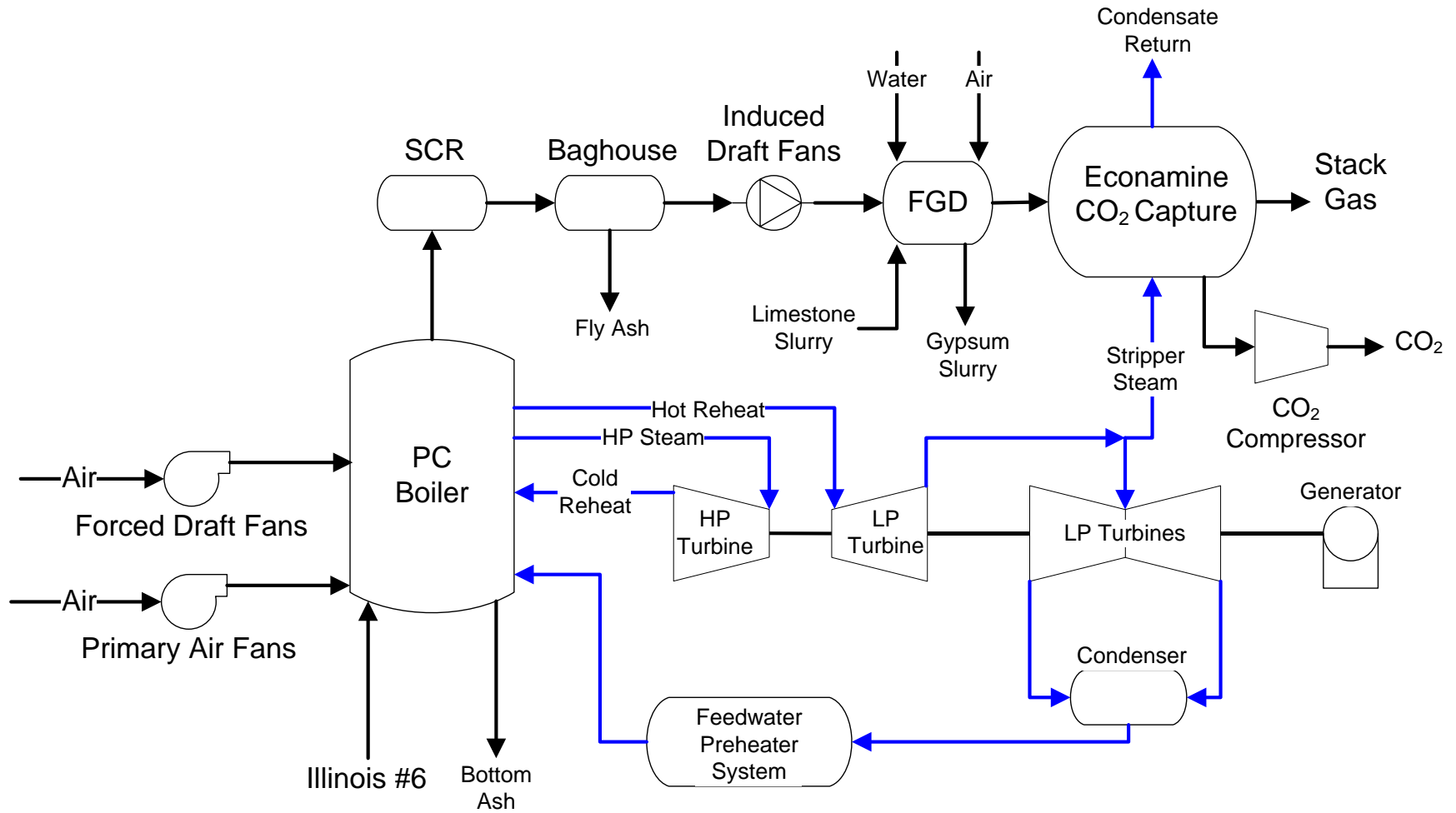


Figure VII-2. Process flow diagram of a PC power plant with CO₂ capture with Econamine process.

Table VII-4. Process Assumptions of a Supercritical Power Plant with Econamine CO₂ Capture

	SRI Supercritical Power Plant w/ Econamine FG+ CO₂ Capture	NETL Supercritical Power Plant w/ Econamine FG+ CO₂ Capture
Net Power Output, MW	550	550
Steam Cycle, (psig, °F, °F)	3500,1100,1100	3500,1100,1100
Coal	Illinois #6	Illinois #6
Condenser pressure, mmHg	50.8	50.8
Cooling water to condenser, °F	64.5	60
Cooling water from condenser, °F	85.5	80
Stack Temperature, °F	74.0	74.0
SO ₂ Control	Wet Limestone Forced Oxidation	Wet Limestone Forced Oxidation
FGD Efficiency, % SO ₂ Removal	98.0	98.0
NOx Control	Low NOx Burners w/OFA and SCR	Low NOx Burners w/OFA and SCR
SCR Efficiency, % NOx Removal	86.0	86.0
Ammonia Slip, ppmv	2.0	2.0
Particulate Control	Fabric Filter	Fabric Filter
Fabric Filter Efficiency, % Ash Removal	99.8	99.8
Mercury Control	Co-Benefit Capture	Co-Benefit Capture
Mercury Removal Efficiency, %	90.0	90.0
CO ₂ Control	Econamine FG Plus	Econamine FG Plus
CO ₂ Capture, %	90	90
CO ₂ Sequestration	Off-site Saline Formation	Off-site Saline Formation

Table VII-5. Comparison of NETL and SRI Results for the Case with Econamine CO₂ Capture

CO₂ Capture	NETL	SRI
	Yes	Yes
Gross Power Output (kW)	663,445	679,911
Auxiliary Power Requirement (kW)	117,450	129,485
Net Power Output (kW)	545,995	550,426
Net Plant HHV Efficiency (%)	27.2%	27.1%
Net Plant HHV Heat Rate (Btu/kW-hr)	12,534	12,590
Coal Flowrate (lb/hr)	586,627	594,000
CO ₂ Emissions (lb/MWh)	254	252
Total Plant Cost (\$ x 1000)	1,567,073	1,586,765
Total Plant Cost (\$/kW)	2,870	2,883
LCOE (¢/kWh)	11.48	11.58

Table VII-6 compares the auxiliary load and the net plant performance of: (1) the case in which CO₂ is captured with Econamine; and (2) the case in which no CO₂ is captured. It shows that, in the case of CO₂ capture, the major contributors to the auxiliary electrical load are the CO₂ compressor, induced draft fans, and the Econamine process load. The electrical load to compress the CO₂ released in the amine stripper to pipeline pressure (150 bar) is about 38% of the increased electrical load. The increase in the electrical load of the fans is due to the pressure drop

across the amine absorber. Note also that about 44% more coal is being burned to produce steam, although only 17% more electricity is produced in the steam turbines. The increase in the fuel use is partly to provide steam for CO₂ stripping from the amine.

Table VII-6. Comparison of Auxiliary Load and Net Plant Performance for the Cases with No-CO₂ capture and CO₂ Capture with Econamine

Parameter	Unit	No CO ₂ Capture	CO ₂ Capture with Econamine
Steam Turbine Gross Power	kWe	581,034	679,911
Auxiliary Load			
Coal Handling & Conveying	kWe	508	729
Limestone Handling & Reagent Preparation	kWe	1,004	1,441
Pulverizers	kWe	3,472	4,981
Ash Handling	kWe	803	1,152
Primary Air Fans	kWe	1,262	1,810
Forced Draft Fans	kWe	1,324	1,900
Induced Draft Fans	kWe	7,165	28,581
SCR	kWe	218	313
Baghouse	kWe	558	788
FGD Pumps & Agitators	kWe	4,664	7,061
Econamine Plus Auxiliaries	kWe	0	16,733
CO ₂ Compressor	kWe	0	48,999
Miscellaneous Balance-of-Plant	kWe	1,453	1,700
Condensate Pumps	kWe	1,085	820
Circulating Water Pumps	kWe	3,977	4,050
Cooling Tower Fans	kWe	2,070	6,728
Transformer Losses	kWe	1,453	1,700
Auxiliary Power Requirements	kWe		
Total	kWe	31,016	129,485
Net Plant Performance			
Auxiliary Load	kWe	31,016	129,485
Net Plant Power	kWe	550,018	550,426
Net Plant Efficiency (HHV)		38.9%	27.1%
Net Plant Heat Rate (HHV)	Btu/kWhr	8,859	12,590
Coal Feed Flowrate	lb/hr	414,000	594,000
Thermal Input ¹	kWth	1,415,453	2,030,867
Limestone Sorbent Feed	lb/hr	41,089	58,953
CO ₂ Emitted	lb/hr	984,315	138,598
CO ₂ Captured	lb/hr	0.0%	1,247,382
CO ₂ Removal		0	90.0%
Water Requirement	lb/s	707	1,417

VII.2 EVALUATION OF THE PROCESS TO CAPTURE CO₂ WITH CARBON SORBENT

Case 3: Capture of CO₂ with Carbon Sorbent.

An overview of the power plant equipped with the carbon sorbent technology is shown below in Figure VII-3. In this case, the Econamine unit is replaced with a carbon sorbent unit. The process is analogous to the Econamine process except that the carbon sorbent microbeads capture CO₂ by adsorption, and direct contact heating is used to strip the CO₂ from the sorbent.

The process assumptions of the SRI carbon sorbent model are shown below in Table VII-7. As in other cases, for the PC-fired boiler and the gas train, process conditions such as pressure drops, slurry weight percentages, operating temperatures, fan efficiencies are matched. However, the assumptions are different for the operating parameters and costs associated with CO₂ capture by carbon sorbents. For this preliminary assessment, the capital cost of carbon sorbent unit is assumed to be equal to that of the Econamine unit. This assumption will be refined when the configuration of the carbon sorbent absorbers and regenerators are finalized. The carbon sorbent bed will absorb CO₂ at 21°C and regenerate at 100°C and has a CO₂ capacity of 6.7 wt%. The sorbent replacement costs were assumed to be similar to those of the amine unit.

The capital and operating cost assumptions for the power plant from the coal preparations to the FGD unit were assumed to vary linearly with the increasing or decreasing size of the particular unit in consideration. For the carbon sorbent bed-based CO₂ capture, the model estimates a coal feed rate of 458,280 lb/hr, compared to 594,000 lb/hr for the Econamine process. This decrease in the coal feed rate is mainly due to the decreased steam requirement for the regeneration of the carbon sorbent and it results in a significant decrease in the capital and operating costs.

Table VII-8 provides a detailed summary of both process and cost results for all three cases based on our model. The net efficiency of a power plant with CO₂ capture by carbon sorbent unit is significantly higher than the Econamine FG+ plant. This higher efficiency causes a decrease in capital and operating costs, which in turn results in a decrease in the cost of electricity.

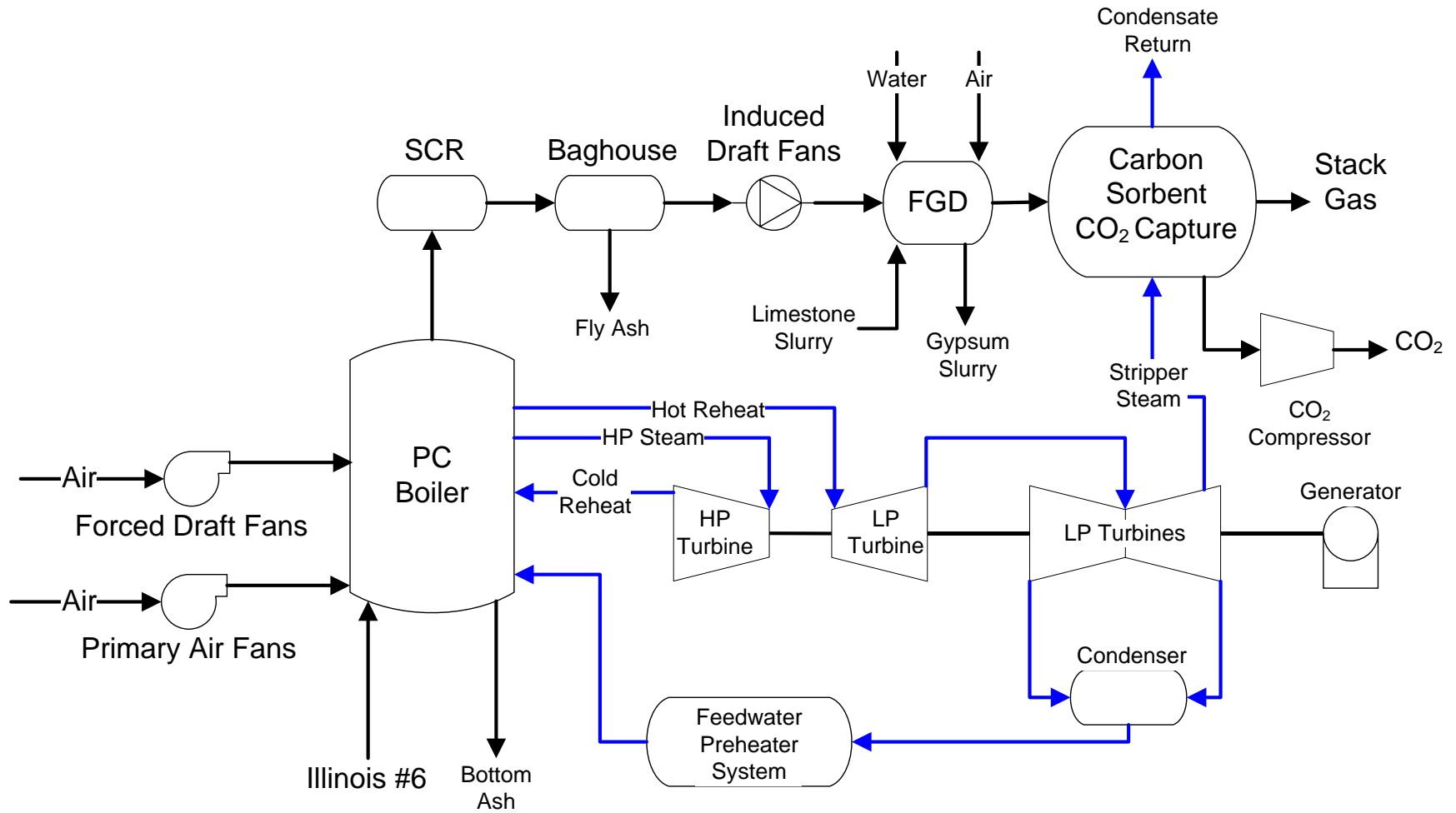


Figure VII-3. Process flow diagram of a PC power plant with CO₂ capture using carbon sorbents.

Table VII-7. Process Assumptions of a Supercritical Power Plant, CO₂ Capture with Carbon Sorbents

	SRI Supercritical Power Plant w/ Carbon Sorbent CO₂ Capture	NETL Supercritical Power Plant w/ Econamine FG+ CO₂ Capture
Net Power Output, MW	550	550
Steam Cycle, (psig, °F, °F)	3500,1100,1100	3500,1100,1100
Coal	Illinois #6	Illinois #6
Condenser pressure, mmHg	50.8	50.8
Cooling water to condenser, °F	64.5	60
Cooling water from condenser, °F	85.5	80
Stack Temperature, °F	74.0	74.0
SO ₂ Control	Wet Limestone Forced Oxidation	Wet Limestone Forced Oxidation
FGD Efficiency, % SO ₂ Removal	98.0	98.0
NOx Control	Low NOx Burners w/OFA and SCR	Low NOx Burners w/OFA and SCR
SCR Efficiency, % NOx Removal	86.0	86.0
Ammonia Slip, ppmv	2.0	2.0
Particulate Control	Fabric Filter	Fabric Filter
Fabric Filter Efficiency, % Ash Removal	99.8	99.8
Mercury Control	Co-Benefit Capture	Co-Benefit Capture
Mercury Removal Efficiency, %	90.0	90.0
CO ₂ Control	Econamine FG Plus	Econamine FG Plus
CO ₂ Capture, %	90	90
CO ₂ Sequestration	Off-site Saline Formation	Off-site Saline Formation

Table VII-8. Comparison of Supercritical Power Plants Using SRI Model

	Base Case	Econamine FG+	Carbon Sorbent
	No	Yes	Yes
CO₂ Capture			
Gross Power Output (kW)	581,034	679,911	640,421
Auxiliary Power Requirement (kW)	31,016	129,485	90,246
Net Power Output (kW)	550,018	550,426	550,175
Net Plant HHV Efficiency (%)	38.9%	27.1%	35.1%
Net Plant HHV Heat Rate (Btu/kW-hr)	8,859	12,590	9,717
Coal Flowrate (lb/hr)	414,000	594,000	458,280
CO ₂ Emissions (lb/MWh)	1,790	252	194
Total Plant Cost (\$ x 1000)	872,118	1,586,765	1,224,213
Total Plant Cost (\$/kW)	1,586	2,883	2,225
LCOE (¢/kWh)	6.40	11.58	9.23
Increase in COE (%)	0.0%	80.9%	44.2%

Table VII-9 compares the auxiliary power loads for the cases in which CO₂ is captured either by carbon sorbent or Econamine process. The coal feed rate is decreased from 594,000 to 458,280 lb/h mainly because of reduced steam requirement to desorb CO₂ from the carbon sorbent. The induced draft fan power requirement is reduced because it is assumed that the pressure drop across the solid sorbent will be lower than that for the liquid amine. The carbon sorbent is not corrosive so that an absorber can be constructed with an inexpensive material such as concrete. The cross-sectional area of the absorber can be increased and height be decreased to allow reduced pressure drop for the flow of flue gases.

Table VII-9. Comparison of SRI Results for the Case with CO₂ Capture by Carbon Sorbent and by Econamine process

Parameter	Units	CO ₂ Capture by	
		Carbon Sorbent	Econamine
Steam Turbine Gross Power	kWe	640,415	679,911
Auxiliary Load			
Coal Handling & Conveying	kWe	563	729
Limestone Handling & Reagent Preparation	kWe	1,112	1,441
Pulverizers	kWe	3,844	4,981
Ash Handling	kWe	889	1,152
Primary Air Fans	kWe	1,397	1,810
Forced Draft Fans	kWe	1,466	1,900
Induced Draft Fans	kWe	13,528	28,581
SCR	kWe	241	313
Baghouse	kWe	615	788
FGD Pumps & Agitators	kWe	5,246	7,061
Carbon Sorbents/Econoamine Plus Auxiliaries	kWe	5,484	16,733
CO ₂ Compressor	kWe	41,966	48,999
Miscellaneous Balance-of-Plant	kWe	1,601	1,700
Condensate Pumps	kWe	1,053	820
Circulating Water Pumps	kWe	5,002	4,050
Cooling Tower Fans	kWe	4,638	6,728
Transformer Losses	kWe	1,601	1,700
Total	kWe	90,246	129,485
Net Plant Performance			
Auxiliary Load	kWe	90,246	129,485
Net Plant Power	kWe	550,170	550,426
Net Plant Efficiency (HHV)		35.1%	27.1%
Net Plant Heat Rate (HHV)	Btu/kWhr	9,718	12,590
Coal Feed Flowrate	lb/hr	458,280	594,000
Thermal Input ¹	kWth	1,566,845	2,030,867
Limestone Sorbent Feed	lb/hr	45,483	58,953
CO ₂ Emitted	lb/hr	106,944	138,598
CO ₂ Captured	lb/hr	962,496	1,247,382
CO ₂ Removal		90.0%	90.0%
Water Requirement	pounds/s	917	1,417

A preliminary sensitivity analysis was performed to understand which parameters will have the greatest impact on the performance of the power plant. Table VII-10 summarizes the results of this sensitivity analysis in which the values of several parameters are changed. Changing the regeneration temperature by using a higher pressure steam than in the base case changes the increase in COE by 1.3%. Doubling the heat of desorption from 250 to 500 Btu/lb CO₂ increases the COE by 2.3%. Note that the carbon sorbent will have minimum water adsorption, and this characteristic will reduce the steam load in comparison to the amine process in which a significant amount of water needs to be heated and evaporated. Similarly an increase in the absorber pressure drop from 0.5 to 2.0 psia increases the COE by 2.4%. A decrease in the absorber temperature from 70° to 50°F with the use of a chiller increased the COE by only 0.7%. The CO₂ capacity of the sorbent has only a minor effect on the cost of electricity.

The variable that has a significant effect on the COE is the capital cost associated with the CO₂ capture unit. Decreasing the capital cost by 30% in relation to the base case decreased the COE increase to 36%, approaching the DOE goals for CO₂ capture.

The sensitivity analysis showed that both capital and operating costs must be reduced to decrease the COE due to CO₂ capture. The operating costs may be reduced by using an absorber configuration that will reduce pressure drop and a regenerator that operates at a relatively low temperature than the amine solvent. The capital costs may be reduced by using inexpensive materials of construction and efficient CO₂ capture process. The compressor used to compress the CO₂ desorbed to pipeline pressure is a significant capital cost that may not be reduced. Using this model and a preliminary estimate of the optimum parameters and characteristics of CO₂ capture using advanced carbon sorbents, we estimated that the cost of electricity will increase by about 33%.

Table VII-10. Sensitivity Analysis of the Parameters for CO₂ capture with Carbon Sorbents

Parameter	Units	Base Case	Reboiler Steam Pressure	Reboiler Steam Pressure	Flue Gas Pressure Drop	Flue Gas Pressure Drop	Reboiler Heat Input	Reboiler Heat Input
Reboiler Steam Pressure	psia	17.7	53.1	131.1	17.7	17.7	17.7	17.7
Flue Gas Pressure Drop	psia	0.54	0.5	0.5	1.0	2.0	0.5	0.5
Reboiler Heat Input	BTU/lb-CO ₂	250	250	250	250	250	350	500
Max Absorber Inlet Temperature	°F	70	70	70	70	70	70	70
Absorbent CO ₂ Capacity	wt%	6.7%	6.7%	6.7%	6.7%	6.7%	6.7%	6.7%
CO ₂ Capture Capital Cost	\$(/lb/hr-CO ₂)	191	191	191	191	191	191	191
Net Plant HHV Efficiency	%	35.1%	34.8	34.5	34.9	34.5	34.8	34.4
Gross Plant Output	MW	640	641	642	644	653	641	643
Coal Flowrate	tons/hr	458	463	467	461	467	462	468
Power Plant Capital	c/kWh	5.23	5.28	5.33	5.26	5.33	5.27	5.34
Power Plant Fuel	c/kWh	2.11	2.13	2.15	2.12	2.15	2.13	2.15
Variable Plant O&M	c/kWh	0.93	0.93	0.94	0.93	0.94	0.93	0.94
Fixed Plant O&M	c/kWh	0.58	0.58	0.58	0.58	0.58	0.58	0.58
CO ₂ Transport, Monitoring, & Storage	c/kWh	0.38	0.38	0.38	0.38	0.38	0.38	0.38
Cost of Electricity (COE)	c/kWh	9.23	9.30	9.38	9.28	9.38	9.30	9.39
Increase in COE	%	44.2%	45.3%	46.6%	45.0%	46.6%	45.3%	46.7%

Table VII-10. Sensitivity Analysis of the Parameters for CO₂ capture with Carbon Sorbents (continued)

Parameter	Units	Base Case	Max Absorb. Inlet Temp	Max Absorb. Inlet Temp	Absorbent CO ₂ Capacity	Absorbent CO ₂ Capacity	CO ₂ Capture Capital Cost	CO ₂ Capture Capital Cost	Optimized Case
Reboiler Steam Pressure	psia	17.7	17.7	17.7	17.7	17.7	17.7	17.7	17.7
Flue Gas Pressure Drop	psia	0.54	0.5	0.5	0.5	0.5	0.5	0.5	0.5
Reboiler Heat Input	BTU/lb-CO ₂	250	250	250	250	250	250	250	250
Max Absorber Inlet Temperature	°F	70	50	100	70	70	70	70	50
Absorbent CO ₂ Capacity	wt%	6.7%	6.7%	6.7%	10.0%	5.0%	6.7%	6.7%	10.0%
CO ₂ Capture Capital Cost	\$(/lb/hr-CO ₂)	191	191	191	191	191	96	127	96
Net Plant HHV Efficiency	%	35.1%	34.9	35.1	35.1	35.0	35.1	35.1	34.9
Gross Plant Output	MW	640	645	640	640	643	640	640	645
Coal Flowrate	tons/hr	458	461	458	458	460	458	458	461
Power Plant Capital	c/kWh	5.23	5.26	5.23	5.23	5.25	4.47	4.72	4.50
Power Plant Fuel	c/kWh	2.11	2.12	2.11	2.11	2.12	2.11	2.11	2.12
Variable Plant O&M	c/kWh	0.93	0.93	0.93	0.93	0.93	0.93	0.93	0.93
Fixed Plant O&M	c/kWh	0.58	0.58	0.58	0.58	0.58	0.58	0.58	0.58
CO ₂ Transport, Monitoring, & Storage	c/kWh	0.38	0.39	0.38	0.38	0.38	0.38	0.38	0.39
Cost of Electricity (COE)	c/kWh	9.23	9.28	9.22	9.22	9.26	8.47	8.72	8.50
Increase in COE	%	44.2%	44.9%	44.1%	44.1%	44.7%	32.3%	36.3%	32.8%

VII.3. UPDATING THE PROCESS ECONOMICS

The preliminary estimate of the cost of CO₂ capture by the carbon sorbents was updated in September 2011. Tables VII-11 through VII-14 summarize the assumptions used in the model, the operating parameters, the auxiliary load, and the cost of CO₂ capture. Table VII-11 compares the parameters used in the original estimate and revised values based on experience with the experimental tests. The pressure drop across the absorber was increased to 1 psi. The heat input to the stripper was increased to 500 Btu/lb CO₂ to include the sensible heat supplied to the sorbent in heating from the absorber temperature to stripper temperature and auxiliary heat to remove steam condensed on the sorbent in the stripper. We also reduced the CO₂ working capacity of the sorbent to 5 wt%, consistent with the experimental results.

Table VII-12 lists the characteristics of a supercritical power plant equipped with either an amine- or carbon-sorbent-based CO₂ capture system. Note that the assumptions for the power plant excluding the CO₂ capture system are the same.

Table VII-13 summarizes the steam turbine gross power, various auxiliary loads, and the calculated power plant performance data for amine- and carbon-sorbent-based CO₂ capture systems. In this model, the net power output is kept constant at 550 MWe, and the coal feed rate is changed to accommodate changes in the auxiliary load. Note that the auxiliary loads are significantly smaller for the carbon-sorbent case than for the amine-based case. Because of the reduced steam requirement in the stripper, the coal feed rate is reduced to obtain the net plant output. The net plant efficiency (HHV) is reduced by only 3.3% in the case of CO₂ capture by the carbon sorbent.

Table VII-14 summarizes the cost of electricity for CO₂ capture using the carbon sorbent and compares costs with the no-CO₂ capture and CO₂ capture with an amine-based system. The increase in the COE is about 37% for CO₂ capture using the carbon sorbent, compared with 80% for an amine-based system, demonstrating the economic advantage of CO₂ capture using the carbon sorbent.

Table VII-11. Characteristics of the CO₂ Capture System

Parameter	Units	Original	Revised
Reboiler Steam Pressure	psia	17.7	17.7
Flue Gas Pressure Drop	psia	0.54	1
Reboiler Heat Input	BTU/lb-CO ₂	250	500
Max Absorber Inlet Temperature	°F	70	70
Absorbent CO ₂ Capacity	wt%	10	5
CO ₂ Capture Capital Cost	\$(/lb/hr-CO ₂)	96	96

Table VII-12. Characteristics of a Supercritical Power Plant with CO₂ Capture

	SRI Supercritical Power Plant with Carbon Sorbent CO₂ Capture	NETL Supercritical Power Plant with Econamine FG+ CO₂ Capture
Net Power Output, MW	550	550
Steam Cycle, (psig, °F, °F)	3500,1100,1100	3500,1100,1100
Coal	Illinois #6	Illinois #6
Condenser pressure, mmHg	50.8	50.8
Cooling water to condenser, °F	64.5	60
Cooling water from condenser, °F	85.5	80
Stack Temperature, °F	74.0	74.0
SO ₂ Control	Wet Limestone Forced Oxidation	Wet Limestone Forced Oxidation
FGD Efficiency, % SO ₂ Removal	98.0	98.0
NO _x Control	Low NO _x Burners w/OFA and SCR	Low NO _x Burners w/OFA and SCR
SCR Efficiency, % NO _x Removal	86.0	86.0
Ammonia Slip, ppmv	2.0	2.0
Particulate Control	Fabric Filter	Fabric Filter
Fabric Filter Efficiency, % Ash Removal	99.8	99.8
Mercury Control	Co-Benefit Capture	Co-Benefit Capture
Mercury Removal Efficiency, %	90.0	90.0
CO ₂ Control	Advanced Carbon Sorbent	Econamine FG Plus
CO ₂ Capture, %	90	90
CO ₂ Sequestration	Off-site Saline Formation	Off-site Saline Formation

Table VII-13. Auxiliary Loads and Power Plant Performance

Parameter	Unit	No CO2 Capture	CO2 Capture with Econamine FG+	CO2 Capture with the Carbon Sorbent
Steam Turbine Gross Power	kW _e	580,400	662,800	642,113
Auxiliary Load				
Coal Handling & Conveying	kW _e	440	510	556
Limestone Handling & Reagent Prep	kW _e	890	1,250	1,078
Pulverizers	kW _e	2,780	3,850	3,703
Ash Handling	kW _e	530	740	860
Primary Air Fans	kW _e	1,300	1,800	1,342
Forced Draft Fans	kW _e	1,660	2,300	1,410
Induced Draft Fans	kW _e	7,050	11,120	17,020
SCR	kW _e	50	70	253
Baghouse	kW _e	70	100	642
FGD Pumps & Agitators	kW _e	2,970	4,110	5,047
Econamine FG Plus Auxiliaries	kW _e	0	20,600	6,000
CO ₂ Compressor	kW _e	0	44,890	43,274
Miscellaneous Balance-of-Plant	kW _e	2,000	2,000	2,395
Steam Turbine Auxiliaries	kW _e	400	400	0
Condensate Pumps	kW _e	800	560	811
Circulating Water Pumps	kW _e	4,730	10,100	4,376
Ground Water Pumps	kW _e	480	910	4,477
Cooling Tower Fans	kW _e	2,440	5,230	1,588
Transformer Losses	kW _e	1,820	2,290	3,922
Total	kW _e	30,410	112,830	98,751
Net Plant Performance				
Auxiliary Load	kW _e	30,410	112,830	98,751
Net Plant Power	kW _e	549,990	549,970	543,362
Net Plant Efficiency (HHV)		39.3%	28.4%	36.0%
Net Plant Heat Rate (HHV)	Btu/kWhr	8,687	12,002	9,472
Coal Feed Flowrate	lb/hr	409,528	565,820	441,178
Thermal Input	kW _{th}	1,400,163	1,934,520	1,508,374
Limestone Sorbent Feed	lb/hr	40,646	57,245	43,508
CO ₂ Emitted	lb/hr	972,382	134,193	102,924
CO ₂ Captured	lb/hr	0	1,207,730	926,317
CO ₂ Removal		90.0%	90.0%	90.0%
Water Requirement	1000s gpd	4,252	7,300	7,072

Table VII-14. Cost of CO₂ Capture

Parameter	Unit	No CO ₂ Capture	CO ₂ Capture with Economine FG+	CO ₂ Capture with the Carbon Sorbent
Capacity Factor		85%	85%	85%
Capital Charge Factor		11.65%	12.43%	12.43%
20-year Levelization Factors				
Fuel		1.2089	1.2089	1.2089
Non-Fuel Variable O&M		1.1618	1.1618	1.1618
Fixed O&M		1.1618	1.1618	1.1618
Plant Operating Life	years	30	30	30
Power Production @100% Capacity	GWh/yr	4,818	4,818	4,760
Power Plant Capital	c/kWh	3.17	5.96	4.40
Power Plant Fuel	c/kWh	1.42	1.96	1.55
Variable Plant O&M	c/kWh	0.51	0.87	0.66
Fixed Plant O&M	c/kWh	0.80	1.30	0.96
Power Plant Total	c/kWh	5.89	10.10	7.56
CO ₂ TS&M	c/kWh		0.56	0.54
BOTTOM LINE TOTAL	c/kWh	5.89	10.66	8.10
Increase in COE	%	0.0%	80.2%	37.2%
CO ₂ Emissions	lb/MWh	1,768	244	189

VIII. CONCLUSIONS AND RECOMMENDATION

On the basis of the experimental and analytical work performed in Budget Periods 1 through 3, we have made the following conclusions:

1. Bench-scale tests with a flue gas from a coal-fired boiler showed that the advanced carbon sorbent process is capable of capturing > 90% CO₂ and producing a product stream that is nearly pure CO₂.
2. The integrated adsorber-stripper system takes advantage of the unique high adsorption and desorption kinetics, high fluidity, and high attrition resistance of the carbon sorbent microbeads. Tests in the bench-scale system demonstrated that a commercially available structural packing is suitable for this application. A stable operation of the integrated system was demonstrated both at SRI using a simulated flue gas and in the field using a flue gas from a coal-fired boiler.
3. The system was able to operate with a flue gas stream containing only 4.5% CO₂ (v/v). When the system operating parameters were adjusted for a target capture efficiency of 90%, a CO₂ level corresponding to 85 to 95% CO₂ capture was observed at the adsorber exit under steady-state conditions. We obtained a CO₂ product gas purity of ~ 100% under those conditions.
4. During the field test, the flue gas flow and sorbent circulation were maintained without any significant problem. The major difficulty encountered during the test period was maintaining the temperatures of the stripper and the dehydrator, especially in the cold weather encountered in Ohio in the middle of winter. When we implemented the external heating of the walls of the stripper and the dehydrator and added additional insulation, we obtained a reliable performance of the integrated system with both high CO₂ capture efficiency and CO₂ product gas purity.
5. The sorbent demonstrated a very high stability with no change in sorption capacity over thousands of adsorption and desorption cycles (~ 7,000).
6. The sorbent has an extremely low attrition loss, with extrapolated sorbent lifetime due to attrition of many years of continuous operation.
7. We demonstrated that sorbent microbeads flow down smoothly even when heated directly with steam because steam condenses inside the pores of the microbeads.
8. We demonstrated that the single column with the adsorber on the top and the stripper on the bottom is an efficient design, minimizing the solid transport.
9. The preliminary estimate of the process using the advanced carbon sorbent indicates that the COE of CO₂ capture and sequestration will increase by 37% over the base case of no-CO₂ capture. Note that the increase in COE using advanced carbon sorbent for CO₂ capture is estimated to be less than half that of an amine-based solvent system for CO₂ capture.
10. A preliminary sensitivity analysis showed that capital costs, pressure drop in the absorber, and steam requirements for the regenerator are the major variables in determining the cost of CO₂ capture.

11. Both the noncorrosive nature and low temperature for the regeneration of the carbon sorbent allow the use of low-cost construction materials, reducing the capital costs. The relatively low heat of desorption and low-temperature operation reduce the steam consumption during regeneration.
12. The results indicate that further long-term testing with a flue gas from a pulverized coal-fired boiler should be performed to obtain additional data relating to the effects of flue gas contaminants, ability to reduce pressure drop by using alternate structural packing, and the use of low-cost construction materials.

The proposed work is a continuation of the current field test (Task 8). In this field test, we will install a bench-scale system at the National Carbon Capture Center and operate the unit using the flue gas from the Gaston power plant for 1,000 h. The development of the ACS process will be accelerated because of the following improvements that are possible from the results of the field test:

1. The performance of the process will be demonstrated using a flue gas stream from an operating PC-fired power plant for an extended period of time.
2. The system design will focus on the materials of construction to reduce the cost of CO₂ capture to acceptable levels. The capital cost of the system is a major factor in the cost of CO₂ capture.
3. Thermal integration concepts can be evaluated at a preliminary level. Although thermal requirements cannot be defined precisely at this scale, we will obtain a reasonable estimate of steam requirements, which is a major operating cost.

The industrial acceptance of the process is enhanced significantly because our method decreases uncertainties in the capital and operating costs and will enable demonstration with an actual flue gas at the NCCC facility.

IX. REFERENCES

- [EIA, 2012] Annual Energy Outlook 2012 with Projections to 2035, Report #DE/EIA-0383, June 2012.
- Alpetkin, G., A. Jayaraman, R. Copeland, “A low cost, high capacity regenerable sorbent for pre-combustion CO₂ capture,” Proceedings of the 2012 NETL CO₂ Capture Technology Meeting. <http://www.netl.doe.gov/publications/proceedings/12/co2capture/>
- Choi, Sunho, Jeffrey H. Drese, Christopher W. Jones, “Adsorbent materials for carbon dioxide capture from large anthropogenic point sources,” *ChemSusChem* 2(9), 796-854 (2009).
- Elliott, J. G. Srinivas, R. Copeland, “Low-cost sorbent for CO₂ capture on existing plants,” Proceedings of the 2012 NETL CO₂ Capture Technology Meeting. <http://www.netl.doe.gov/publications/proceedings/12/co2capture/>
- Figuroa, J.D., Carbon dioxide capture and sequestration potential and issues in the United States. APPA New Generation Meeting, Washington, DC (2006). http://www.netl.doe.gov/publications/carbon_seq/presentations/APPANewGenerationMeetingFinal.zip
- Hornbostel, M., “Development of novel carbon sorbents for CO₂ capture,” Presentation at the Annual NETL CO₂ Capture Technology for Existing Plant R&D Meeting, March 2009.
- Jockenhövel, T., R. Schneider, H. Rode, “Development of an economic post-combustion carbon capture process,” *Energy Procedia* 1(1), 1043-1050 (2009).
- Klara, J., “Cost and performance baseline for fossil energy plants, Volume 1: Bituminous coal and natural gas to electricity,” Final Report, DOE/NETL-2007/1281, Revision 1: August 2007.
- Kozak, F., V. Telikapalli, R. Hiwale, “CCS Project: Chilled ammonia process at the AEP Mountaineer Plant,” presented to the Coal-Gen Conference and Exhibition, August 17, 2011.
- Krishnan, G., “Development of novel carbon sorbents for CO₂ capture,” Presentation at the Annual NETL CO₂ Capture Technology for Existing Plant R&D Meeting, September 2010.
- Marsh, H. and T. Siemieniowska, “The surface area of coals as evaluated from the adsorption isotherms of carbon dioxide using Dubinin-Polanyi equation,” *Fuel* 44, 453 (1965).
- Mason, J.A., K. Sumida, Z. Herm, R. Krishna, J.R. Long, “Evaluating metal-organic frameworks for post-combustion carbon dioxide capture via temperature swing adsorption,” *Energy Environ. Sci.* 4, 3030-3040 (2011).
- Sjostrom, S. and Krutka, H. “Evaluation of solid sorbents as a retrofit technology for CO₂ capture,” *Fuel* 89, 1298-1306 (2010).
- Walker, P. L. and R. L. Patel, “Surface areas of coals from carbon dioxide adsorption at 298 K,” *Fuel* 49, 91-94 (1970).